Applications of Whispering Gallery Microcavities

- Yang Yong

- April 14, 2008

Contents

- Introduction of WG microcavities
- Applications of Passive micro resonators
- Applications of Active microcavity
- Recent Progress for microcavity in cavity QED

Principle of WG mode

Lord Rayleigh

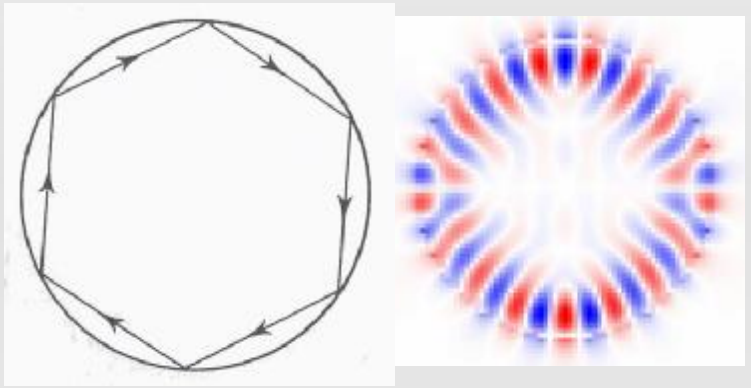

Whispering Gallery Mode (WGM)

Current microcavity

	Fabry–Perot	Whispering gallery		Photonic crystal
High Q	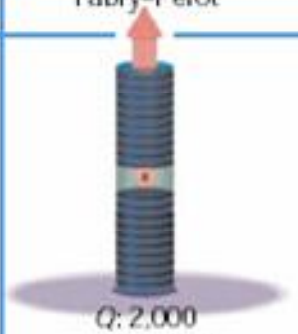 Q: 2,000 V: 5 $(\lambda/n)^3$	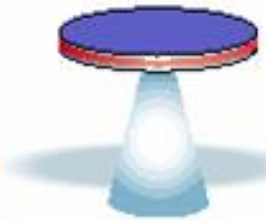 Q: 12,000 V: 6 $(\lambda/n)^3$	Q_{III-V}: 7,000 Q_{Poly}: 1.3x10^5	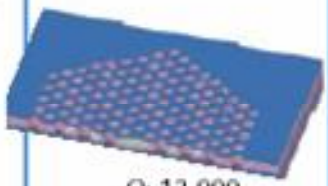 Q: 13,000 V: 1.2 $(\lambda/n)^3$
Ultrahigh Q	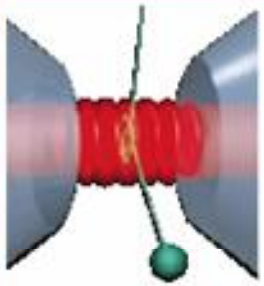 F: 4.8×10^5 V: 1,690 μm^3	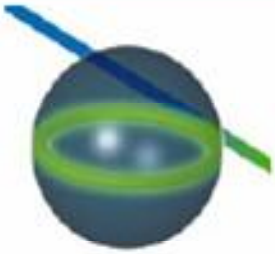 Q: 8×10^9 V: 3,000 μm^3	Q: 10^8	

Mode charecteristics of WGM

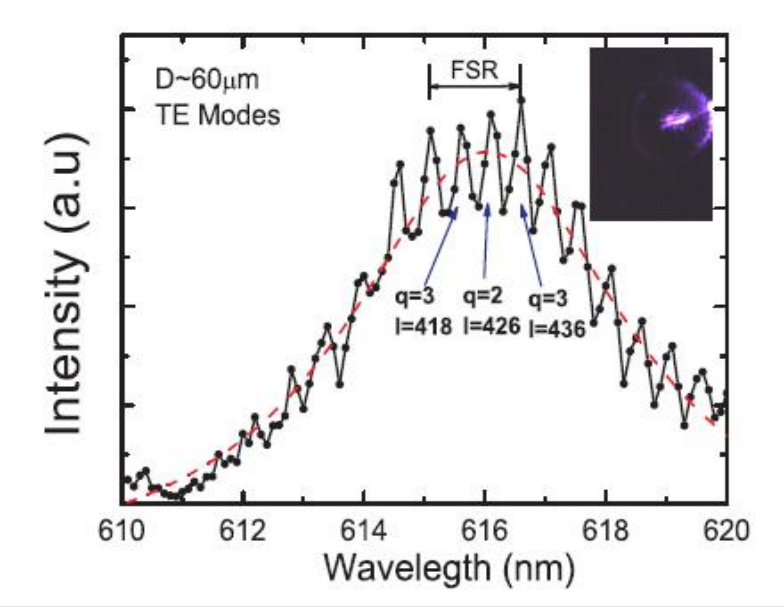

Mode distribution of a Eu-doped microsphere

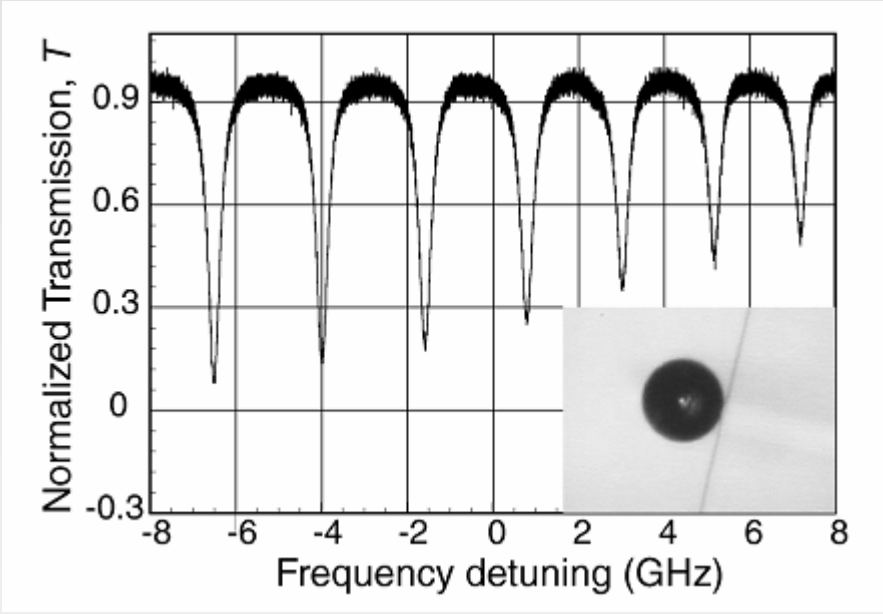

$$\gamma_{qlm}^{E,H} = \Delta_0 \left[l + 1/2 - A_q \sqrt[3]{(l+1/2)/2} - \Delta_{E,H} \pm \varepsilon^2 (l - |m|)/2 \right],$$

Modes of fiber taper coupled microsphere

Taper coupled microcavity

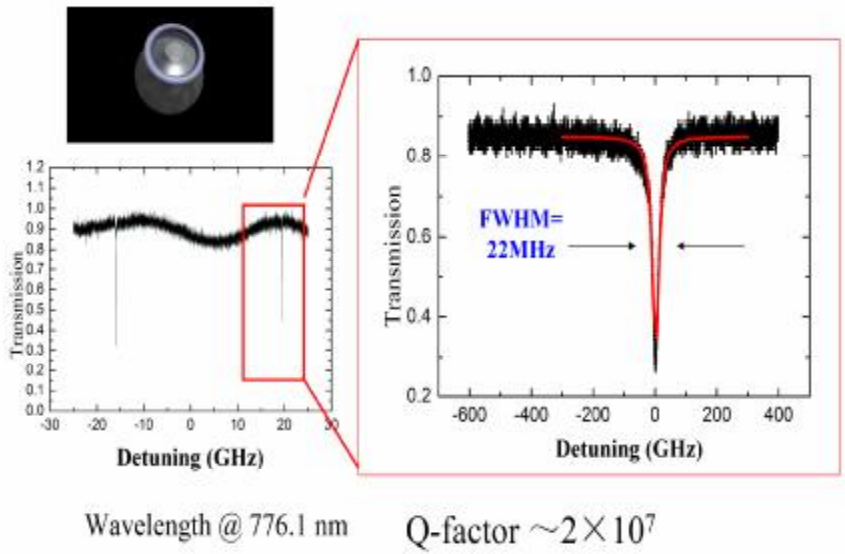

Wavelength @ 776.1 nm Q-factor ~2×10^7

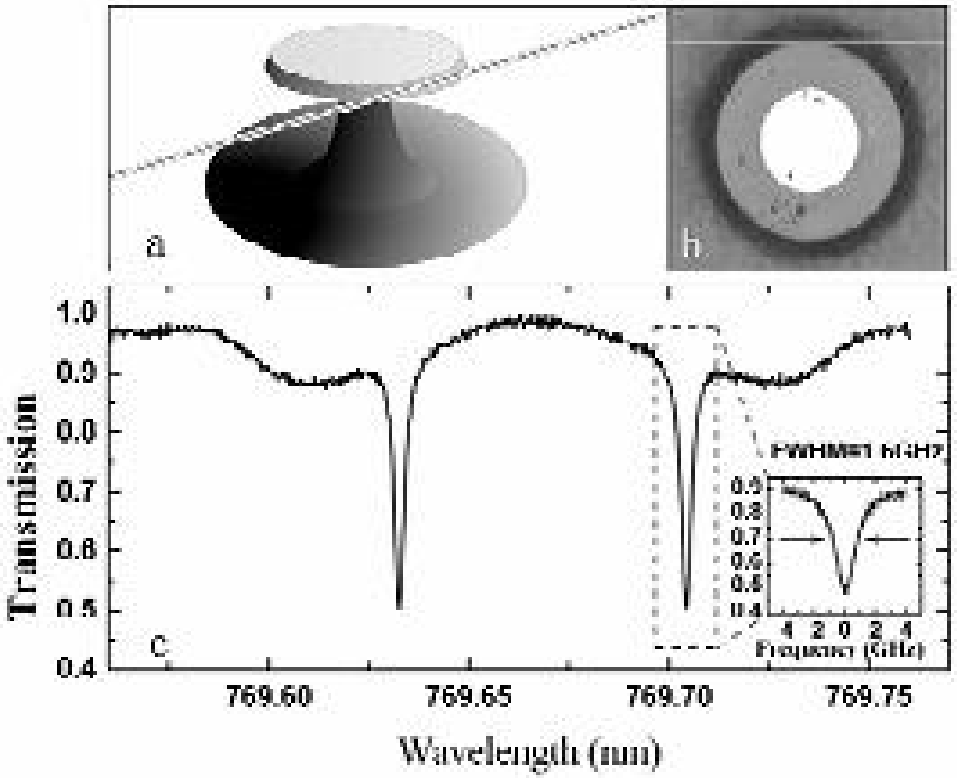

Q factor of taper-coupled microtoroid

Q factor of taper-coupled microdisk

CHINESE OPTICS LETTERS / Vol. 5, No. 11 / November 10, 2007

Passive WGM:Add-Dropper

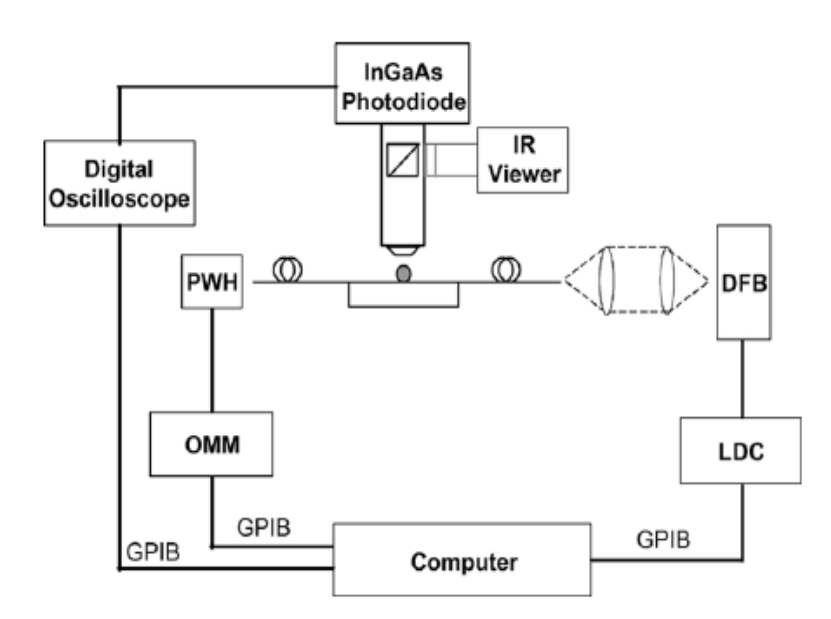

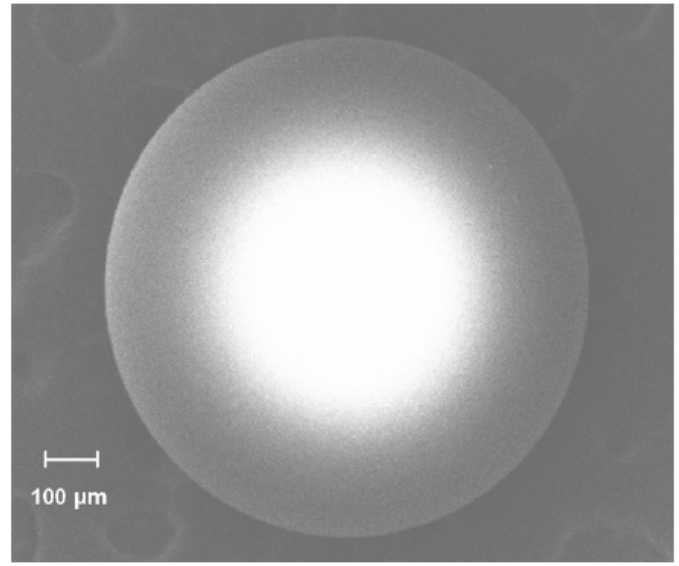

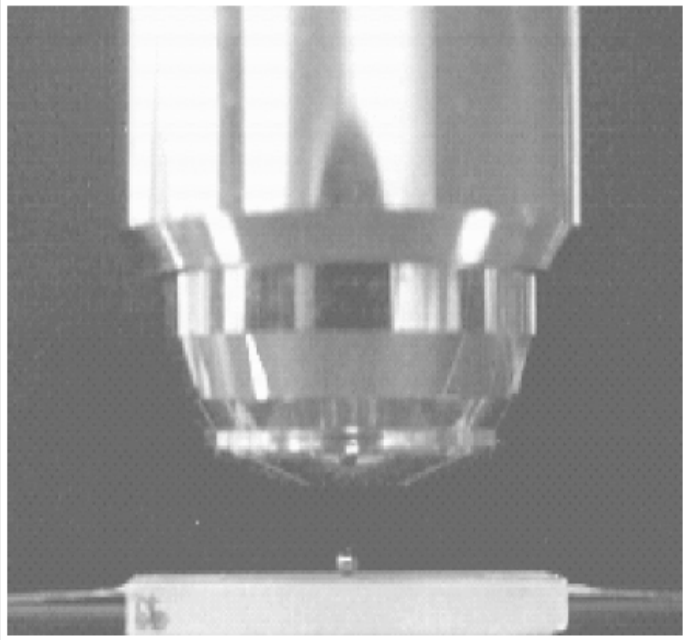

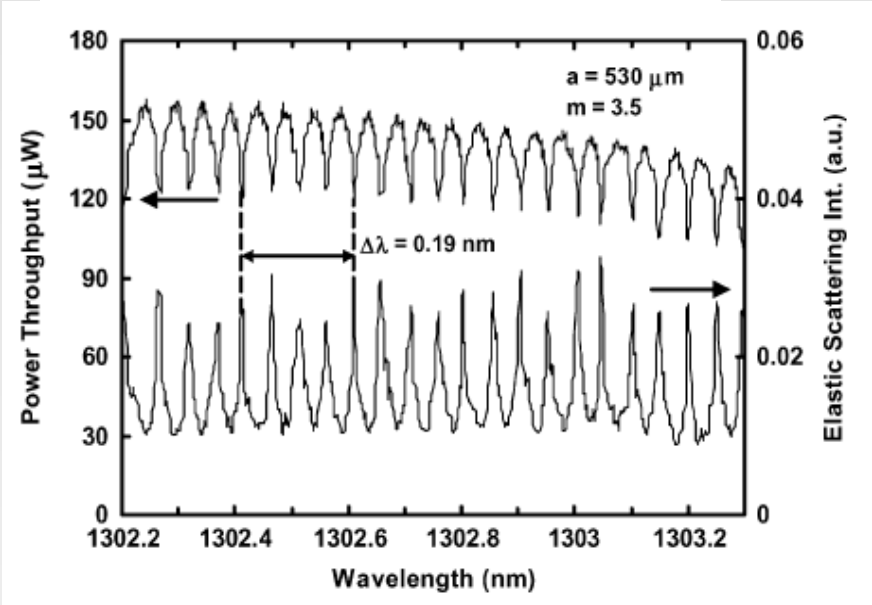

IEEE PTL Vol. 17 No. 8 ,2005

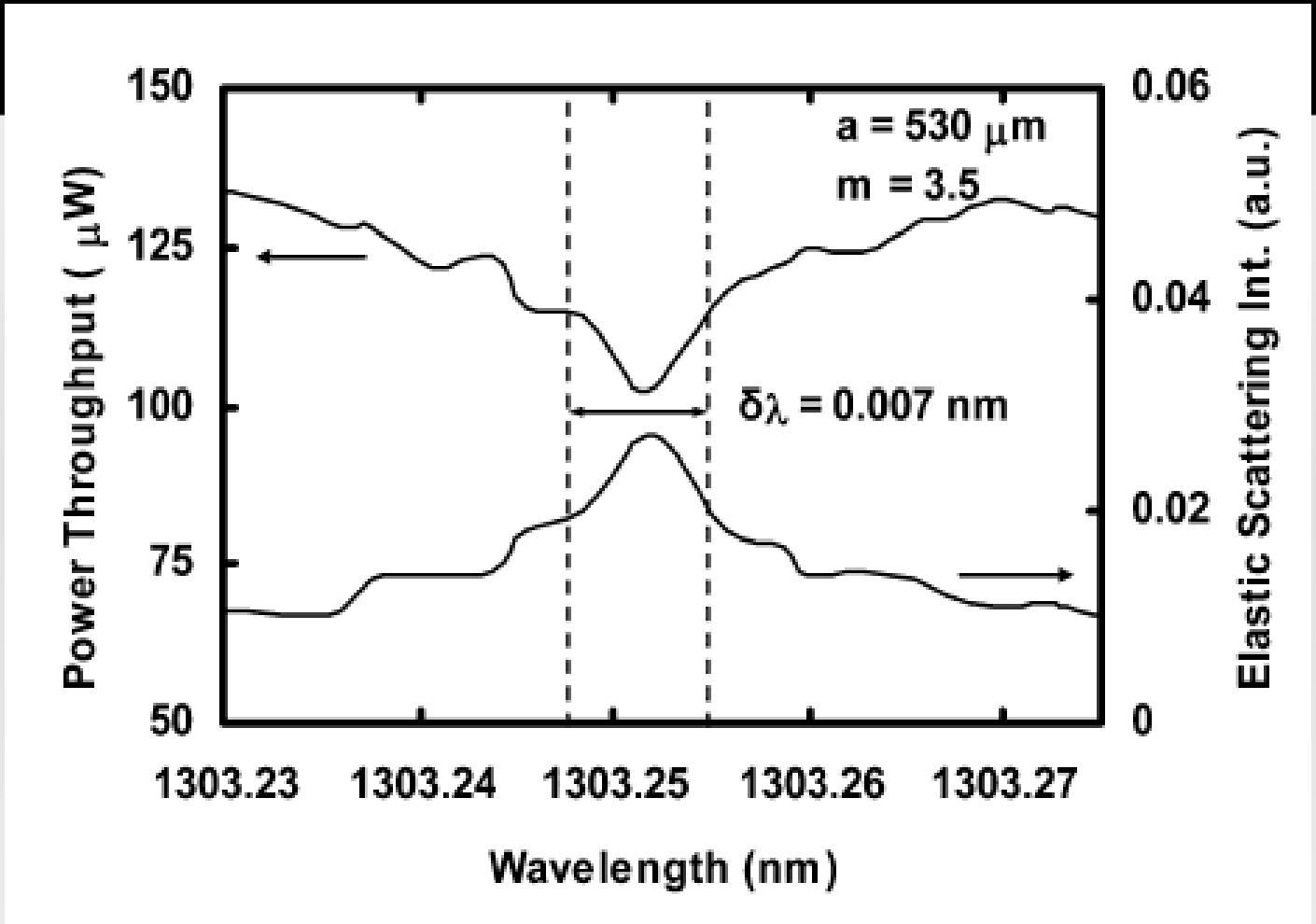

High-resolution elastic scattering and transmitted power spectra from
the silicon microsphere.

Passive WGM: High-Order Filter

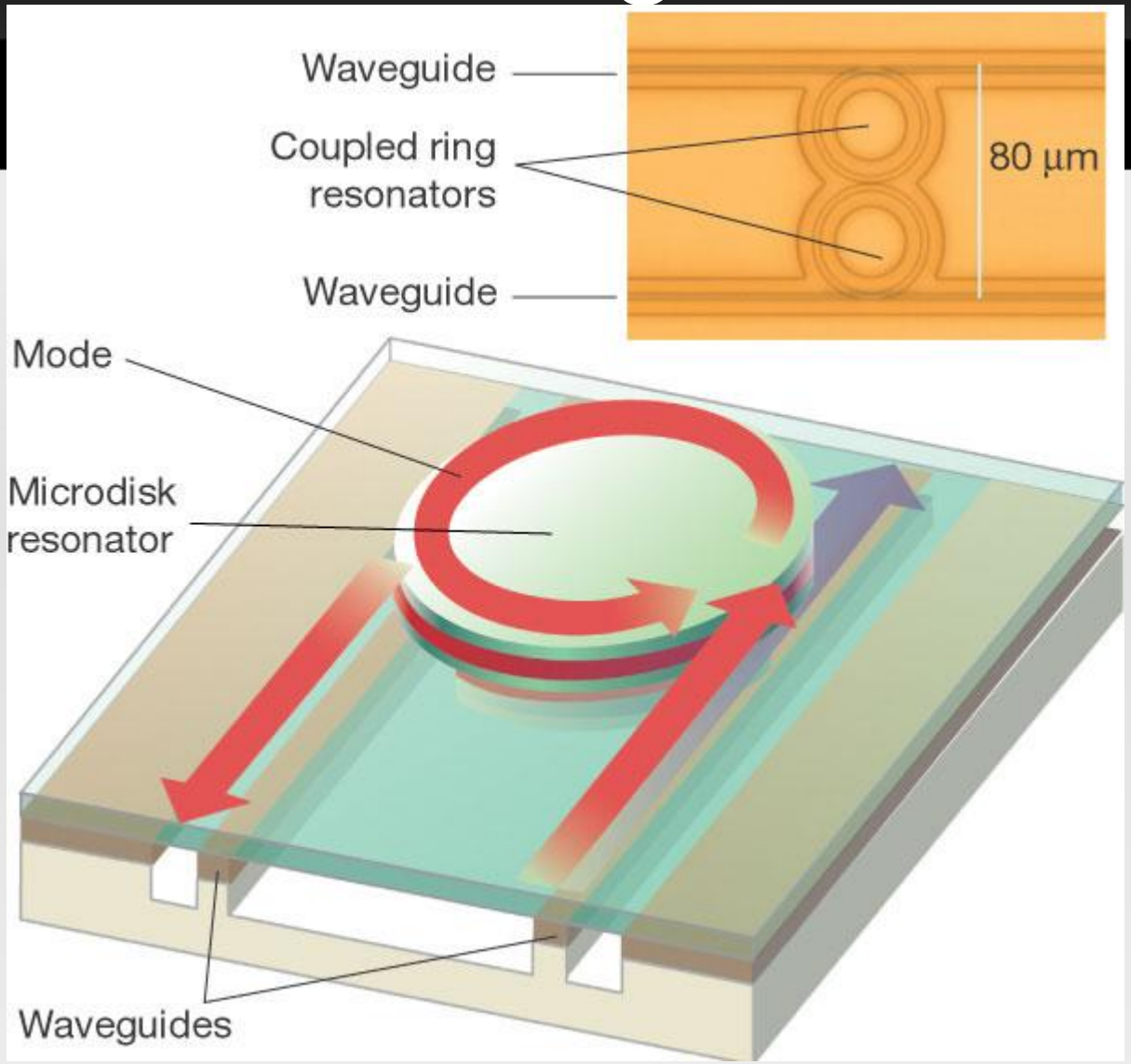

Illustration of a microcavity add/drop filter in which two buried waveguides (shown in brown) are vertically coupled to a disk whispering gallery

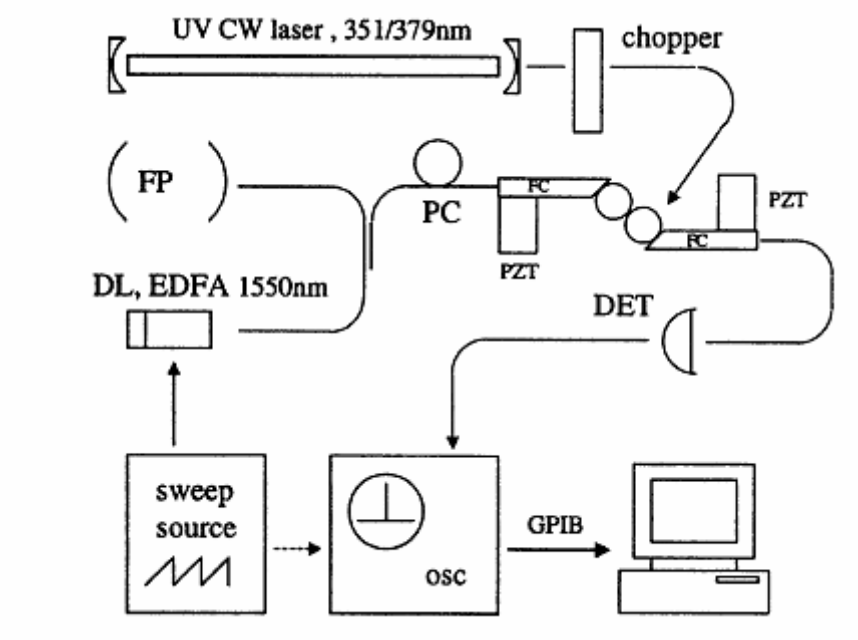

Installation to fabricate a second-order filter.

Filter spectrum. Thin line depicts experimental results, thick line—Lorentzian fit.

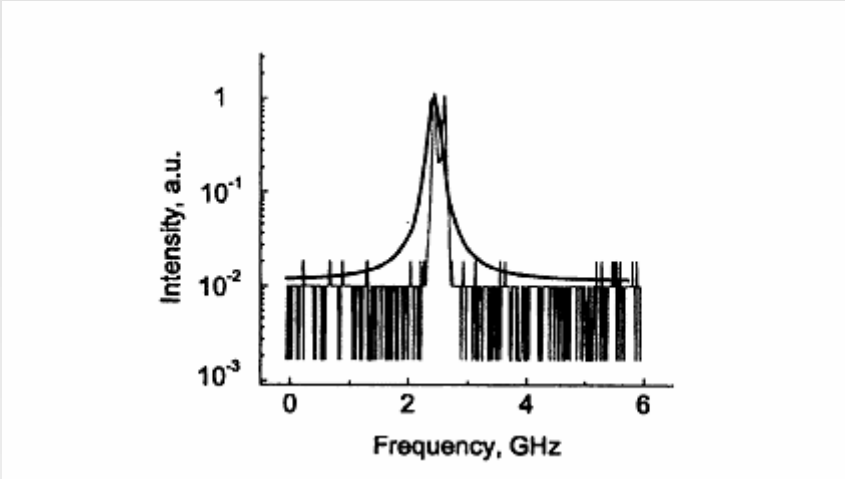

IEEE PTL Vol. 15 no. 4, 2003

Passive WGM: Tunable Filters

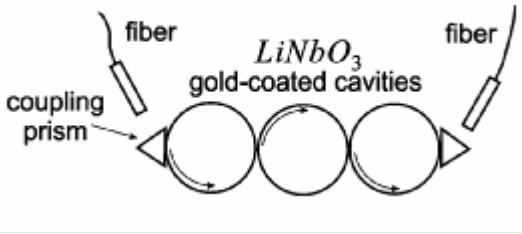

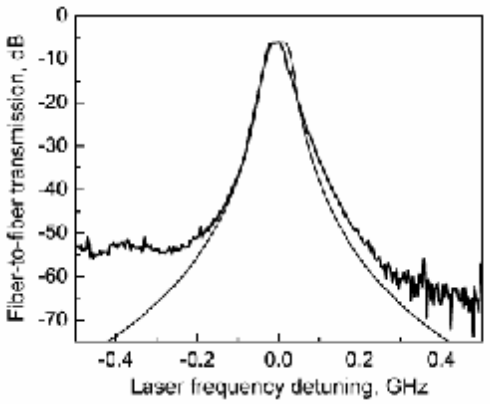

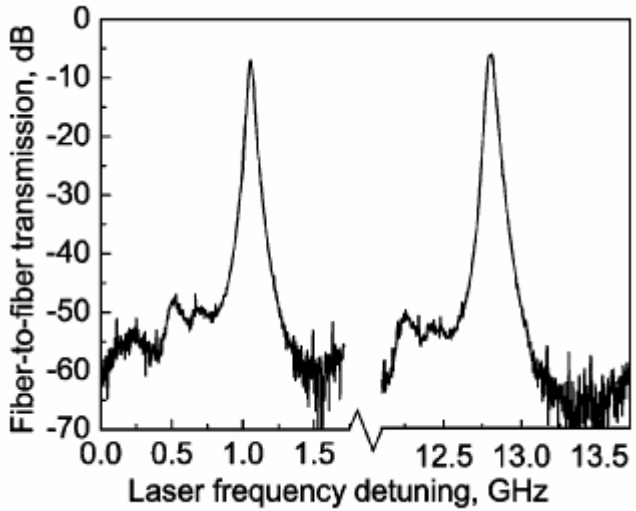

IEEE PTL Vol. 17 no. 1 2005

$$\Delta\nu_{\mathrm{TE}} = \nu_0 \frac{n_e^2}{2} r_{33} E_Z, \quad \Delta\nu_{\mathrm{TM}} = \nu_0 \frac{n_o^2}{2} r_{13} E_Z$$

Tunable third-order optical filter fabricated from the three voltage-controlled lithium niobate whispering gallery-mode resonators. The filter operates at 1550 nm with 30-MHz bandwidth and can be electrooptically tuned by 12 GHz in the linear regime with approximately 80-MHz/V tuning rate. With this filter, we have demonstrated 6-dB fiber-to-fiber insertion loss and 30-ns tuning speed, limited by the resonator buildup time.

Passive WGM: Polarization Convert

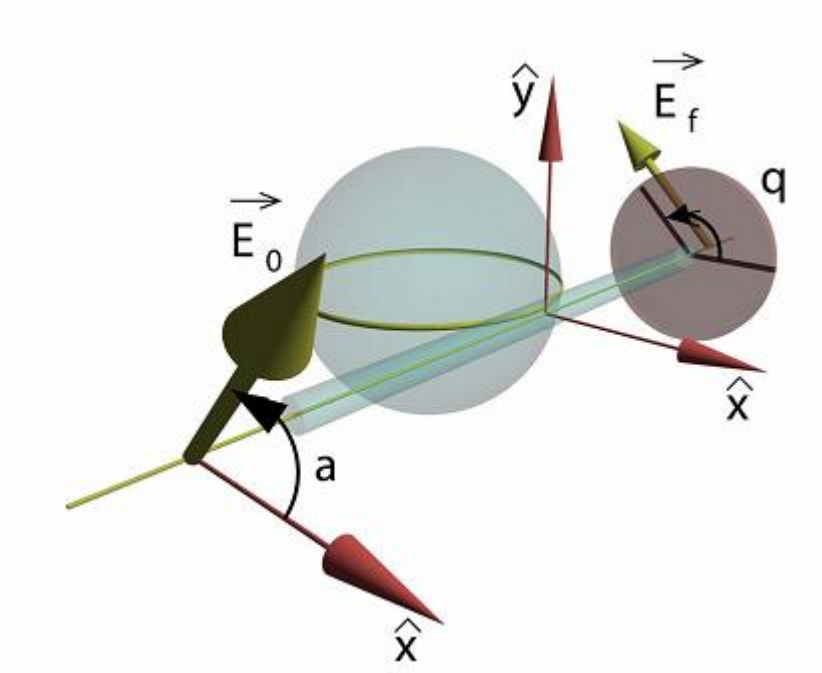

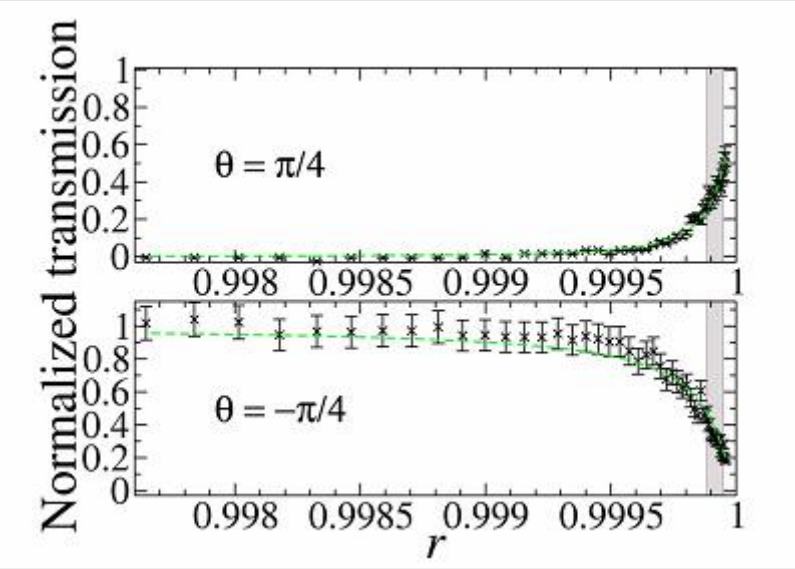

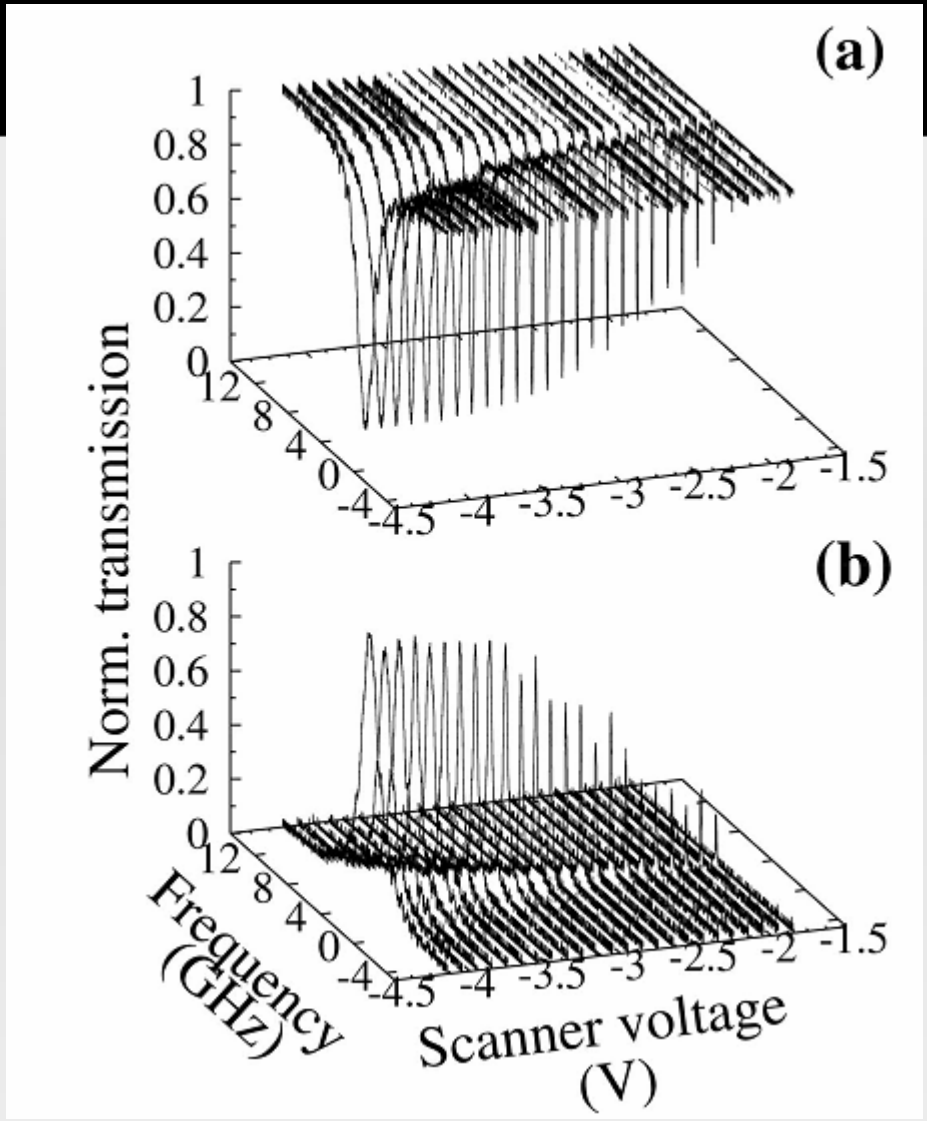

Passive WGM: Laser Applications

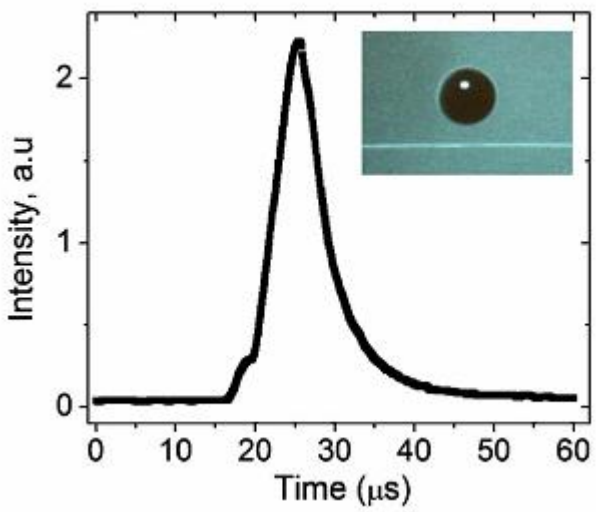

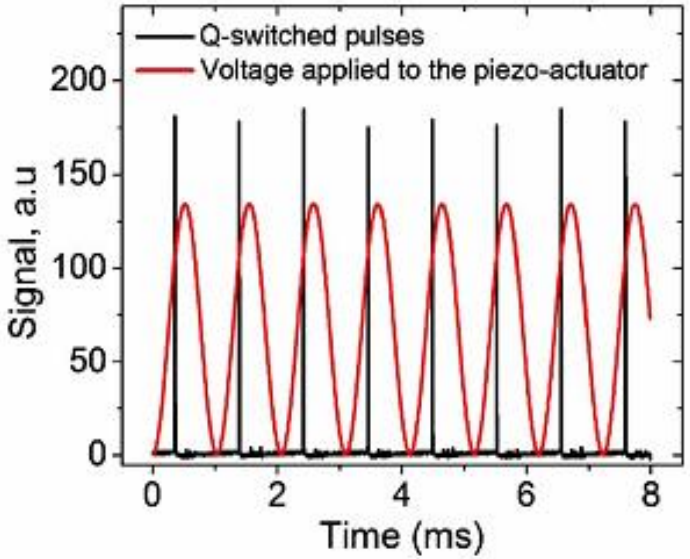

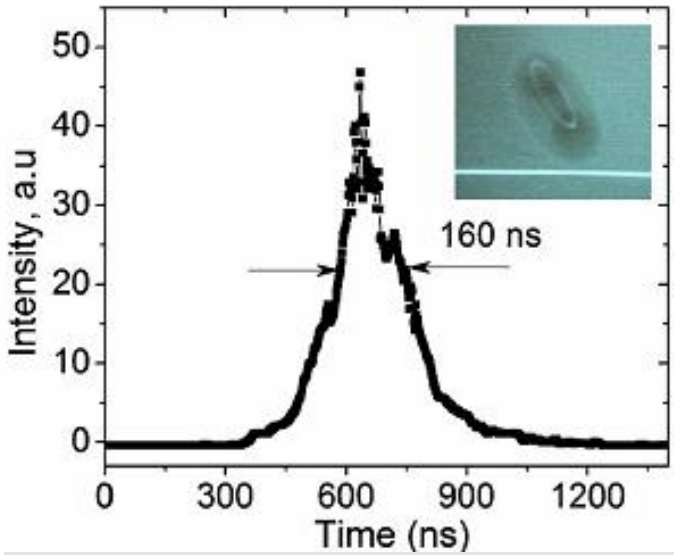

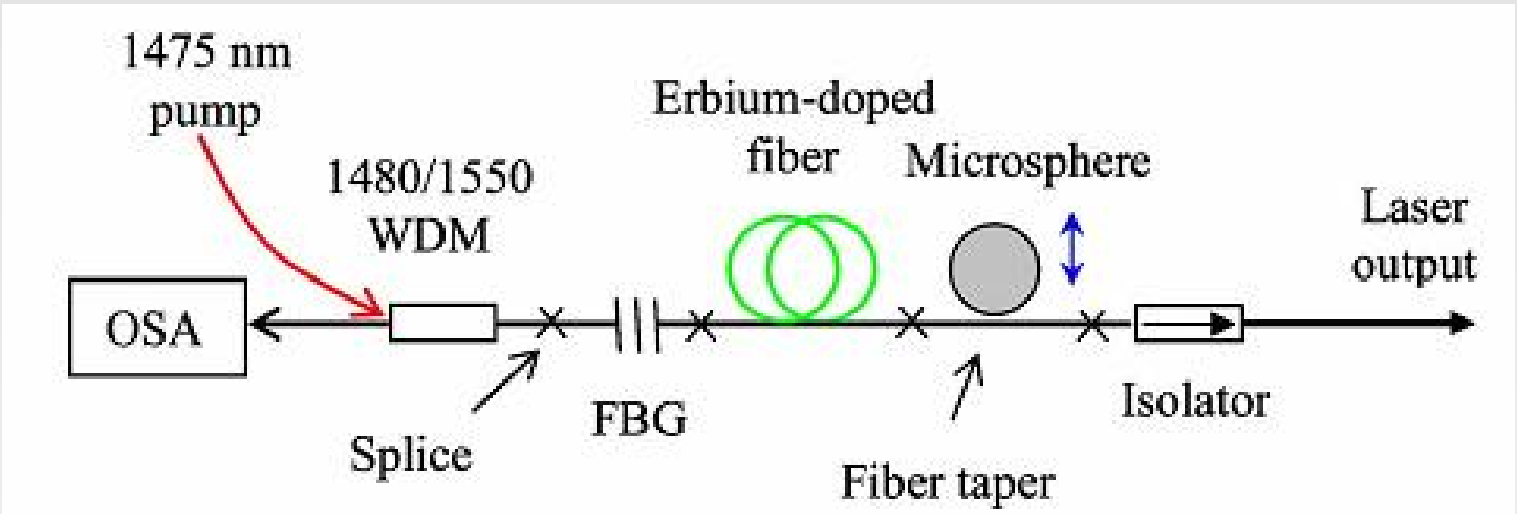

Q Switch for a fiber laser.

Narrow diode's linewidth: Microsphere as feedback

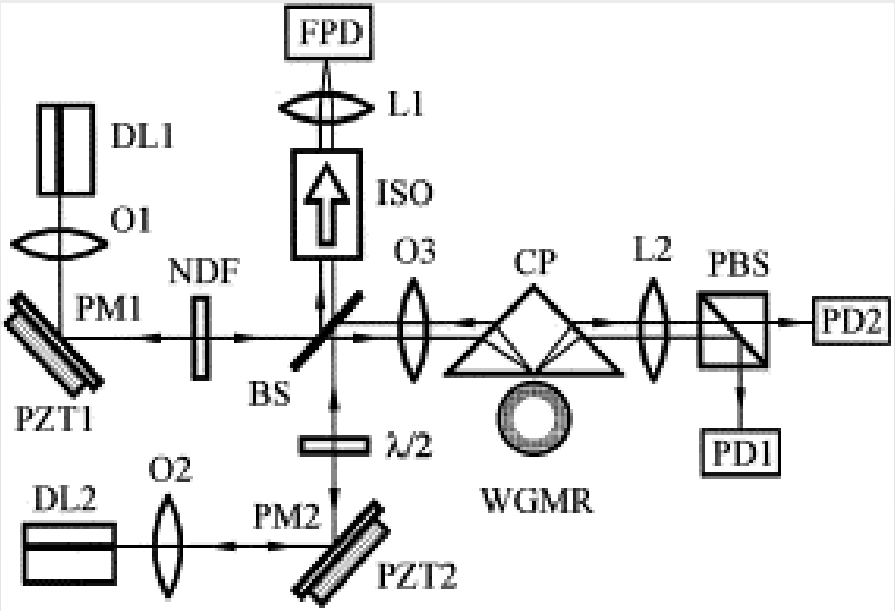

The setup for locking of two lasers to orthogonally polarized modes of the microsphere.

Opt. Comm. Vol. 158, 1999

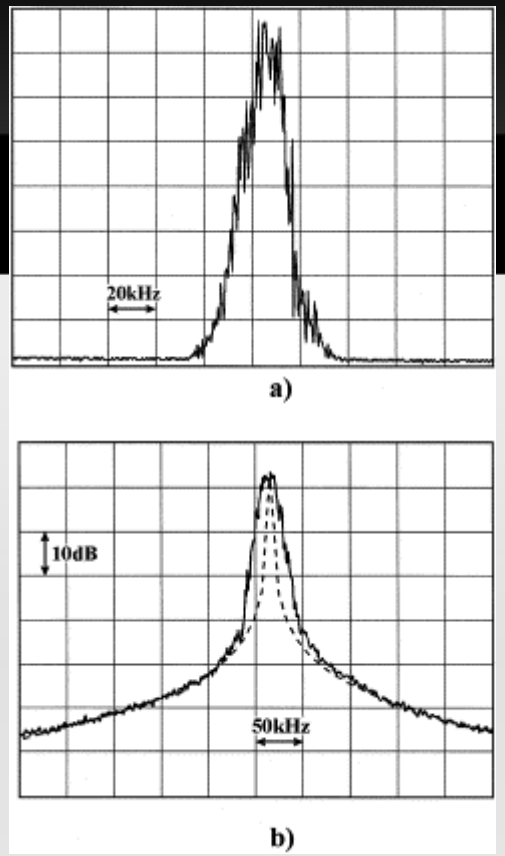

The beatnote spectrum of two DLs optically locked to the orthogonal modes of the WGMR. (a) Linear scale, frequency span 200 kHz, resolution 10 kHz, sweep time 5 s, video bandwidth 30 Hz. (b) Logarithmic scale, frequency span 500 kHz, resolution 10 kHz, sweep time 10 s, video bandwidth 30 Hz. The dashed curve is the Lorentzian best fit with FWHM of 790 Hz.

Laser lock to the microcavity: Pound-Drever-Hall Method

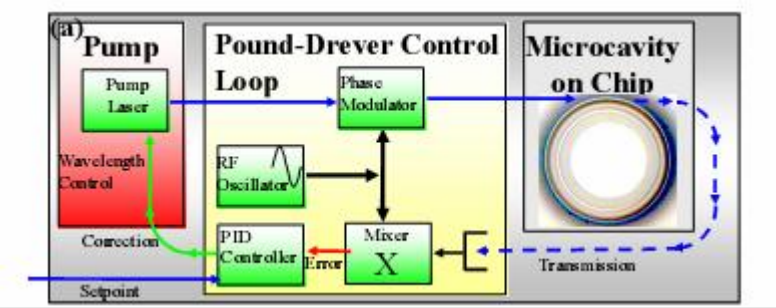

Experimental Setup

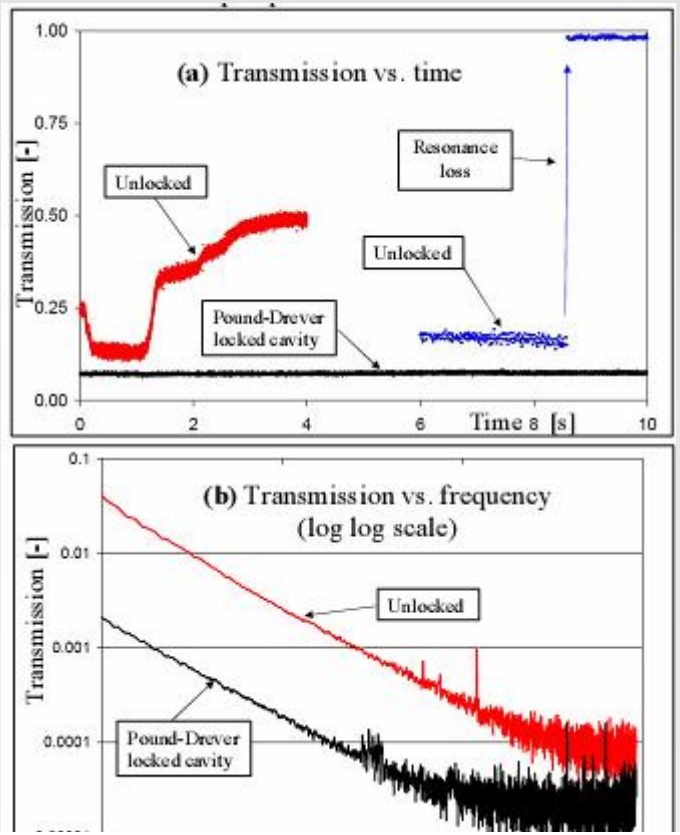

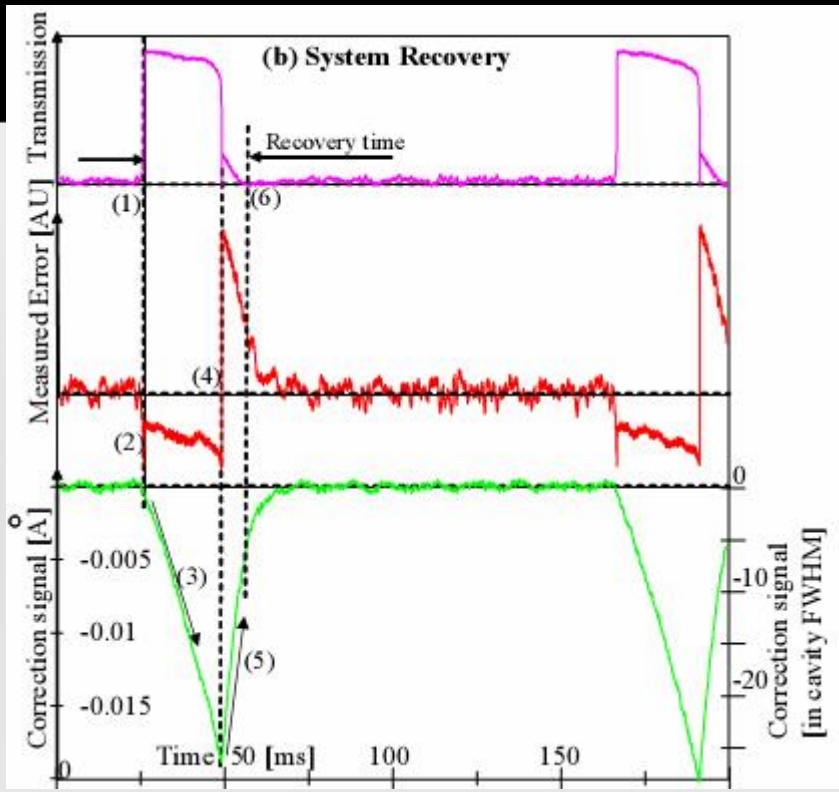

System recovers from perturbation in the regime of thermal instability.

a) Transmission vs. time of a locked system.
b) Spectra property of a locked system

Opt. Lett. Vol. 13 no 9, 2005

Vice Vesa: Lock microcavity to a Frequency stabilized Laser

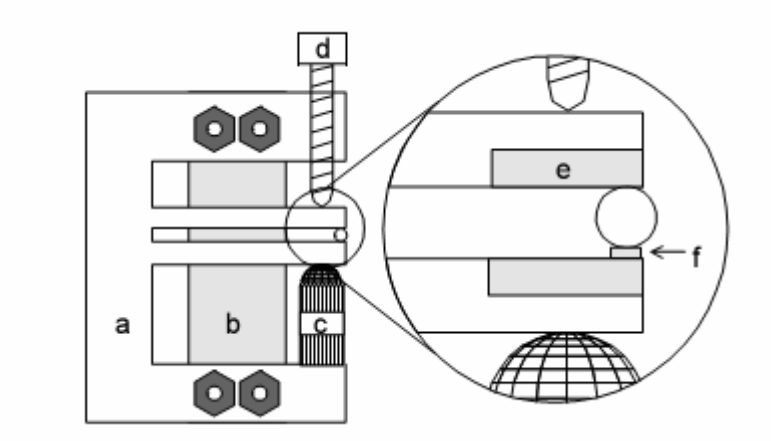

Experimental Setup for Tuning WGMs

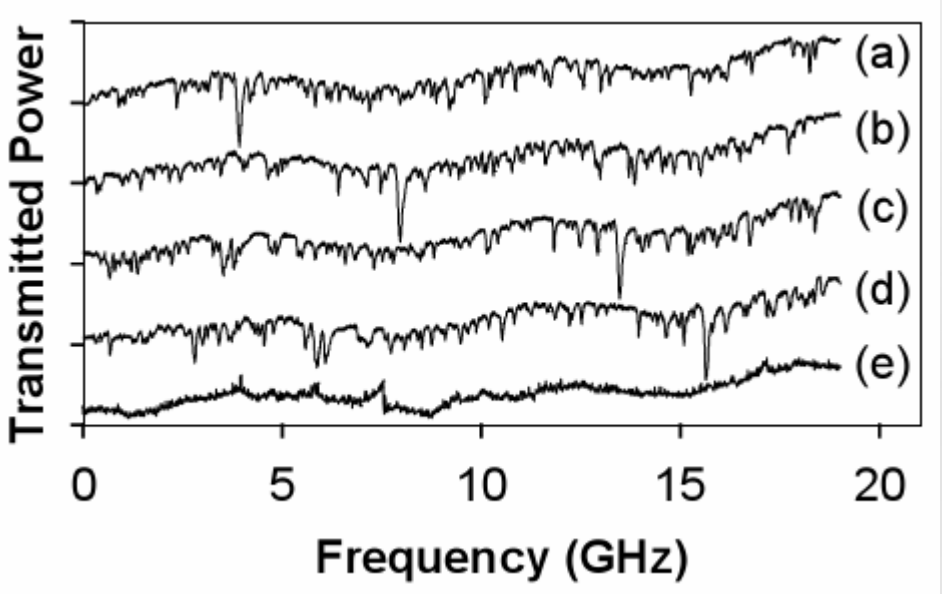

Transmission spectra of unlock and lock WGMs

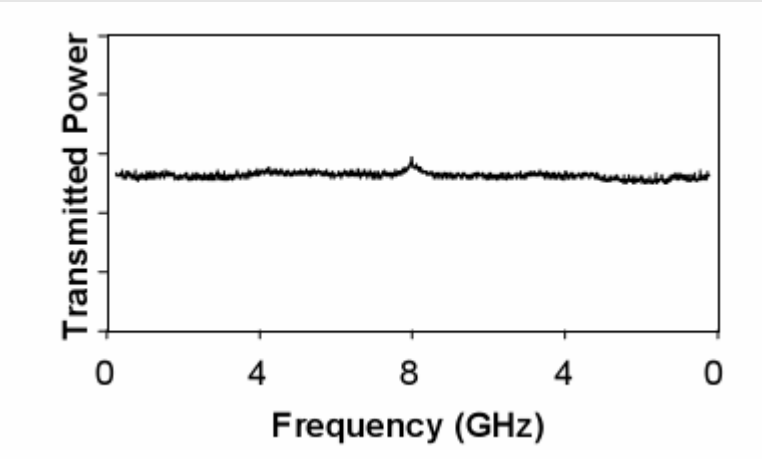

Opt. Exp. 2001

So WG microcavity may be a good candidate for frequency reference

Please refer to a review paper written by A. Savchenkov if interested!

J. Opt. Soc. Am. B/Vol. 24, No. 6/June 2007 Matsko et al.

Passive WGM: Sensor

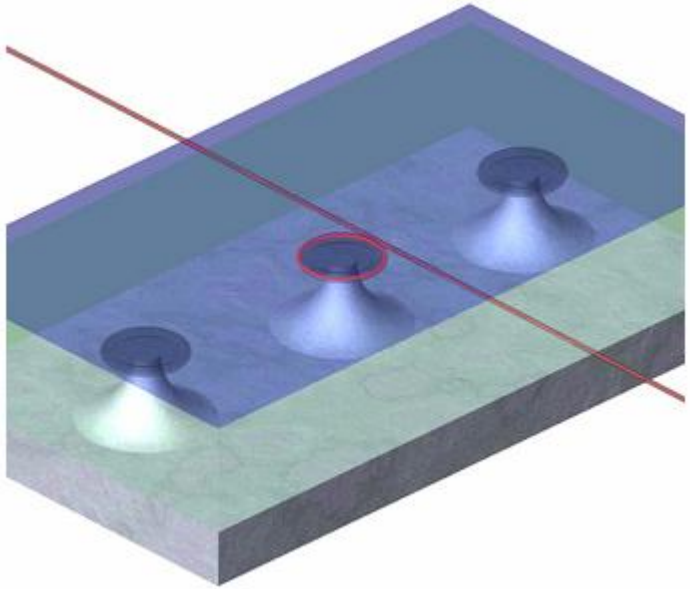

The ultra-high-Q silica microtoroid is coupled to the fiber taper waveguide. After being immersed in either H2OorD2O, a coverslip is placed on top.

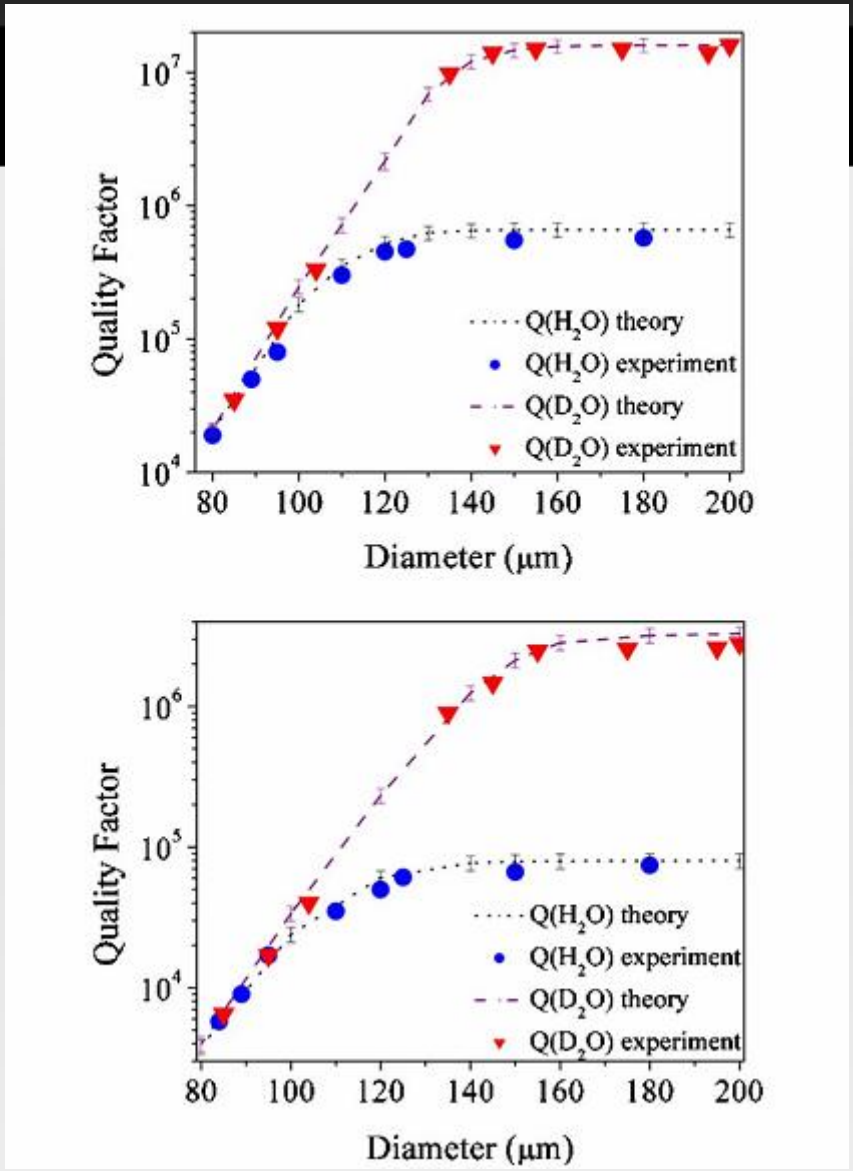

APL 87 151118, 2005

Chemical sensor

Passive WGM: Single Particle Detection

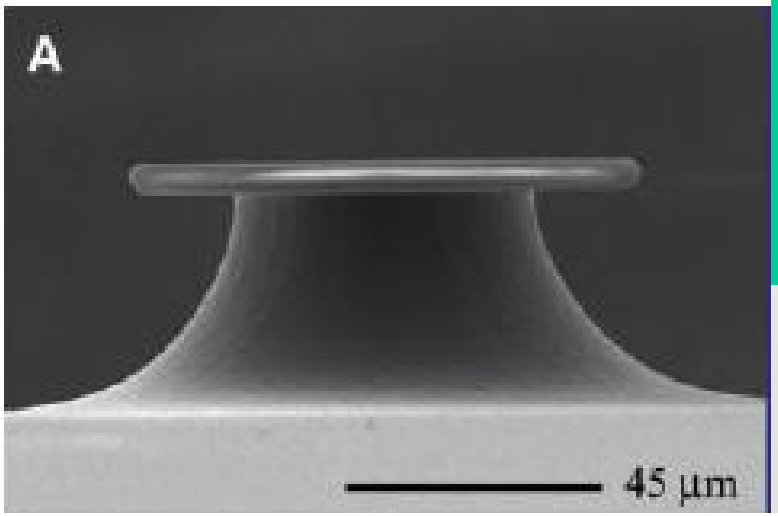

Label-Free, Single-Molecule Detection with Optical Microcavities

SCIENCE VOL 317 10 AUGUST 2007

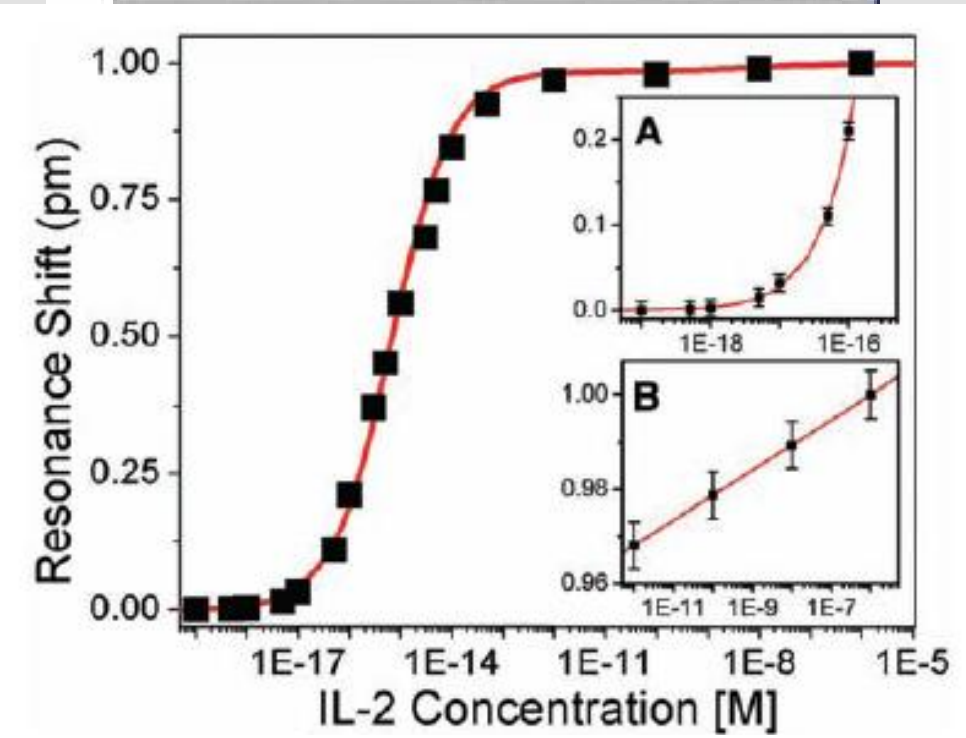

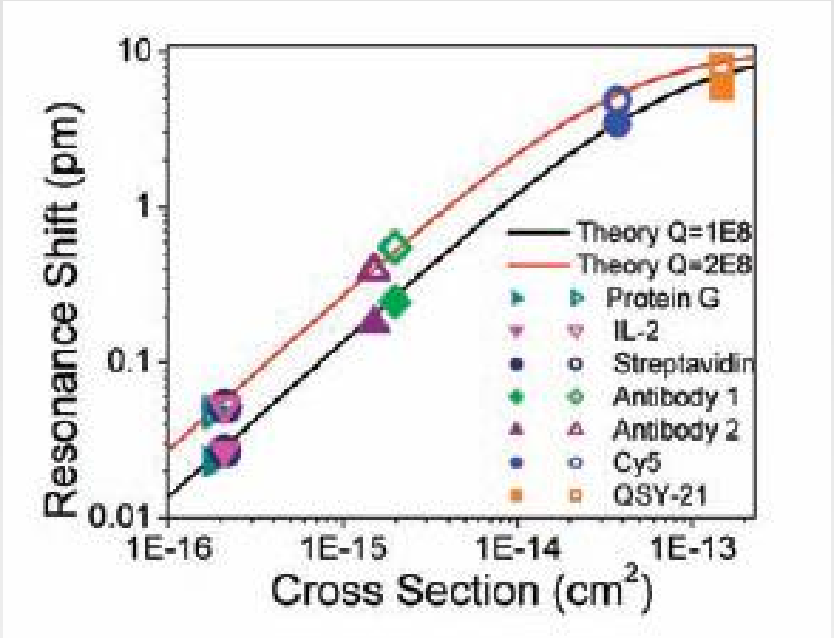

Sensor for nanopaticles

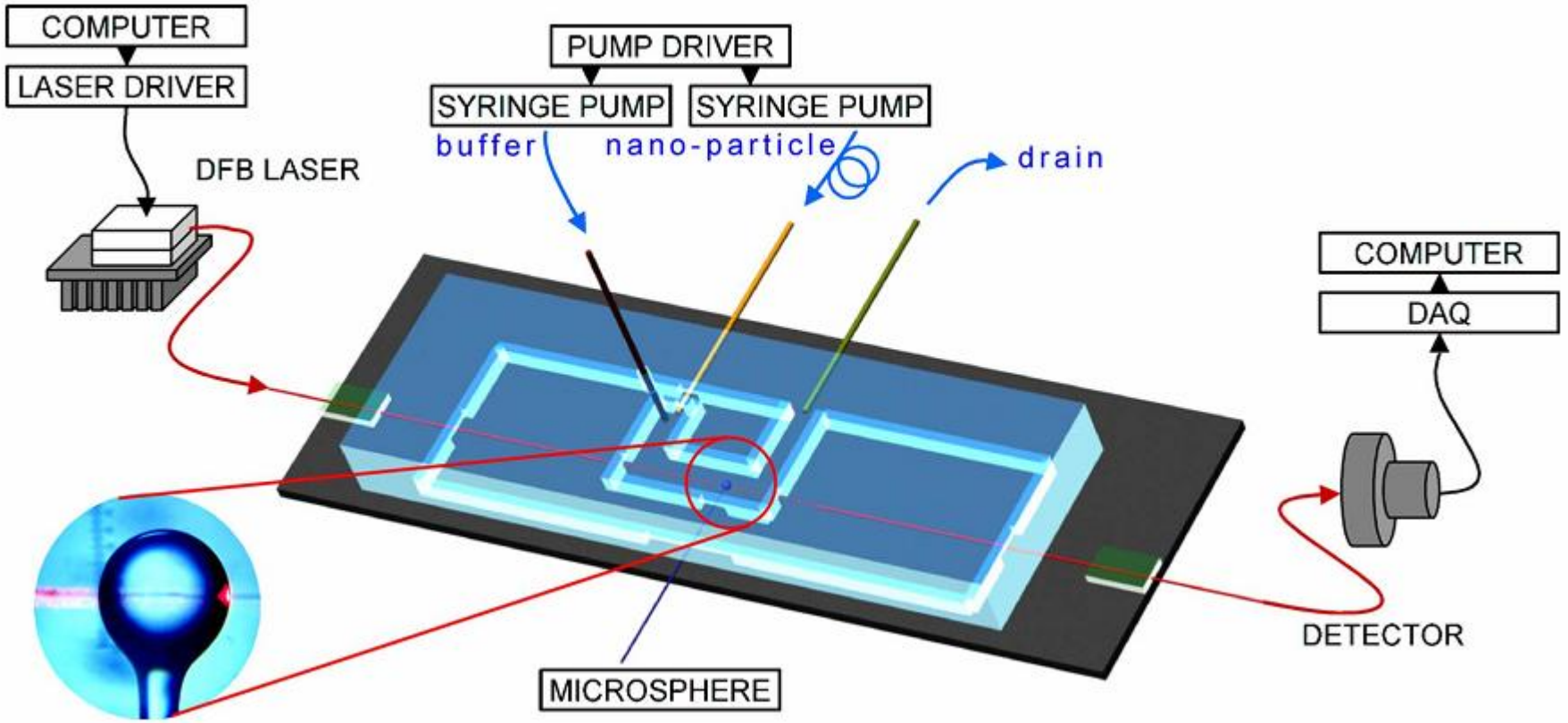

Microfluidic system incorporating a microsphere resonator and a coupling fiber.

APL 91, 103902, 2007

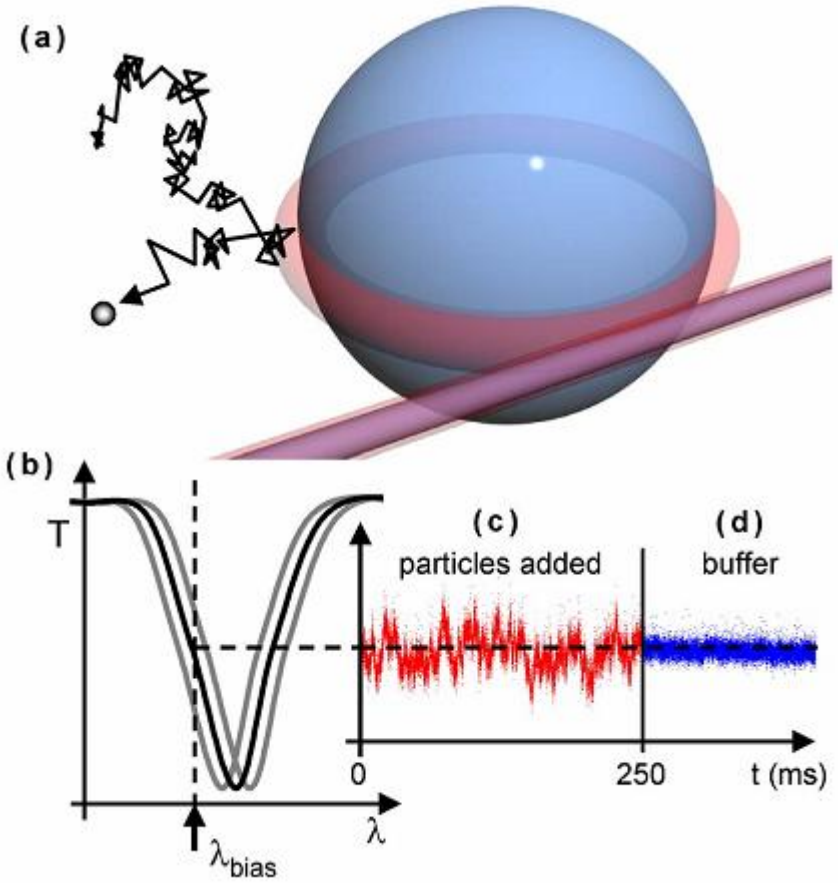

Measurement principle

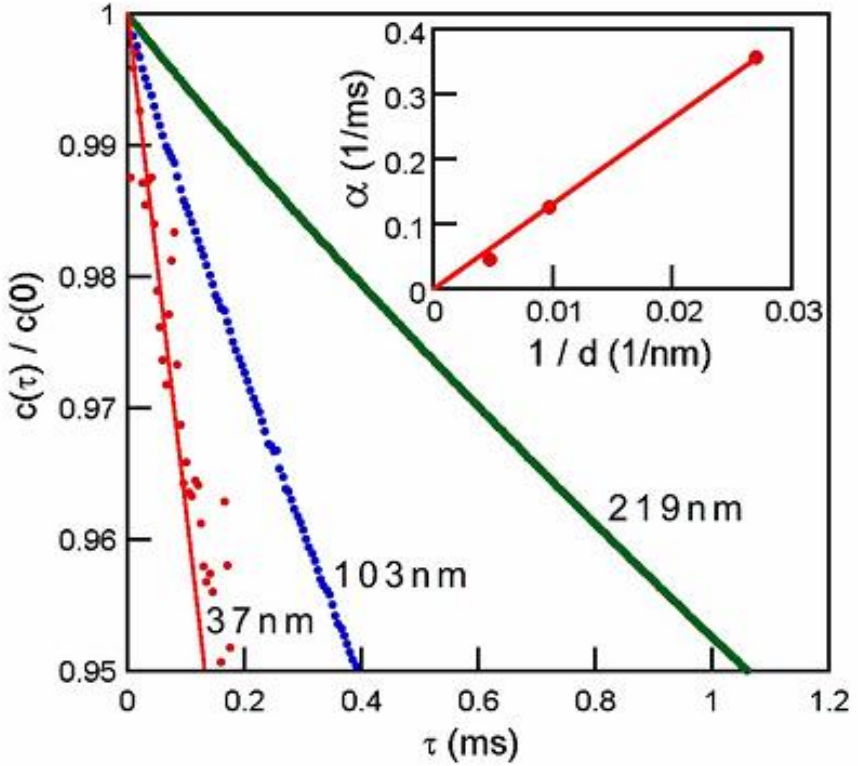

Normalized autocorrelation of resonance wavelength fluctuations for several particle diameters.

Sensor for living things

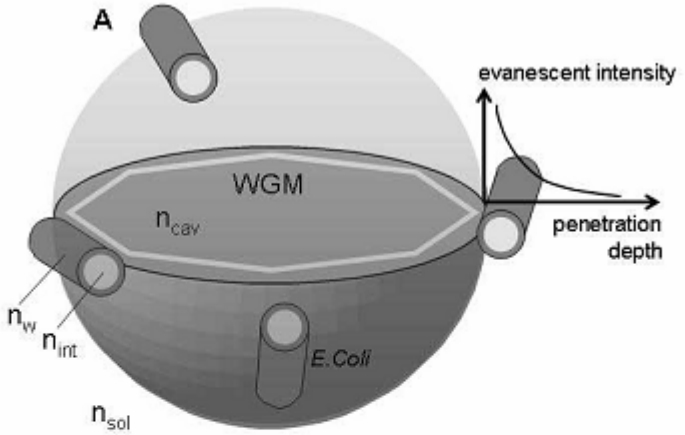

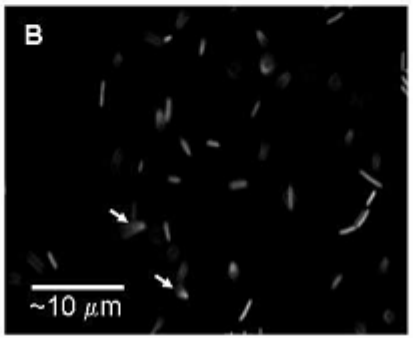

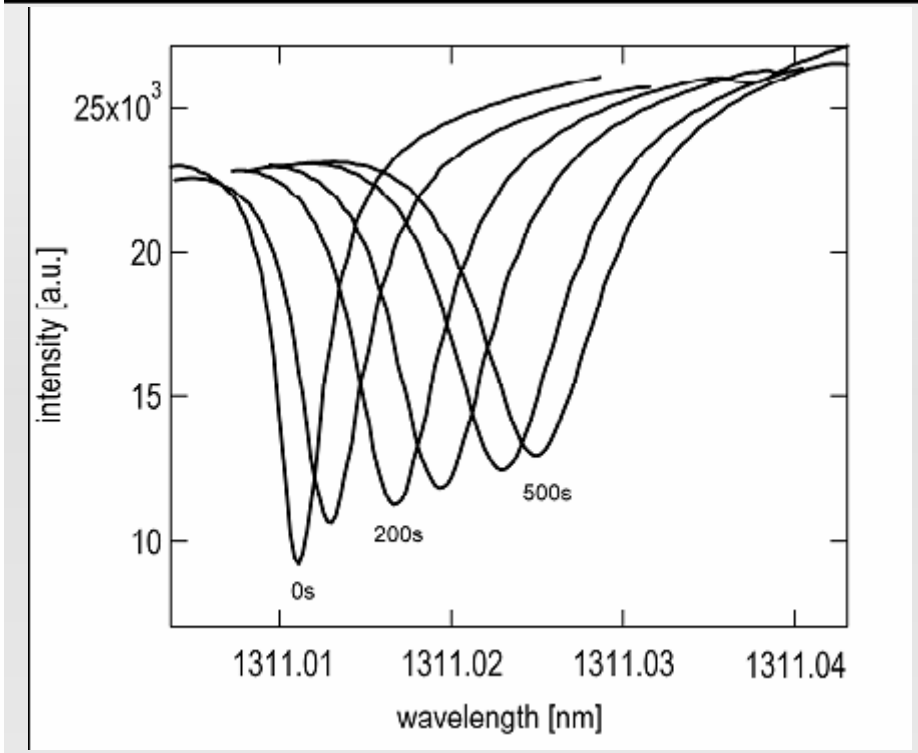

Microsphere for detection of bacteria.

Opt. Exp. Vol. 15 no. 25 , 2007

Shift of resonance wavelength and broadening of linewidth of a WGM due to adsorption of E.coli bacteria. The spectra were recorded in 100 s intervals. In parallel, bacteria surface densities where determined from optical micrographs.

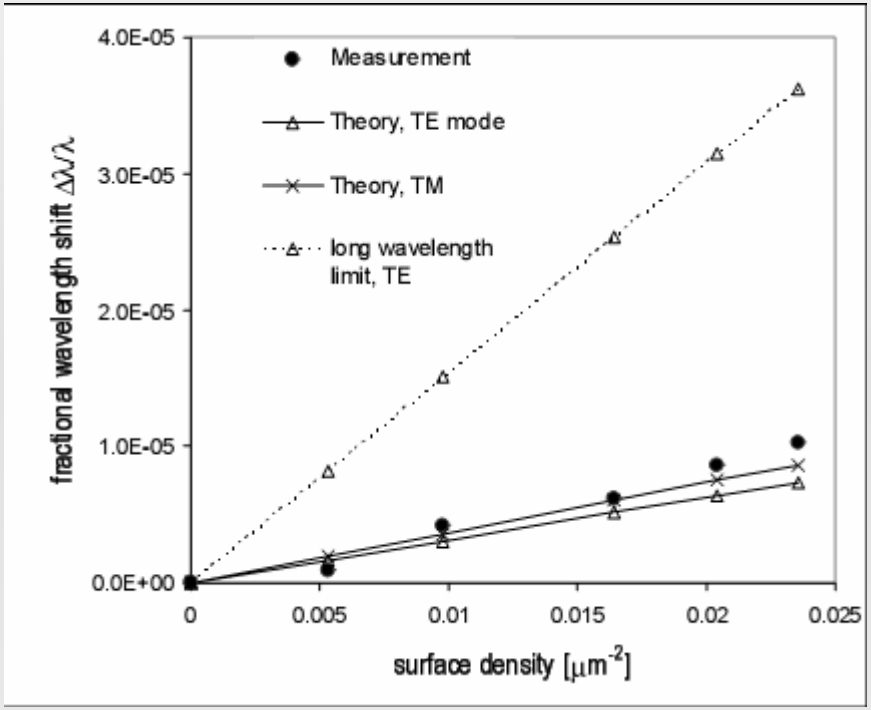

linear relationship between measured fractional wavelength shift and surface density of adsorbed E.coli bacteria (data points).

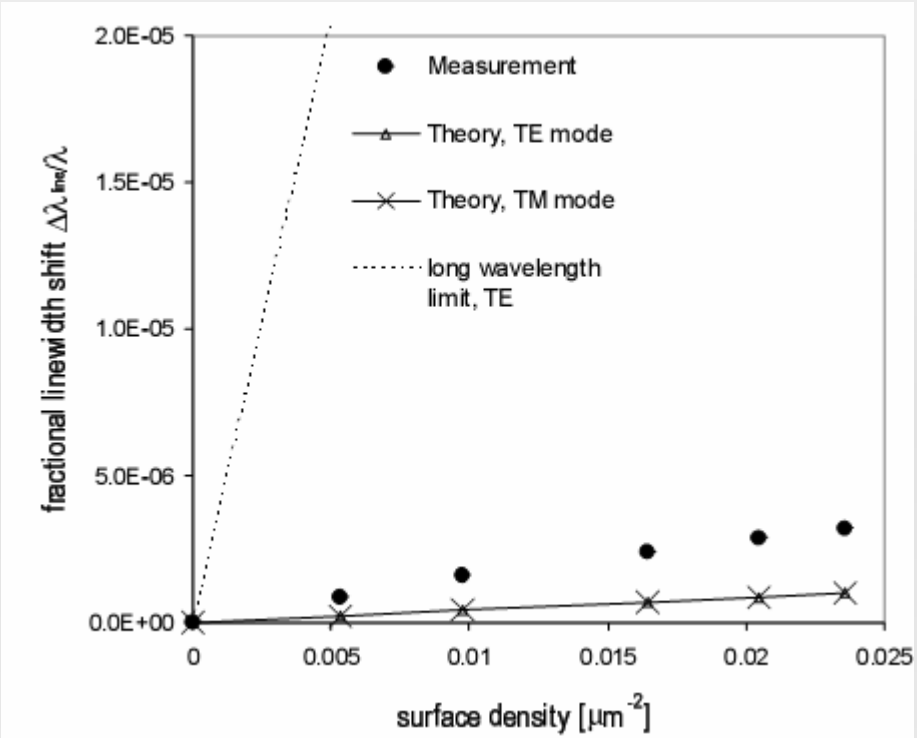

Measured fractional linewidth shift versus E.coli surface density

$$\frac{\delta\lambda}{\lambda} \approx \frac{A_{fp}\sigma_b L}{(n_{cav}^2 - n_{sol}^2)R}\left[(1-e^{-t/L})\left(n_w^2 - n_{sol}^2\right) + e^{-t/L}\left(n_{\text{int}}^2 - n_{sol}^2\right)\right]$$

$$\Gamma = \frac{16\pi^3\sigma\left[\Delta\varepsilon v + (\Delta\varepsilon' - \Delta\varepsilon)v'\right]^2}{3n_{\text{sol.}}(n_{\text{cav}}^2 - n_{\text{sol}}^2)\lambda^4 R}\rho\eta$$

Mechanical Sensor

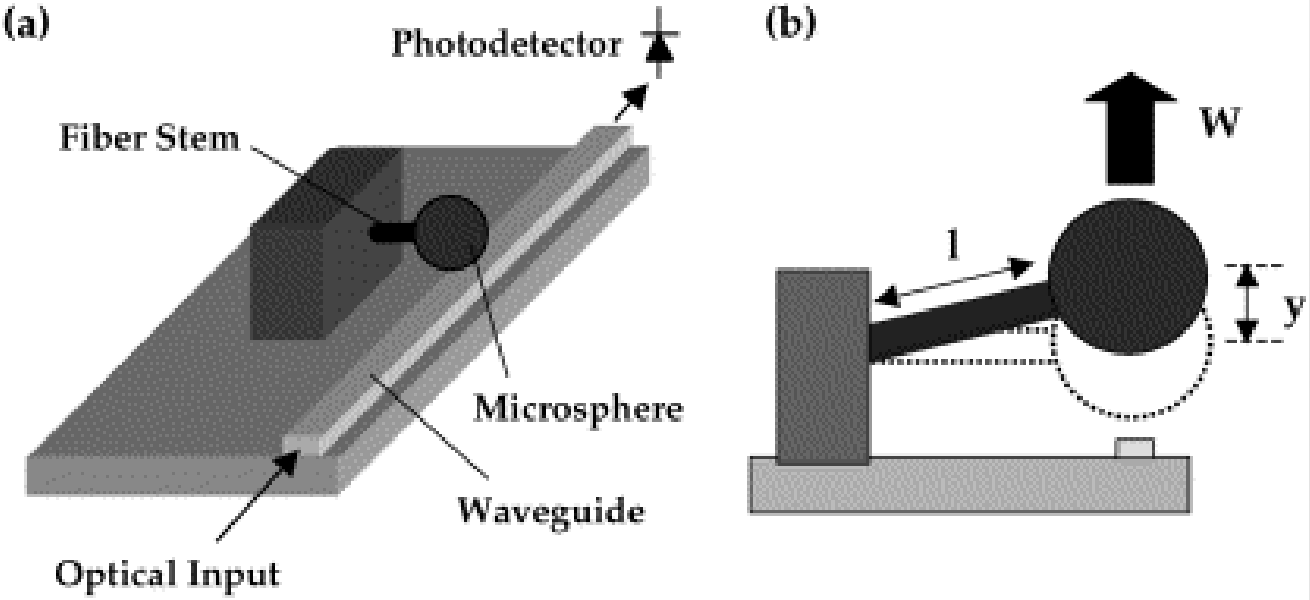

Microsphere resonator, flexure stem, and SPARROW waveguide configuration

$$Q_r(d) = 102\left(\frac{r}{\lambda}\right)^{5/2}\frac{n^3(n^2-1)}{4q-1}e^{2\gamma a}$$

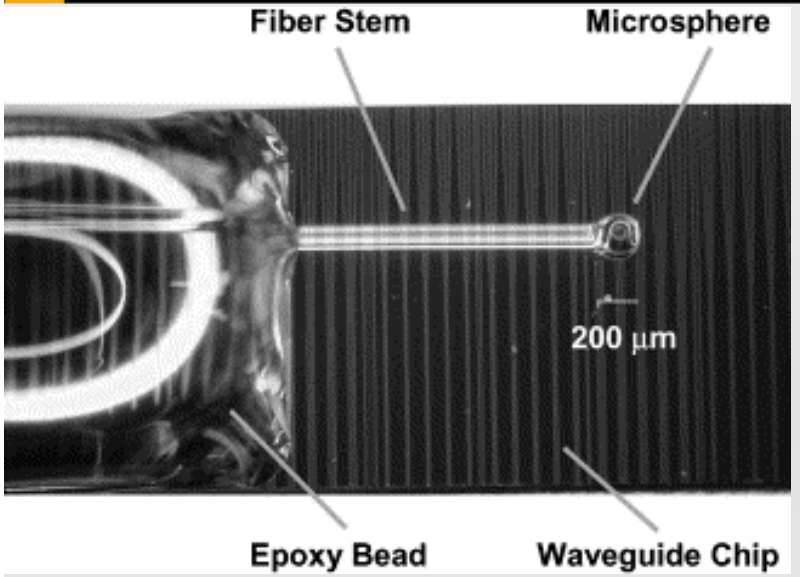

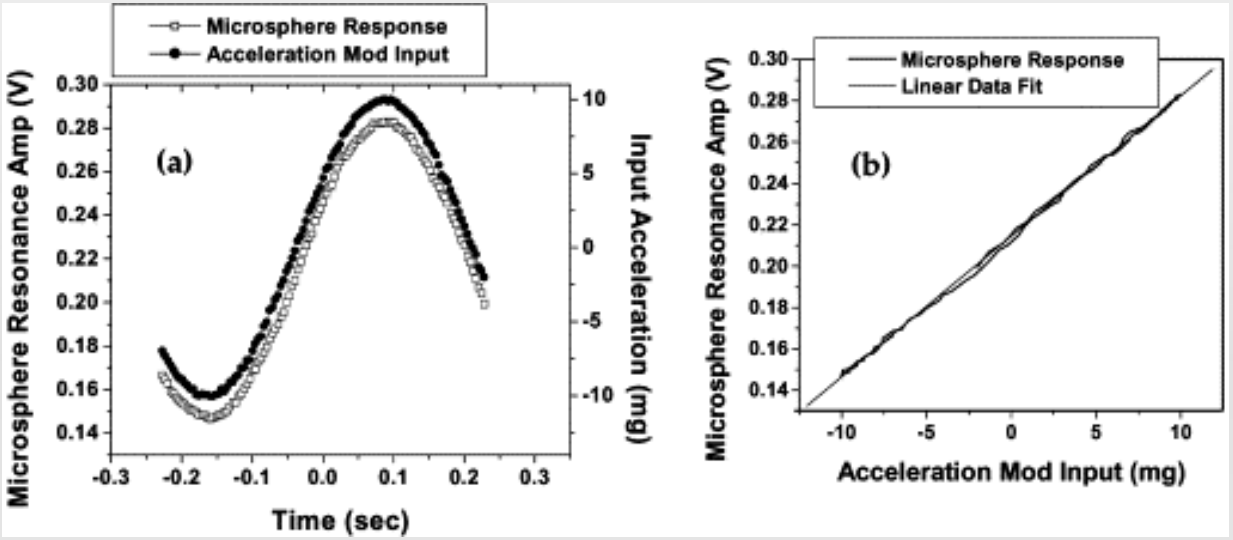

(a) Plots of microsphere-resonance amplitude and input acceleration as a function of time, (b) plot of resonance amplitude as a function of input acceleration. Acceleration of 1mg at 250Hz bandwidth can be measured with a noise of 100ug.

Passive WGM: gyroscope

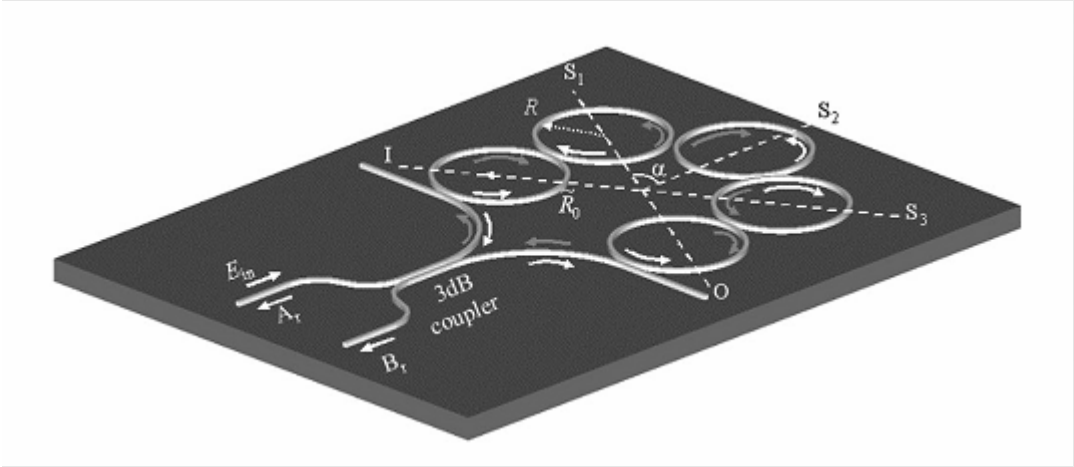

Schematic of the coupled-resonator slow-light rotation sensor.

PHYSICAL REVIEW LETTERS Volume: **96** Issue: **5**

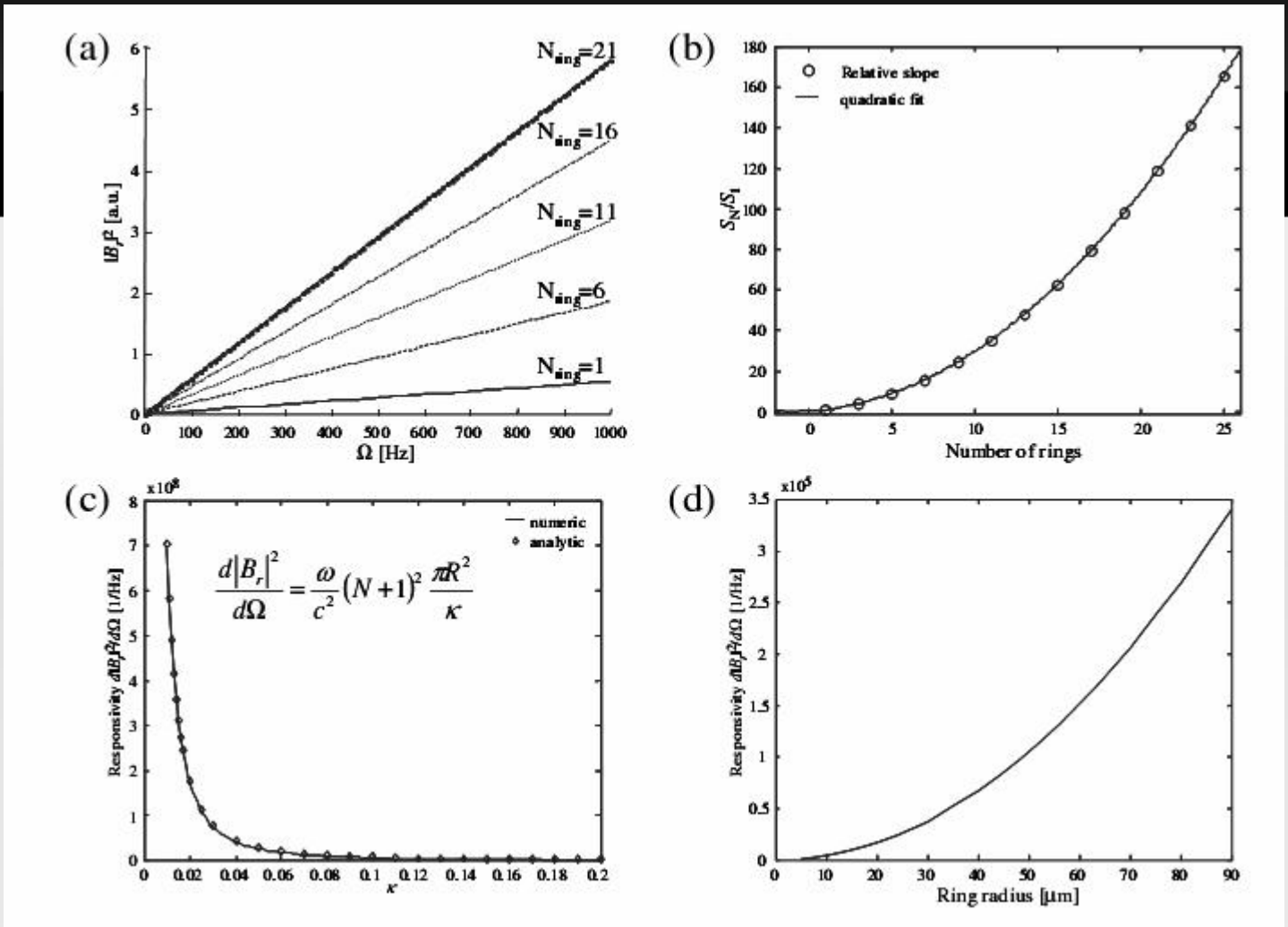

(a) Output signal intensity as a function of the structure angular velocity for various numbers of rings, R=25um (b) Dependence of the relative sensitivity on the number of microrings, R=25um Dependence of the sensitivity on:(c) the coupling coefficient (R=25um, N=9) and on (d) the microrings' radius (N=9, 0:01).

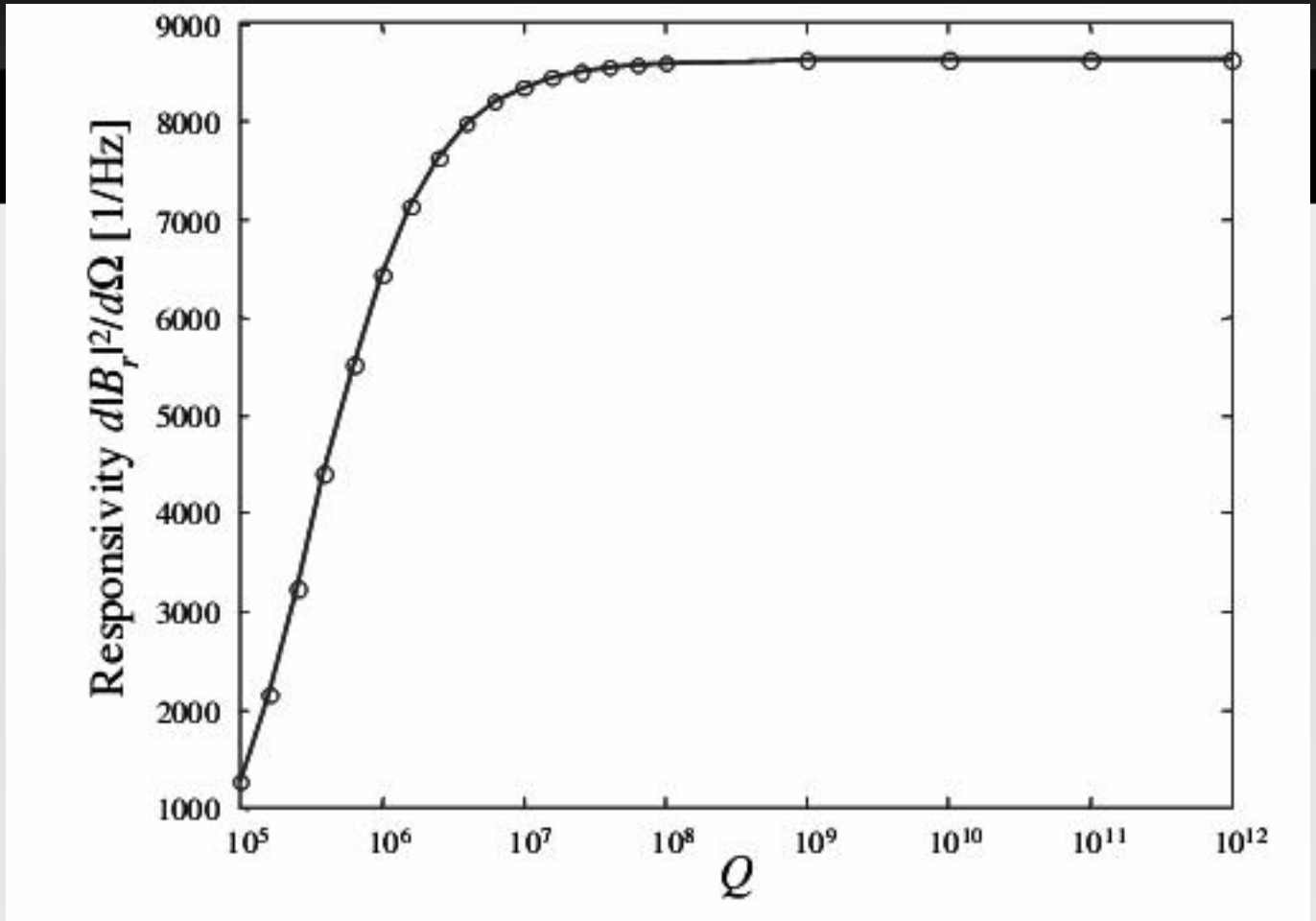

The impact of the quality factor onthe sensitivity.

“Slow Light”

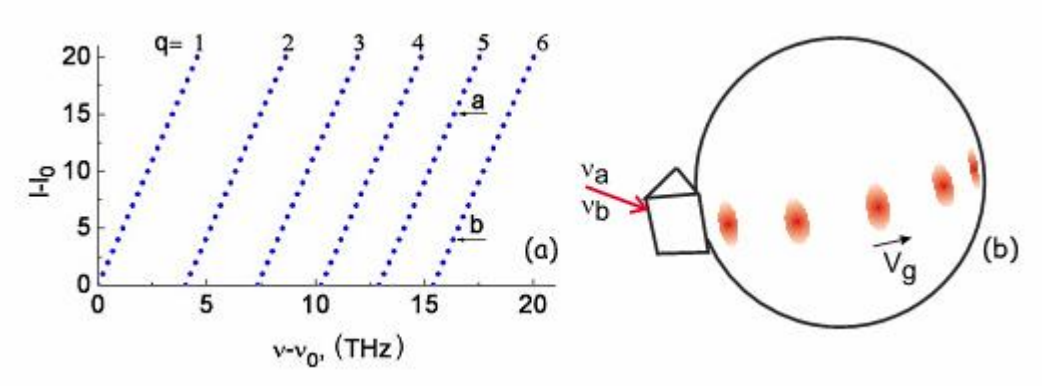

Principle of stopping light

$$P \simeq P(\theta)[1 + \cos(\Delta\omega_{ab}t - \Delta m_{ab}\phi)],$$

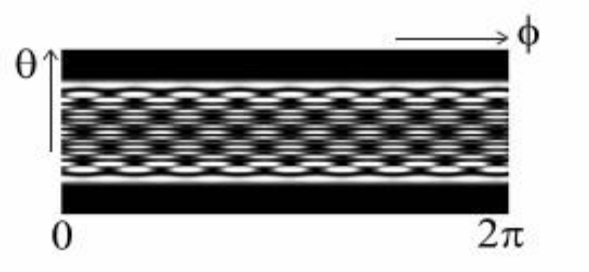

Theoretical model

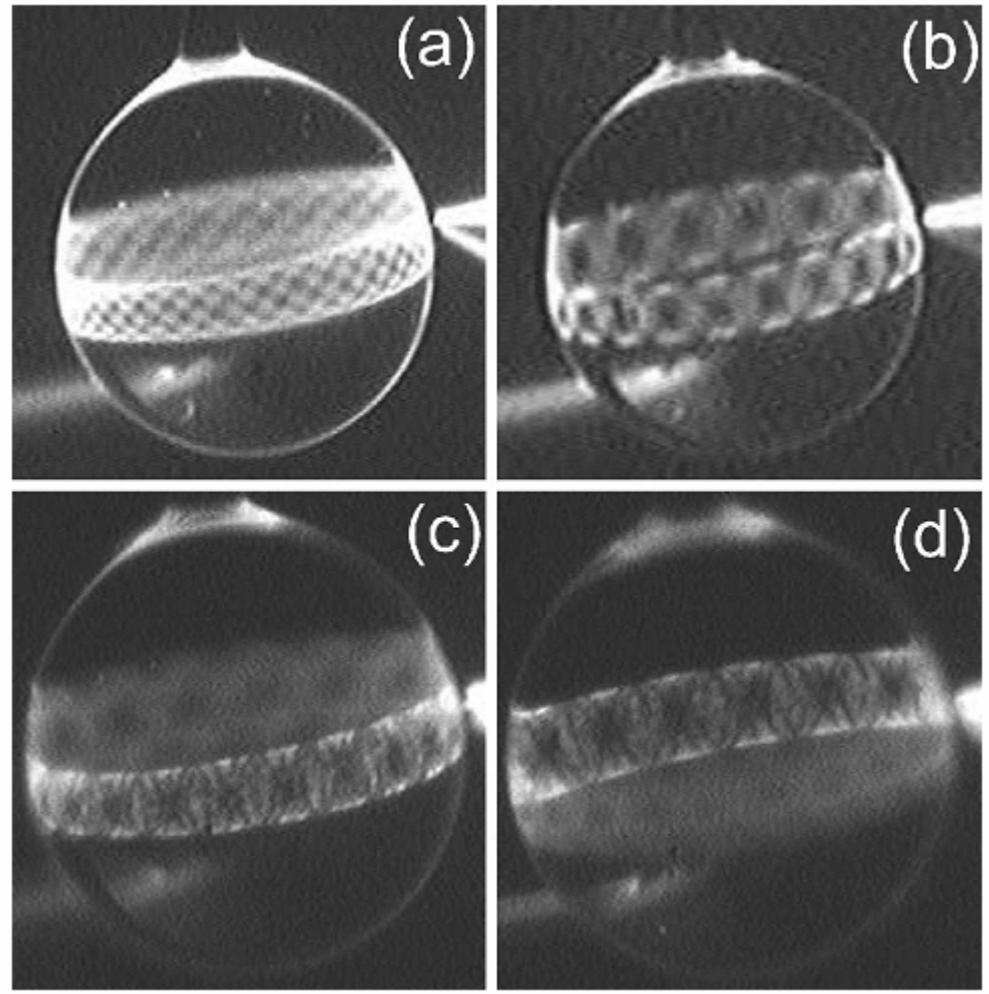

Interference patterns on surface

PRA 76, 023816, 2007

Also found in Micro toroids

PRL 100, 103905 (2008)

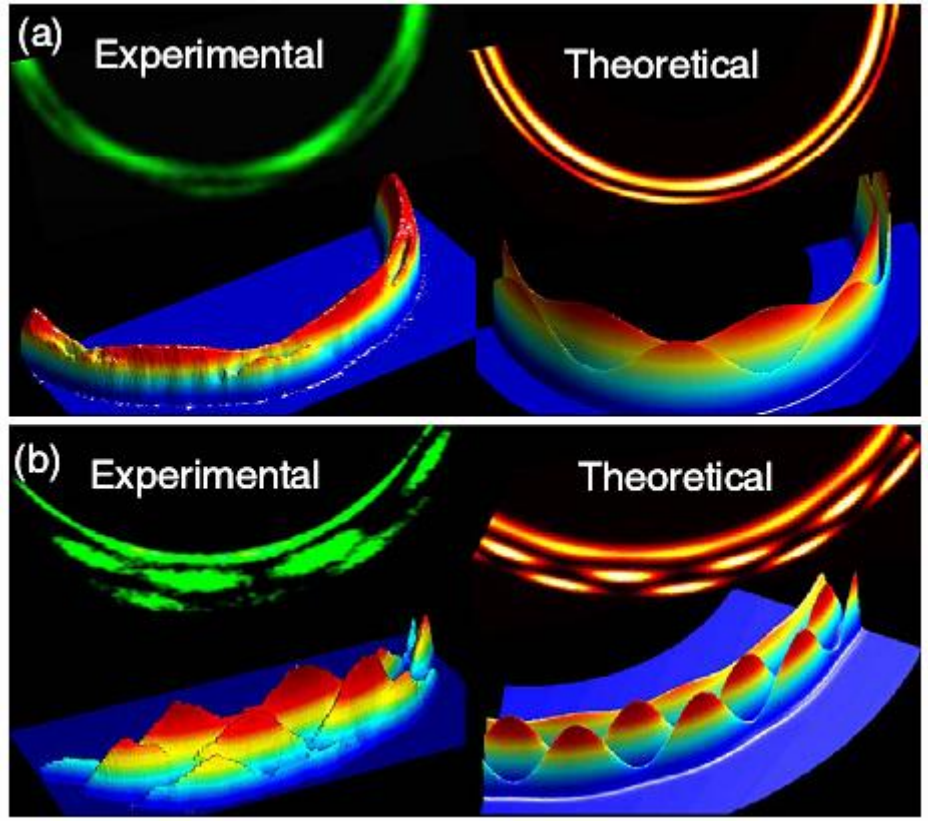

Crossed modes with azimuthal as well as radial profiles.

Summary

- Biosensor
- Gyroscope based on slow light microresonator
- Frequency Reference

Active WGM: Nonlinear Effect

- Raman Scattering
- Kerr Nonlinearity
- Parametric Oscillation
- Frequency Double
- Photorefractive Effect

Active WGM: Raman Effect

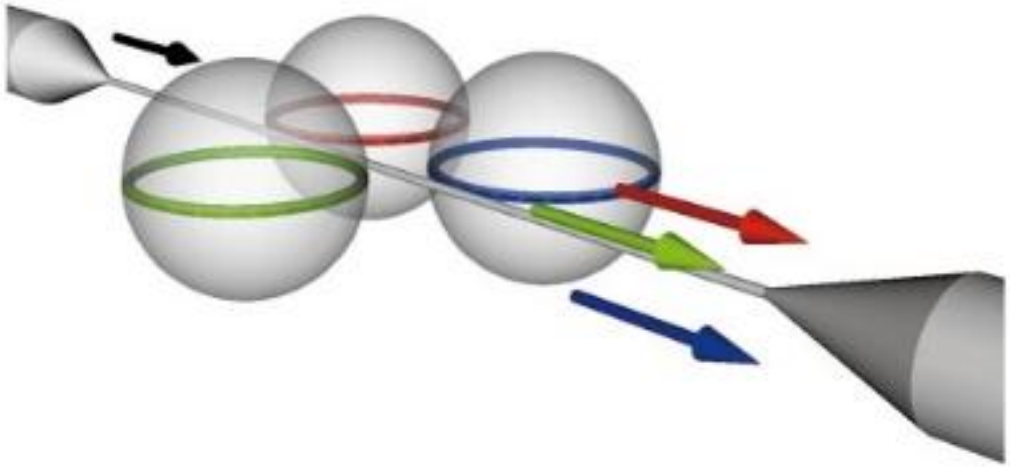

Nature 415, 7, 2002

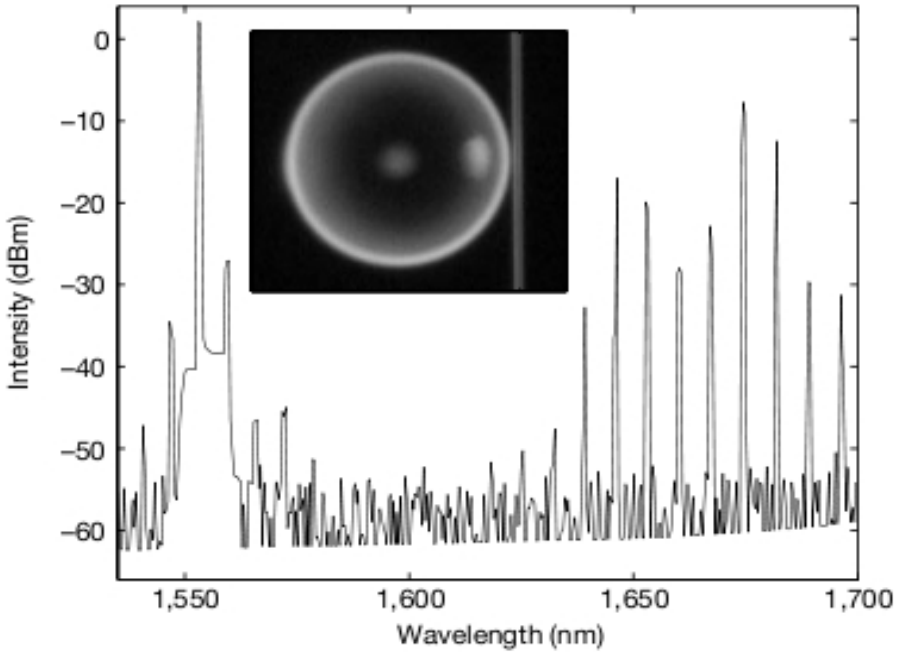

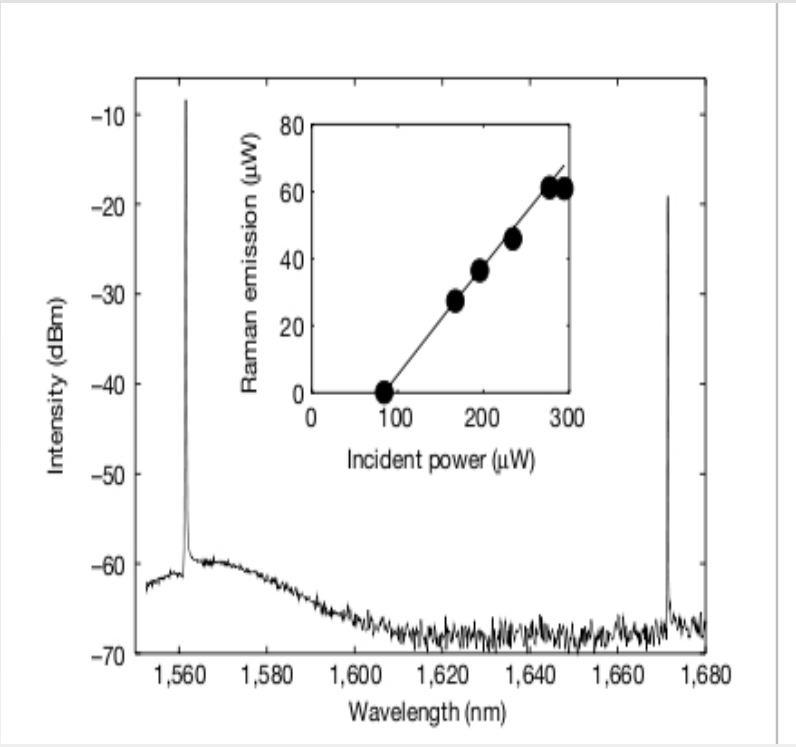

Figure 2 Spectrum of a 70-μm-diameter Raman microsphere laser with pump powers of 2 mW. The pump is at 1,555 nm. Peaks located around 1,670 nm are Raman oscillations, separated by the free spectral range of the microsphere. Secondary lines around 1,555 nm are due to four-wave mixing between the pump and two Raman waves. Inset, a microsphere coupled to a fibre taper.

$$P_{\text{threshold}} \quad \frac{\pi^2 n^2}{\lambda_P \lambda_R} \frac{V_{\text{eff}}}{\Gamma B g} Q_e^P \quad \frac{1}{Q_T^P} \quad ^2 \frac{1}{Q_T^R}$$

Application: Cascade Raman Laser

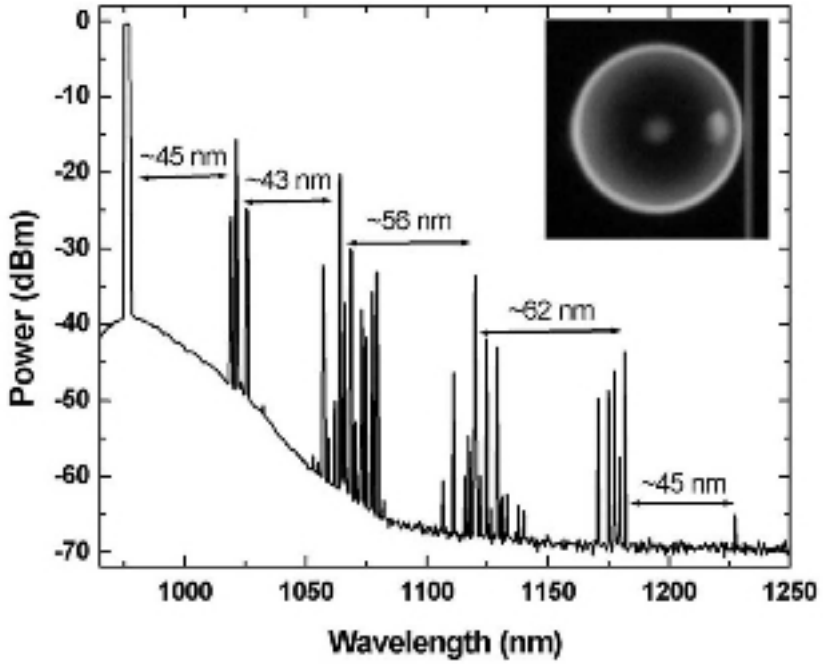

Fig. 1. Typical emission spectrum of the microsphere cascaded Raman laser. The pump wavelength is at 976.08 nm. Inset: optical micrograph of a microsphere taper system used in the experiment.

Opt. Lett. 28, 17, 2003

$$P_{\text{th}} = \frac{\pi^2 n^2}{\lambda_0 \lambda_1} \frac{V_{\text{eff}}}{g_R B} \left(\sum_{k=0}^{N/2} \frac{1}{Q_{t,N-2k}} \right)^2 \times \sum_{k=1}^{N/2} \frac{Q_{e,0}}{Q_{t,N-(2k-1)}} \qquad (N \text{ even}),$$

$$P_{\text{th}} = \frac{\pi^2 n^2}{\lambda_0 \lambda_1} \frac{V_{\text{eff}}}{g_R B} \left(\sum_{k=1}^{(N+1)/2} \frac{1}{Q_{t,N-(2k-1)}} \right)^2 \times \sum_{k=0}^{(N-1)/2} \frac{Q_{e,0}}{Q_{t,N-2k}} \qquad (N \text{ odd}),$$

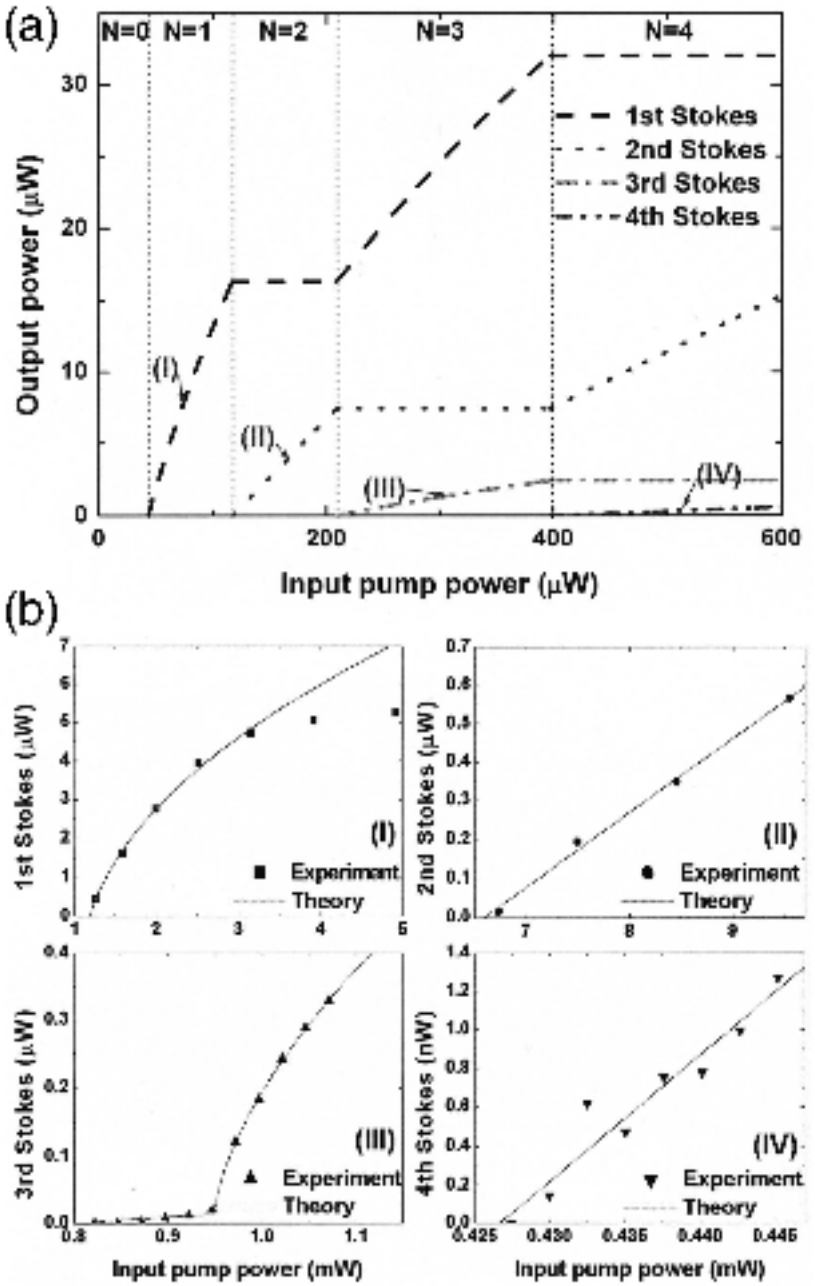

Silicon Cascade microring Raman Laser

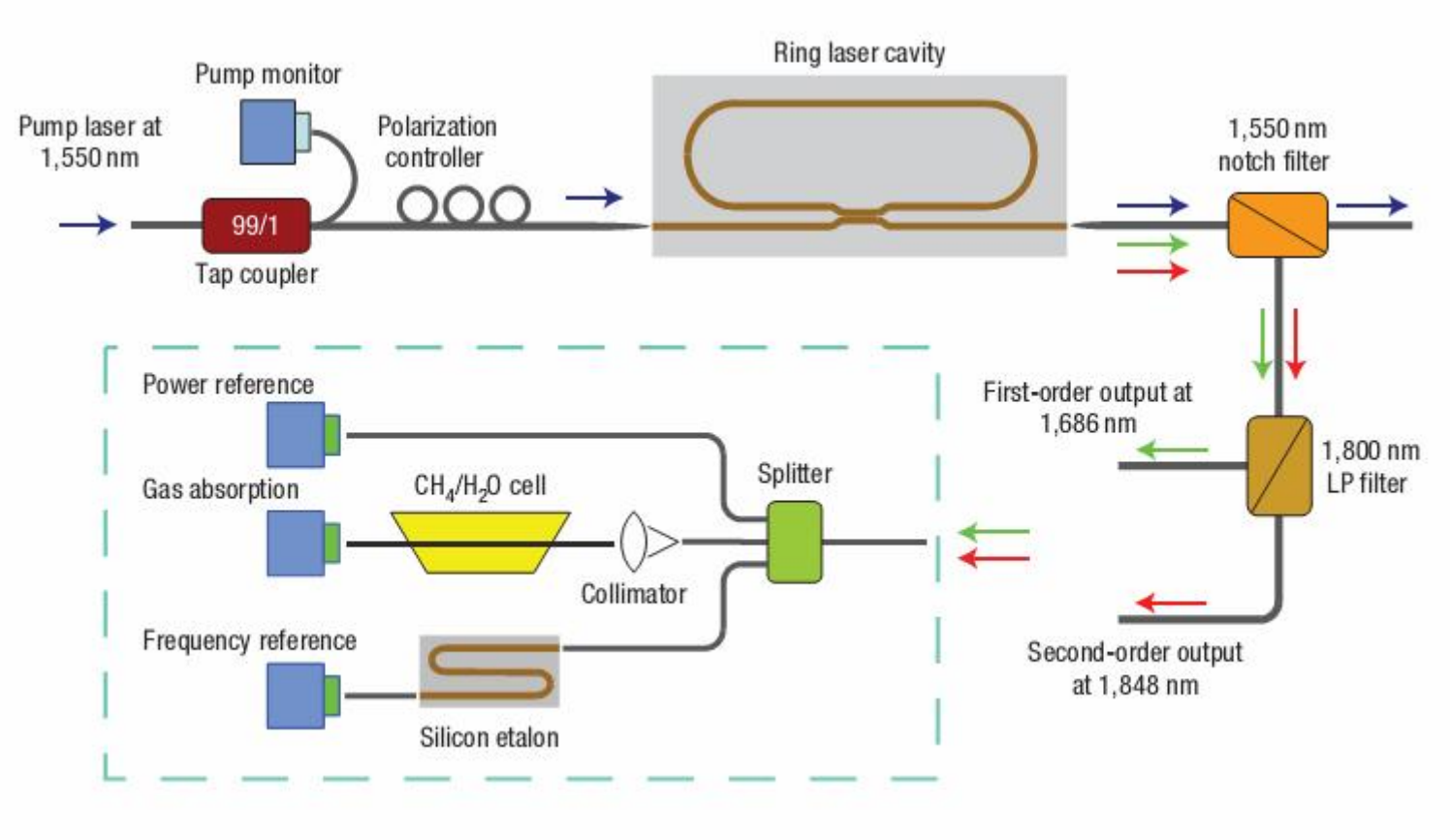

Nature Photonics Vol.2 ,170, 2008

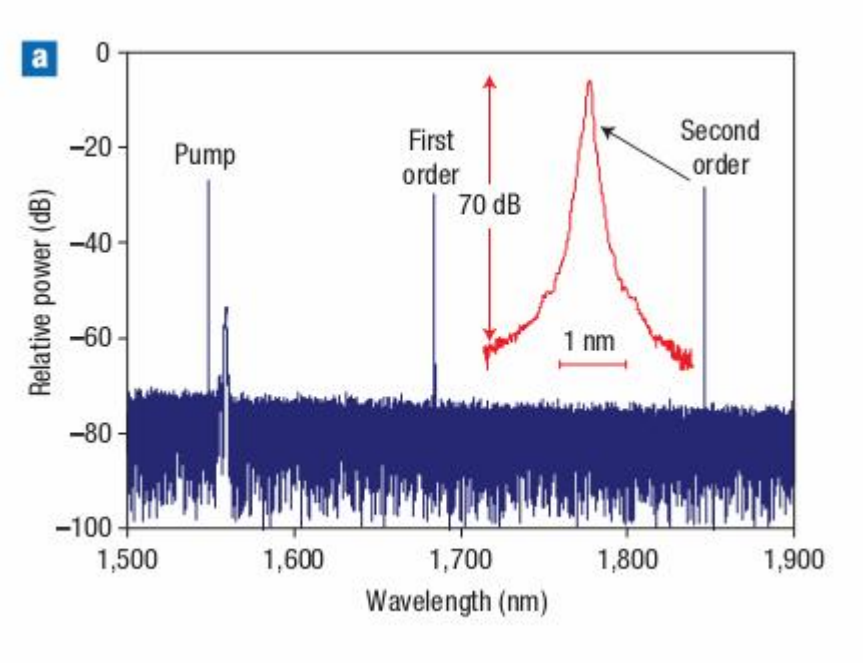

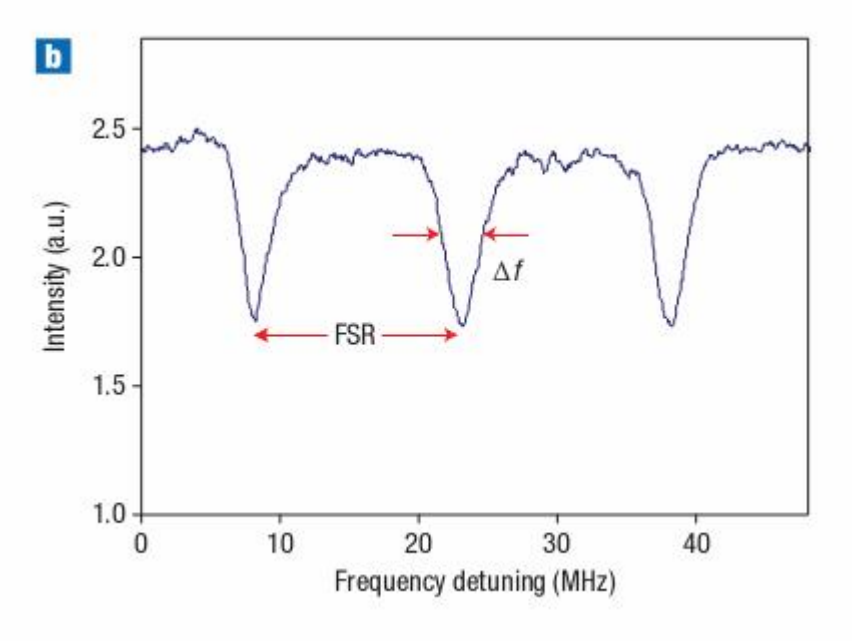

By using silicon instead of silica ,the laser wavelength extends to MID-IR, which is of great use in many fields But the cavity here needs improvements.

Active WGM: Kerr Nonlinearity, Parametric Oscillation

Stimulated Raman Scattering

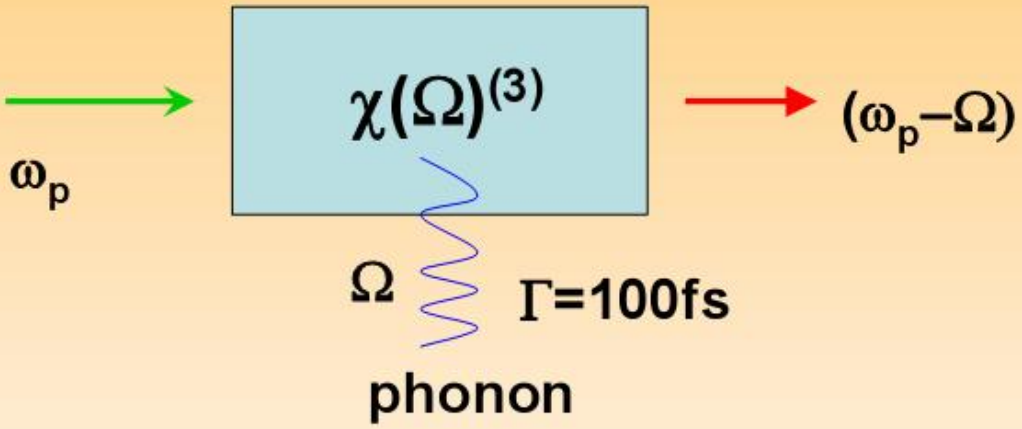

- Coupling to a dissipative phonon bath
- Phase insensitive amplification
- Intrinsically phase-matched process

Parametric Interactions

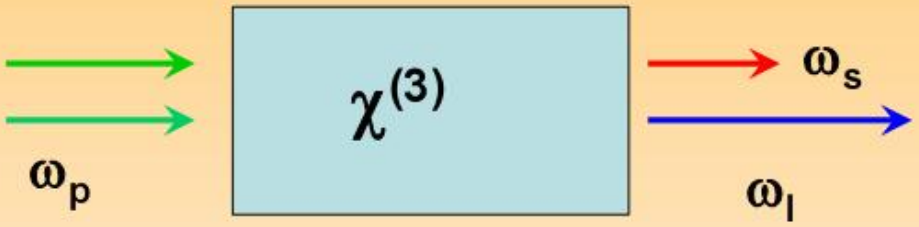

$$n = n_0 + n_2 I$$

- Mediated by the Kerr-nonlinearity
- Energy conservation
- Momentum conservation
- Phase sensitive amplification

Competition of Raman and Parametric Oscillation

Parametric Oscillation Threshold

$$P_t^K = \frac{\omega_0^2 Q_0^{-2}(1+K)^2 + (\Delta\omega/2)^2}{2\gamma\Delta\omega\,(c/n_{eff})} \cdot \frac{\pi^2 R n_{eff}}{C(\Gamma)\lambda_0} \frac{1}{Q_0} \frac{(K+1)^2}{K}$$

Raman Oscillation threshold

$$P_t^R = \frac{\pi^2 n^2}{C(\Gamma) g_R \lambda_p \lambda_R} V_{eff} \cdot \left(\frac{1}{Q_0}\right)^2 \frac{(1+K)^3}{K}$$

⇒***Parametric Regime*** $P_{Param}(\Delta\omega,K) < P_{Raman}$

⇒***Raman Regime*** $P_{Param}(\Delta\omega,K) > P_{Raman}$

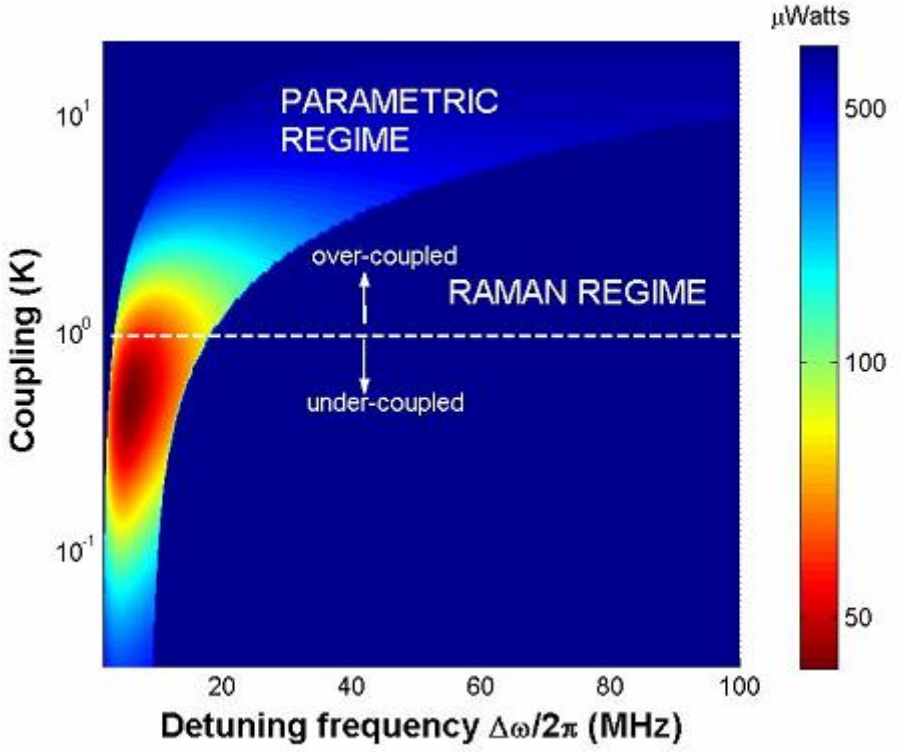

- Near Unity Signal to Idler ratio
- Up to 40uW of parametric power
- Kerr-Optical nonlinear effect in microcavity

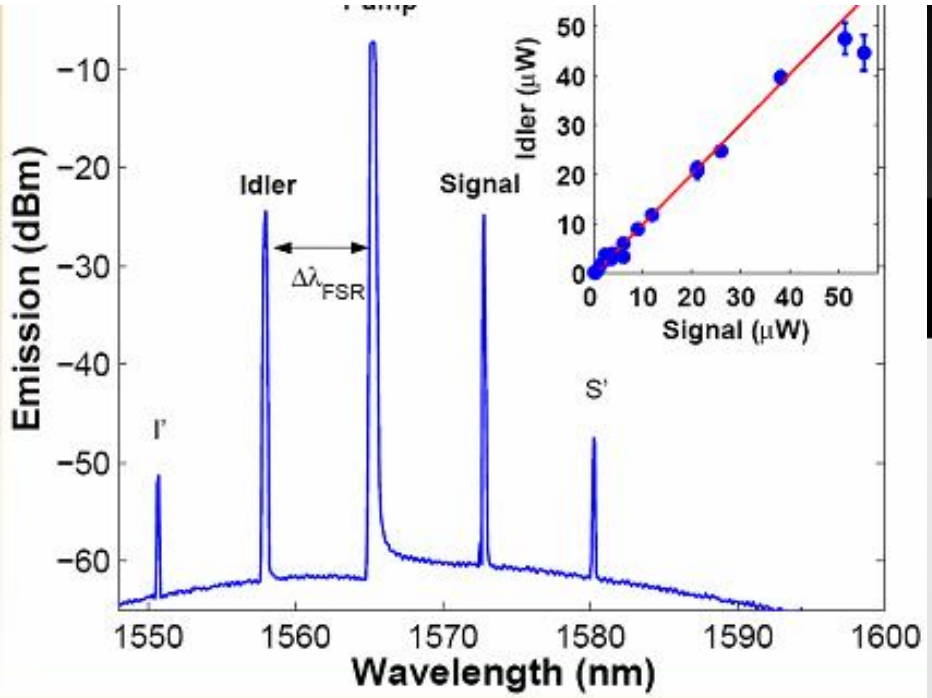

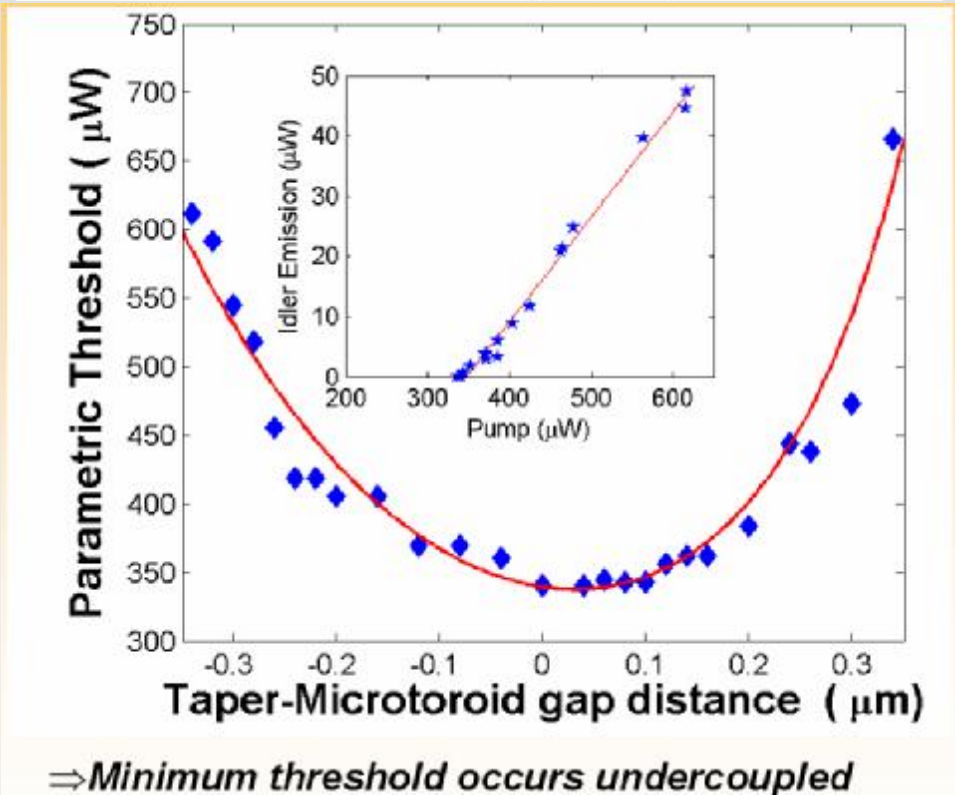

⇒*Minimum threshold occurs undercoupled*

Phys. Rev. Lett. 93, 083904 (2004)

Applications: Toroid of many colours

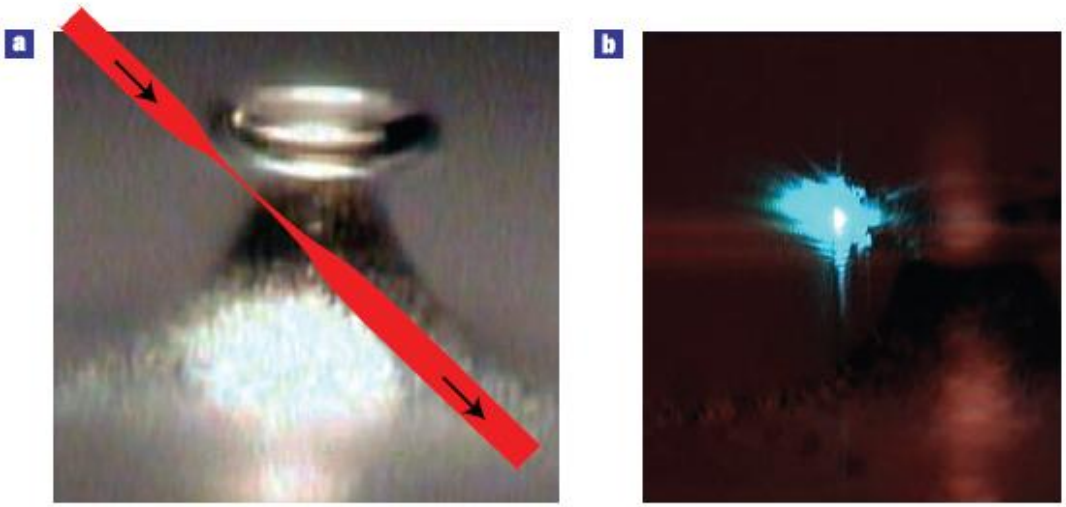

A demonstration of continuous sum-frequency generation of visible light in a microscopic silica resonator could provide a light source for on-chip silicon photonics and applications in the UV.

nature physics VOL 3 JUNE 2007

Application: Frequency Comb

Nature Vol. 450, 20, 2007

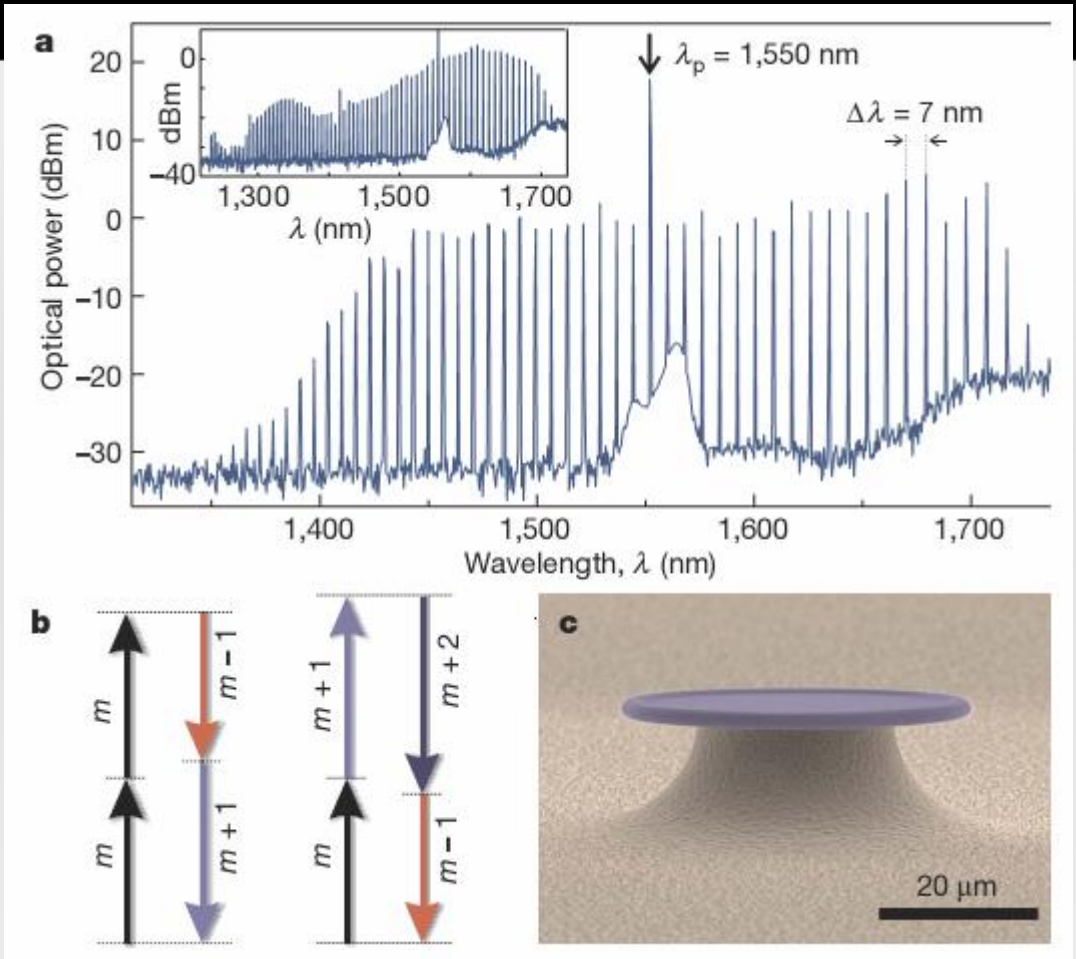

Broad band parametric frequency conversion from a monolithic toroidal microresonator.

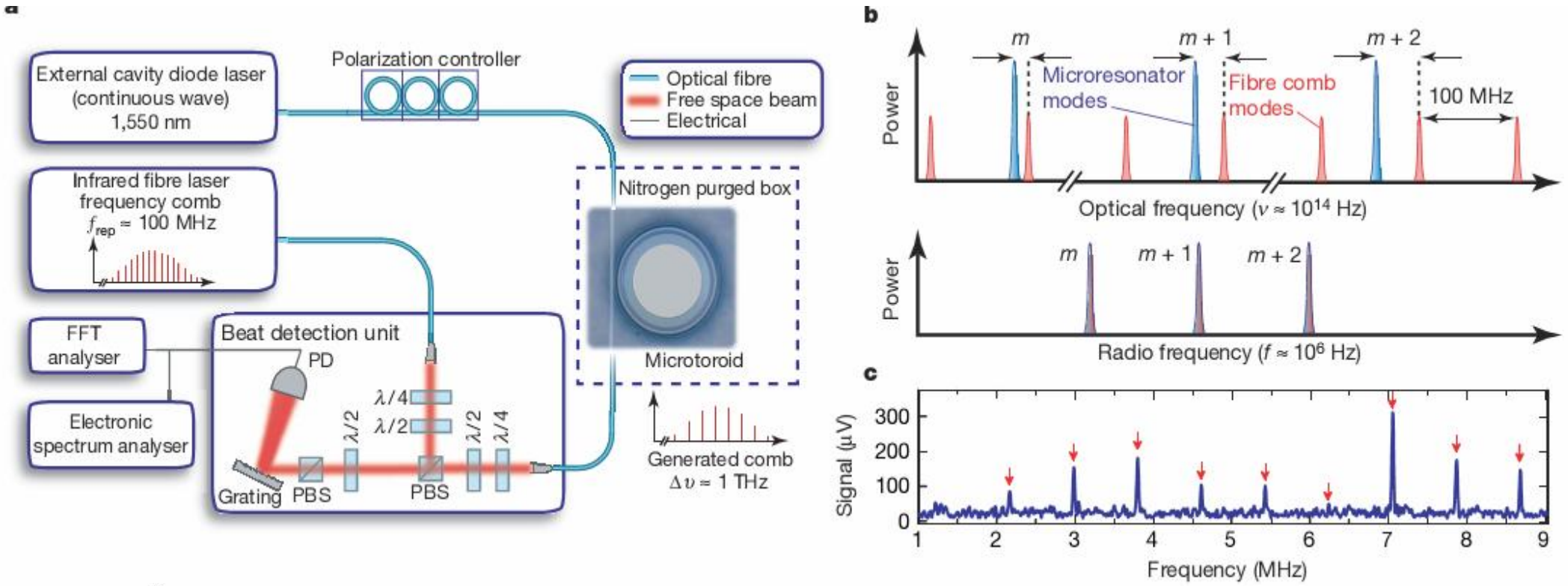
a
External cavity diode laser (continuous wave) 1,550 nm
Polarization controller
Optical fibre
Free space beam
Electrical
Infrared fibre laser frequency comb
f_{rep} ≈ 100 MHz
Nitrogen purged box
Microtoroid
FFT analyser
Beat detection unit
PD
λ/4
λ/2
λ/2
λ/2
λ/4
Electronic spectrum analyser
Grating
PBS
PBS
Generated comb
Δυ ≈ 1 THz
b
m
m + 1
m + 2
Microresonator modes
Fibre comb modes
100 MHz
Power
Optical frequency (ν ≈ 10^14 Hz)
Radio frequency (f ≈ 10^6 Hz)
c
Signal (μV)
Frequency (MHz)

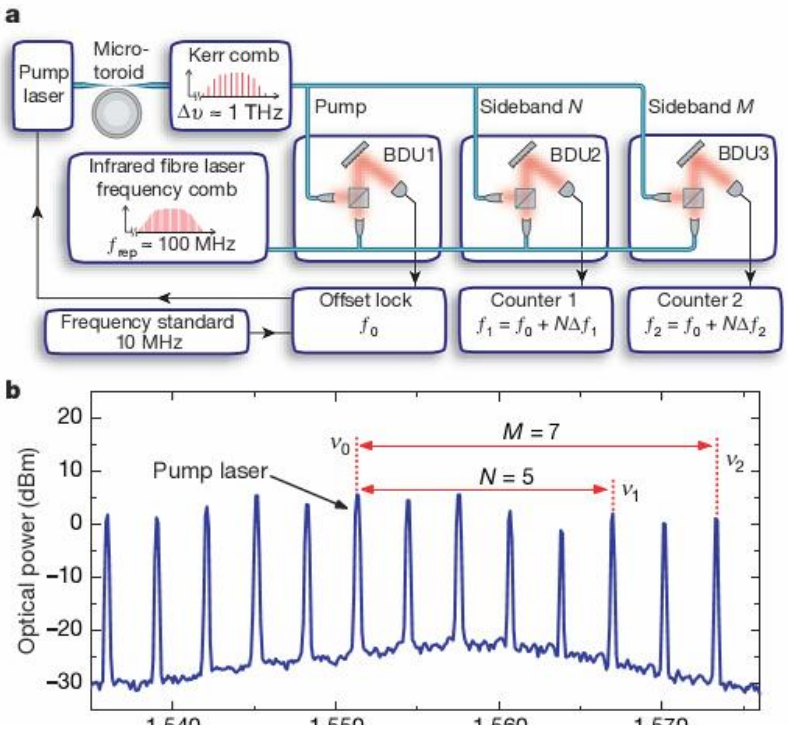
a
Pump laser
Micro-toroid
Kerr comb
Δυ = 1 THz
Pump
Sideband N
Sideband M
BDU1
BDU2
BDU3
Infrared fibre laser frequency comb
f_{rep} = 100 MHz
Offset lock
f_0
Counter 1
$f_1 = f_0 + N\Delta f_1$
Counter 2
$f_2 = f_0 + N\Delta f_2$
Frequency standard 10 MHz
b
Optical power (dBm)
Pump laser
ν_0
M = 7
N = 5
ν_1
ν_2

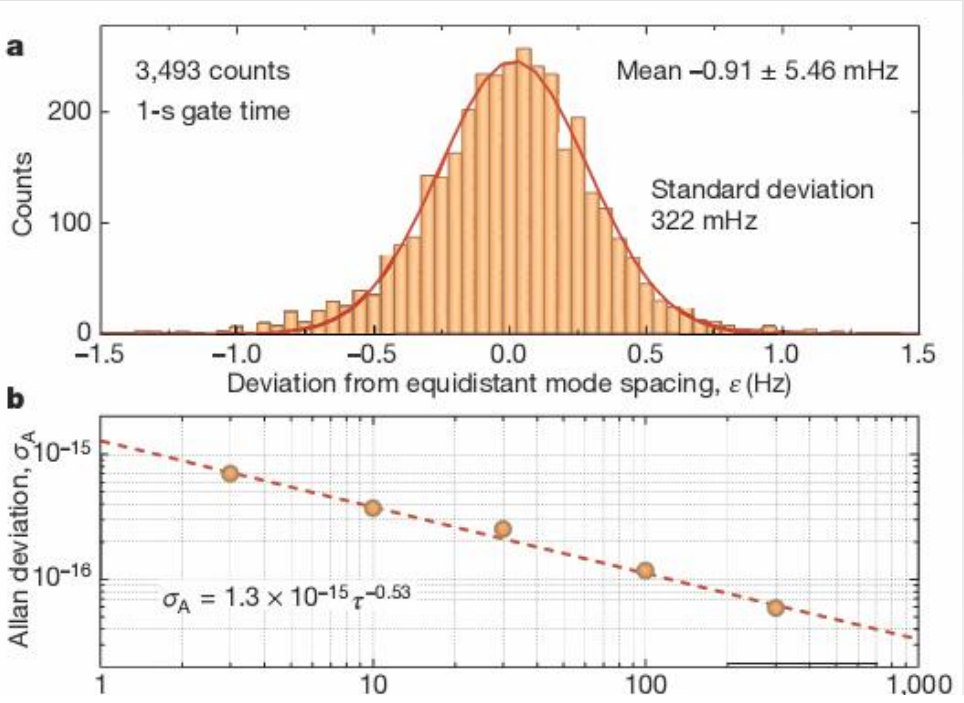
a
3,493 counts
1-s gate time
Mean –0.91 ± 5.46 mHz
Standard deviation 322 mHz
Counts
Deviation from equidistant mode spacing, ε (Hz)
b
Allan deviation, σ_A
$\sigma_A = 1.3 \times 10^{-15} \tau^{-0.53}$

Crystalline WGR: OPO

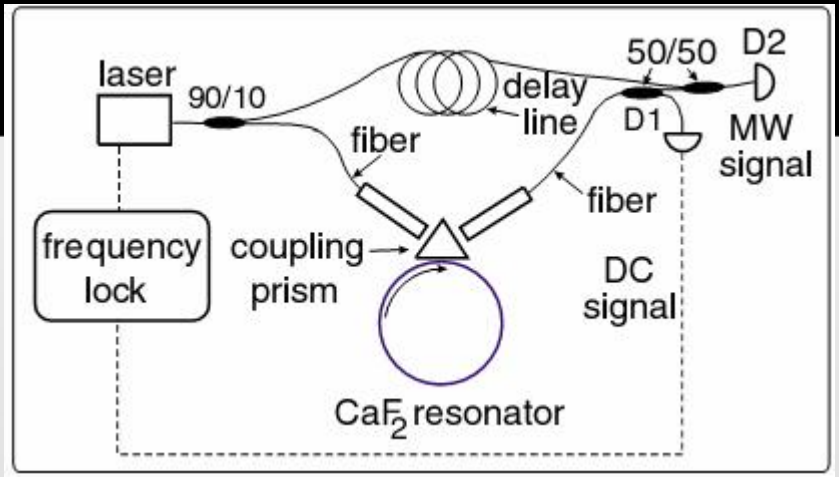

Experimental Setup

PRL 93, 243905 (2004)

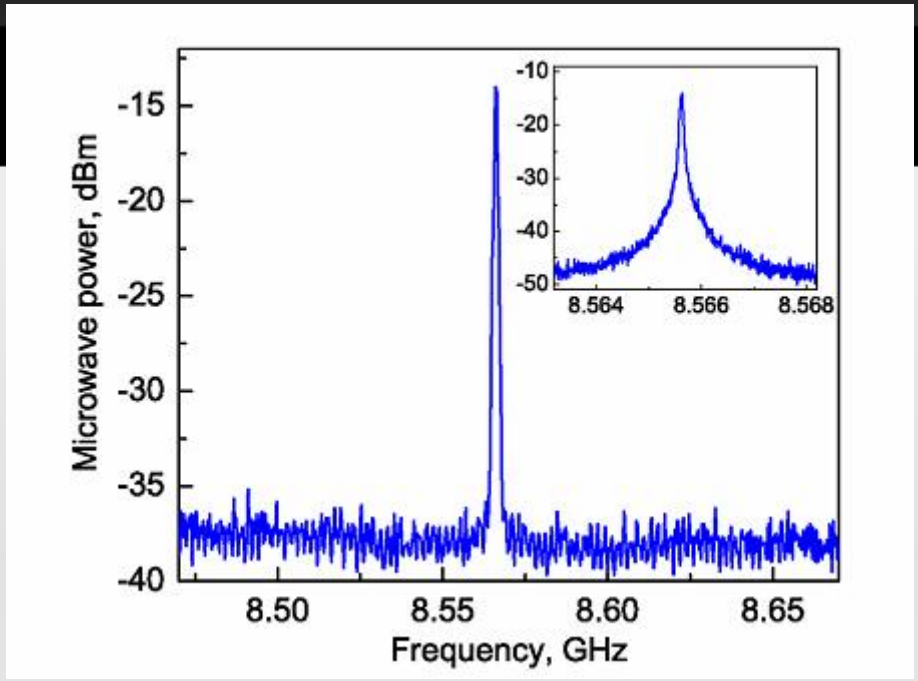

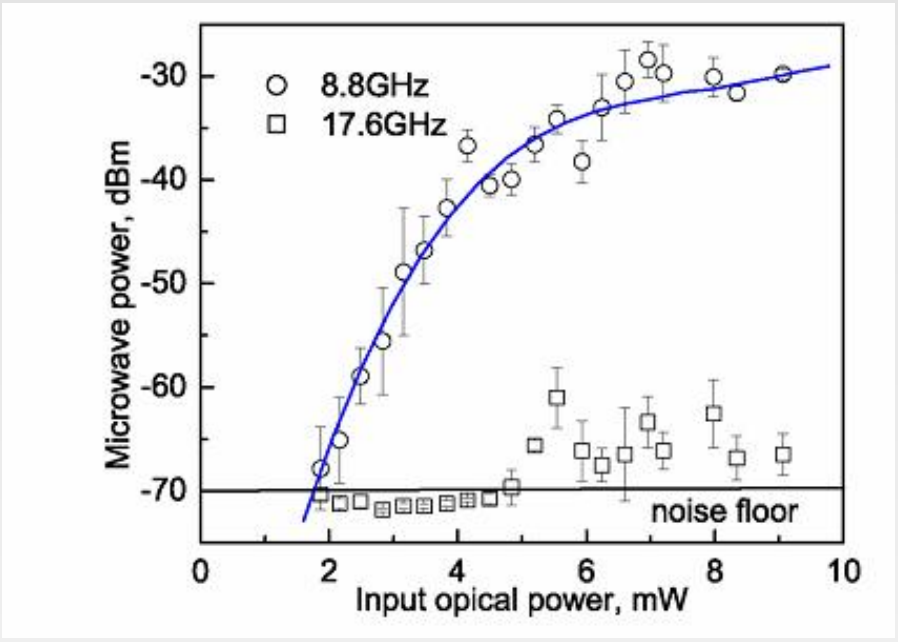

Crystalline WGR: Frequency Doubling

PRL 92, 043903, 2004

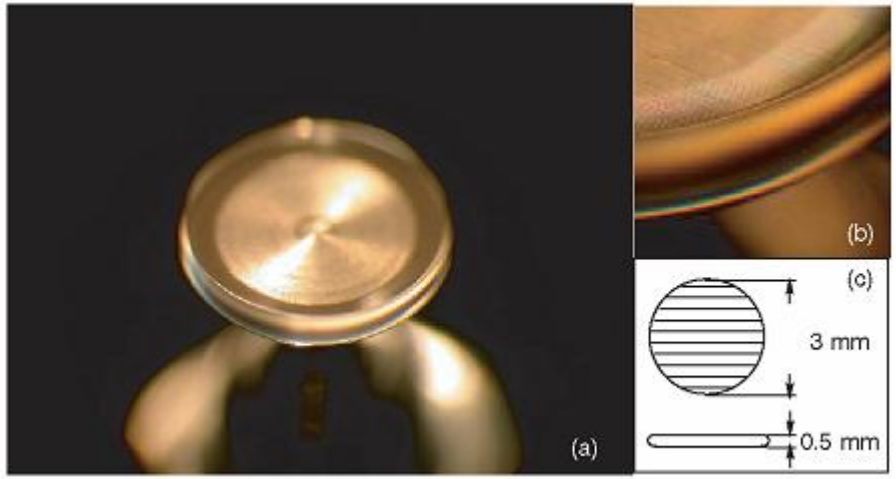

(a) Toroidal whispering gallery mode cavity made of periodically poled lithium niobate. (b) Enlarged fragment of the cavity rim. (c) Schematic of the cavity.Poling has planar structure and 14m period.Q=2*10^8.

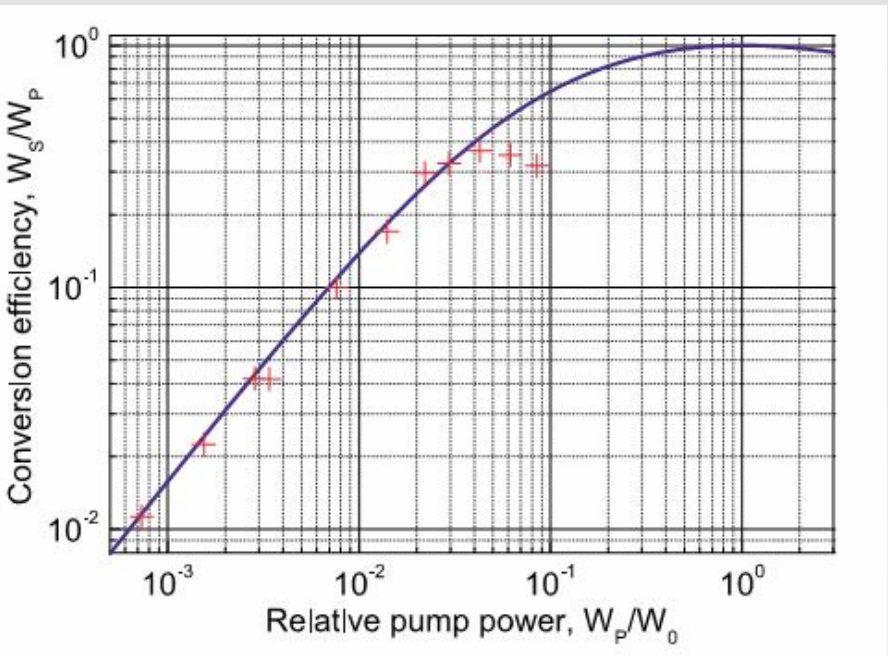

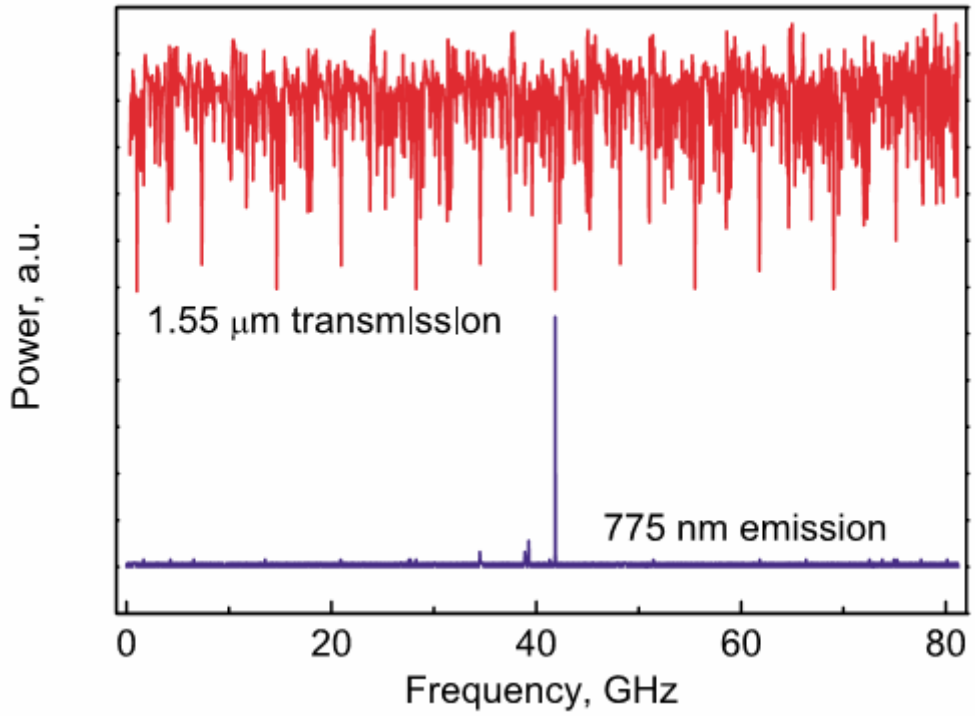

Crystalline WGR: Photorefractive

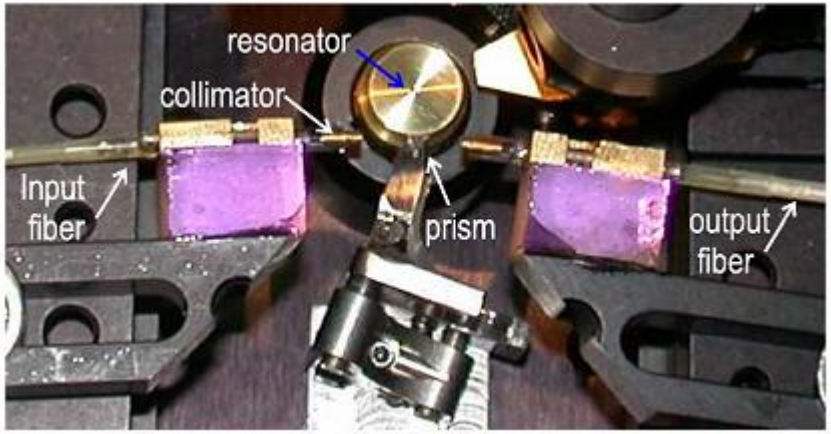

Experimental Setup
APL 88, 241909, 2006

Active WGM: Micro Laser

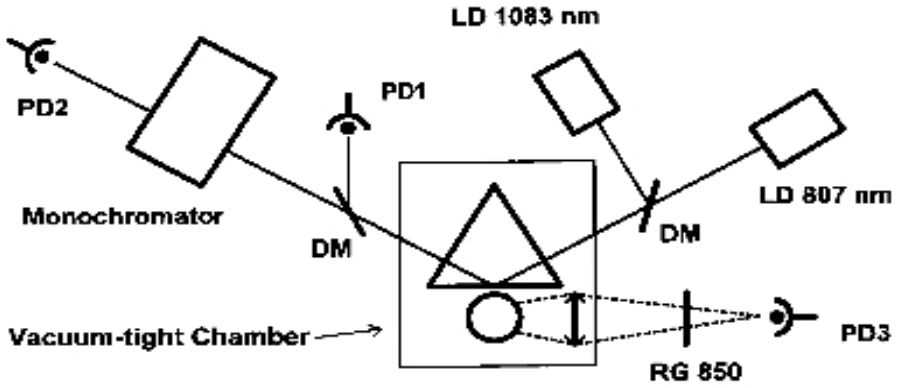

Fig. 3. Experimental setup for the microlaser experiment: WGMs are excited by evanescent wave coupling with a high index prism across the sphere–prism gap g, which can be adjusted with nanometric precision. The pump source is a diode laser (Sharp LT017MDO) operating at 807 nm. By adjusting the diode current, resonant excitation of a sphere's WGM can be observed as a dip on the light transmitted to the photodiode PD1. A 1080 nm probe beam can be superimposed with a dichroic mirror (DM) to measure the cold-cavity Q factor as a function of the gap g. The laser light (or fluorescence) emitted out of WGMs in the fluorescence band and recoupled into the prism is separated from the reflected pump beam by a second dichroic mirror and then passed through a monochromator (resolution 0.02 nm) onto photodiode PD2. The side-fluorescence of the doped sphere is measured with photodiode PD3, after elimination of the scattered pump light with the RG850 filter. The microsphere can also be viewed with a CCD camera coupled to a stereomicroscope (not shown here).

Fused Sillica microsphere laser
very low threshold~200nW

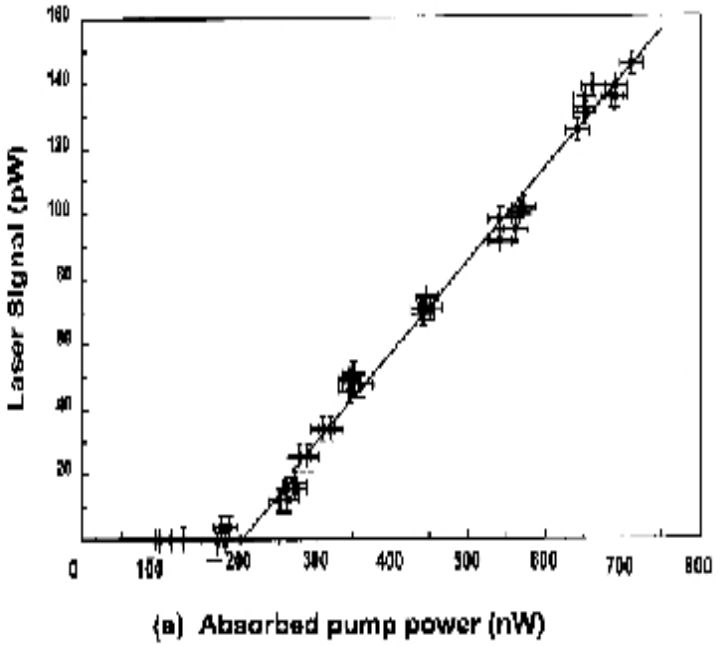

PRA 54, 3, 1996

Er-Yb codoped microlaser

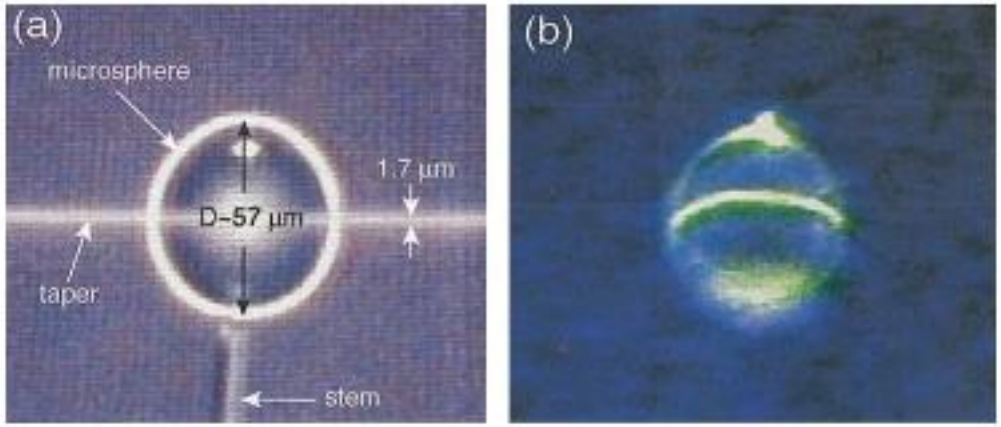

Fig. 1. (a) Image of the taper in contact with the equator of the microsphere. (b) Color image of the green upconverted photoluminescence from the taper-pumped microsphere, where the pump wavelength is tuned close to a fundamental ($|m| = l$) WG mode.

- Taper is tailered so that the 980nm pump light is near critical coupled into the microsphere.85% pump light is absorbed by sphere
- From the picture of the upconversion of the Er3+, pumping volume is estimated to 1000

Taper coupled microsphere laser

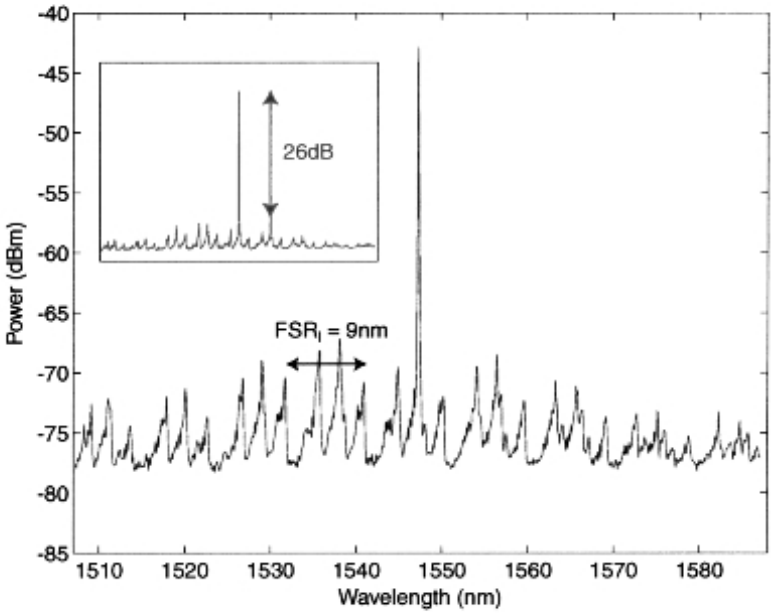

Fig. 2. Photoluminescence spectra [taken at point (a) in Fig. 3, below] of the microsphere for an annular pump region about the equator. The photoluminescence (inset) is taken at point (b) in Fig. 3 (wavelength range matching that of the main spectra), where the side-mode suppression is 26 dB.

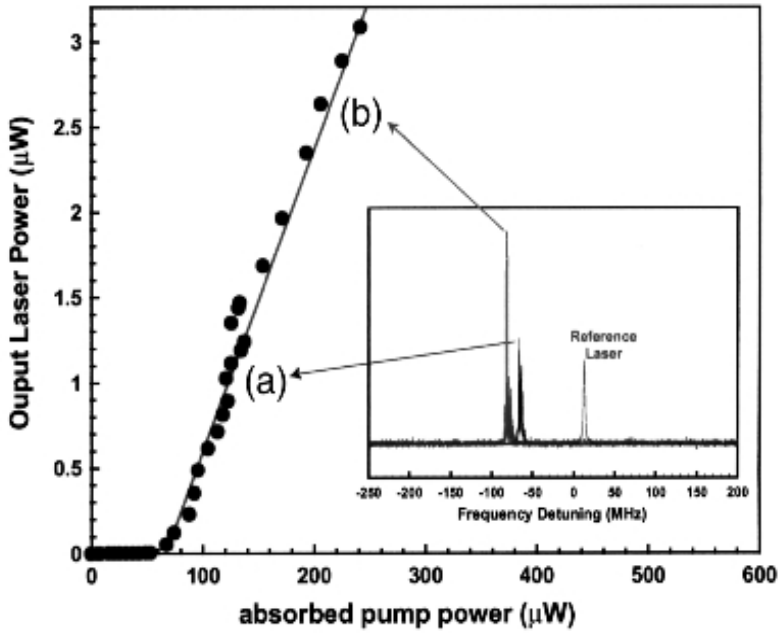

Fig. 3. Collected laser output power versus absorbed pump power in the microsphere ($L_{out} - L_{in}$). Inset, spectral output of a Fabry–Perot filter, showing the single-mode nature of the microsphere laser, where for reference a single-frequency laser with a known linewidth of 300 kHz is also shown.

Measured with FP ethanol
60 microWatts, output power 3 microW

Opt. Lett. Vol. 25, no.19 ,2000
Opt. Lett. Vol. 26, no. 12, 2001

Sol-gel coated micro laser

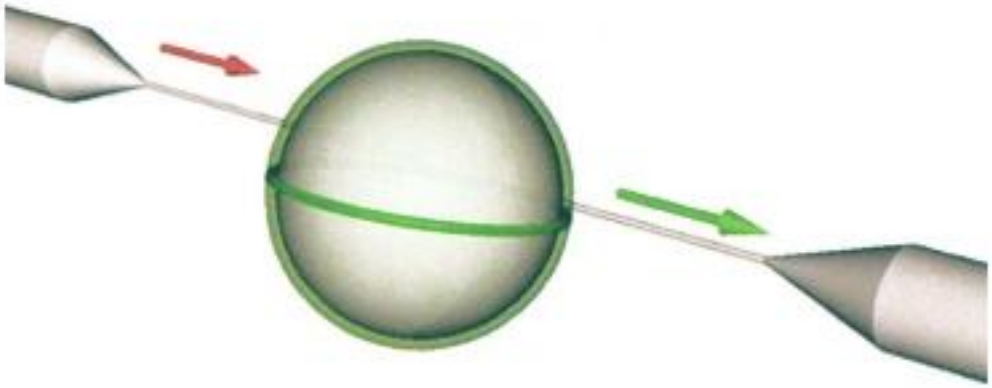

Fig. 1. Schematic of a thin-film-coated microsphere laser coupled with a fiber taper. The red and green arrows represent input pump and output lasing waves, respectively.

0.2wt%
buildup rate
0.3 μ m/cycle

Thickness of the sol-gel film can affect the lasing behavior:
1 μ m make cw operation possible
thick sol-gel as to 5 μ m can provide conditions for pulse operation

Opt. Lett. Vol. 28 no. 8, 2003

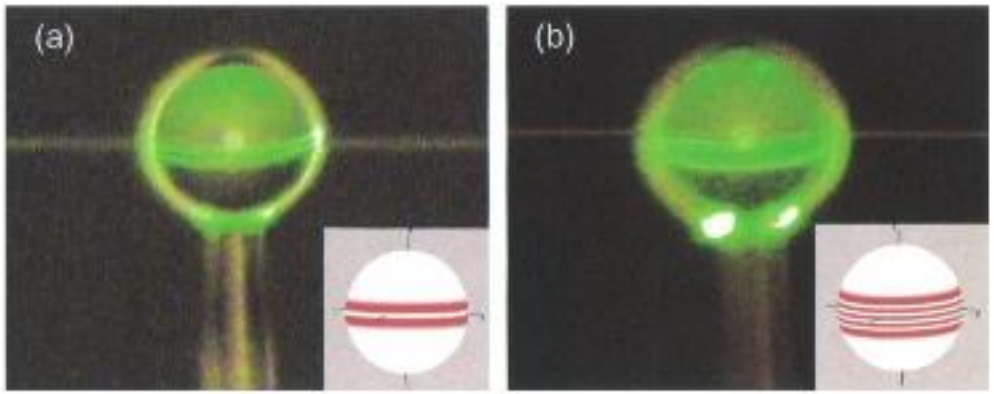

Fig. 2. Images of the WGMs in the taper–sphere coupling zone: (a) $l - m = 1$, (b) $l - m = 4$. The green rings are upconverted photoluminescence. The inset shows spherical harmonics[13] $Y_{lm}(\theta, \varphi)$ for (a) $l - m = 1$ and (b) $l - m = 4$.

APL Vol. 83, 5, 2003

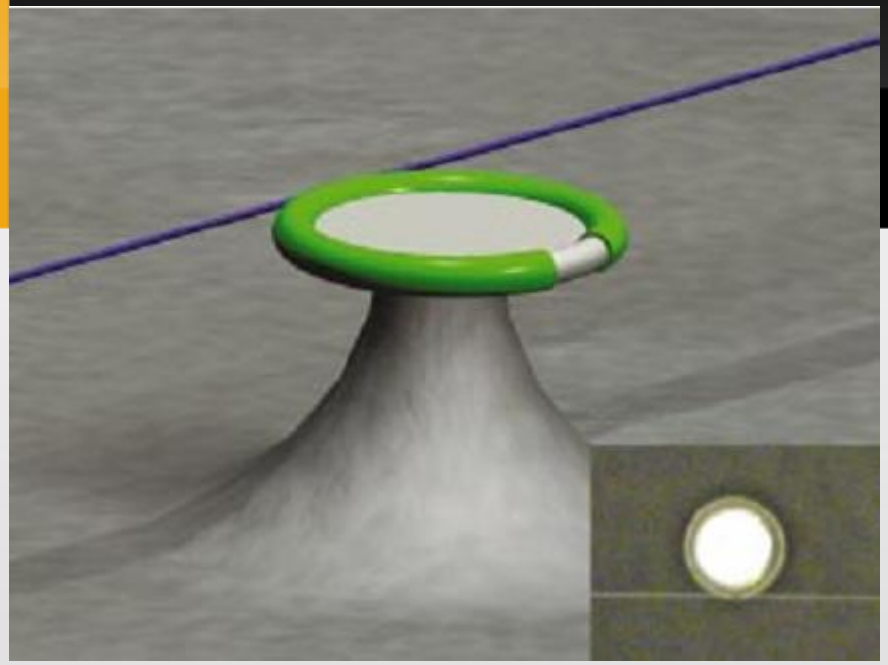

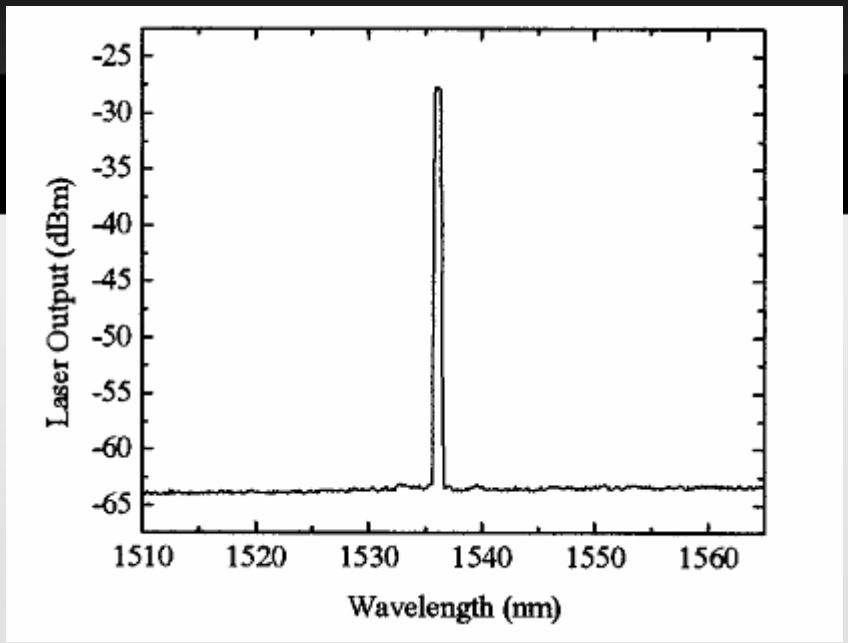

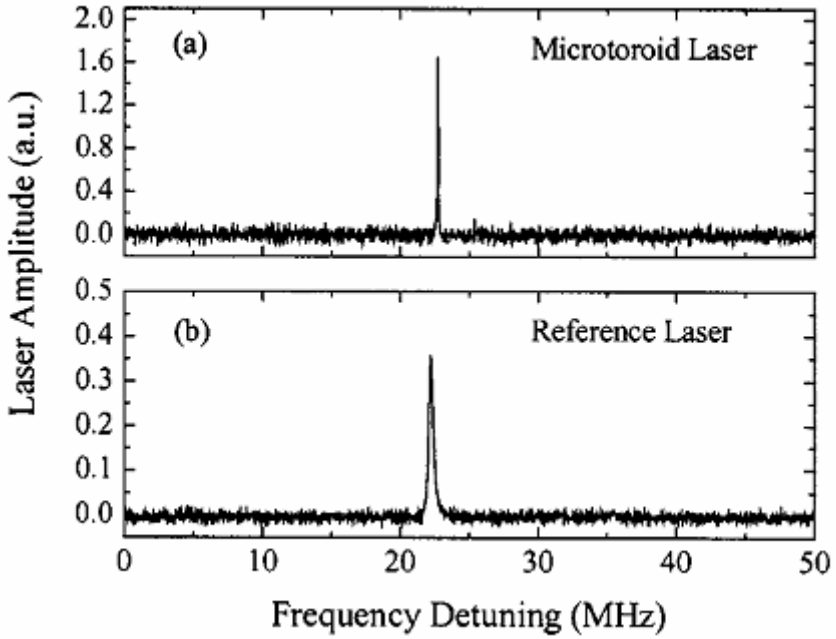

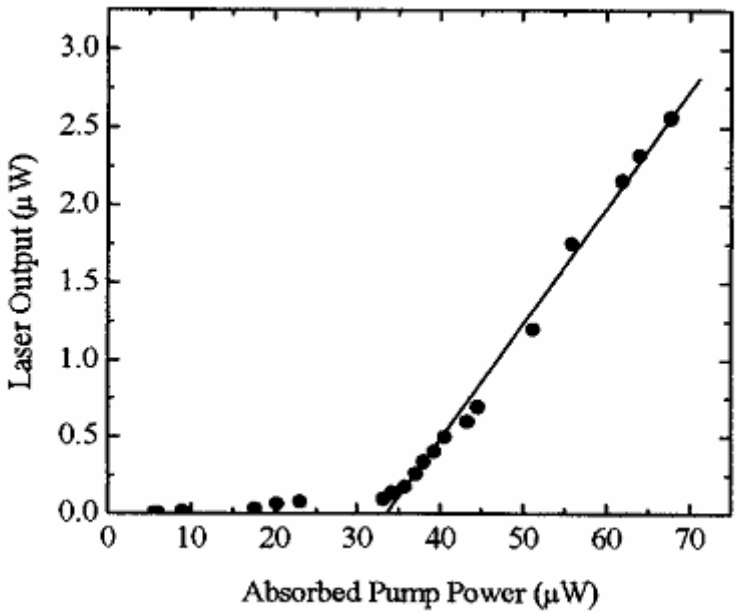

High power output via Sol-gel

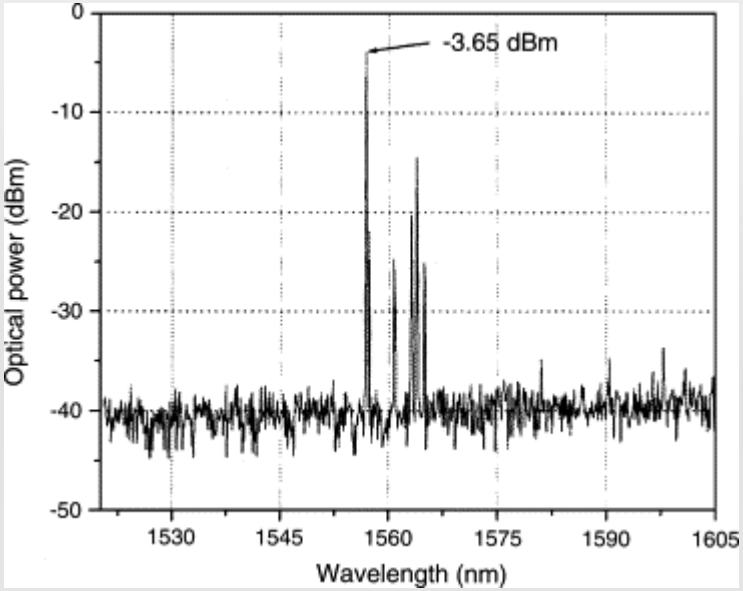

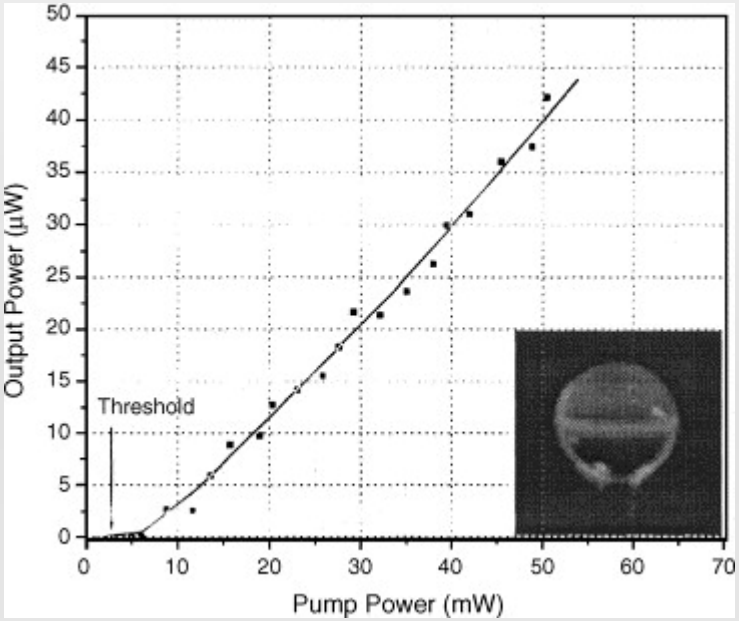

WGM-laser output power of −3.65 dBm measured by the half-taper fiber coupling to sol–gel bulk-glass microsphere laser under optical pump power of 70 mW at 976 nm.

Laser output power at 1557 nm vs. pump power at 976 nm. *Inset*: up-conversion luminescence observed in laser.

MATERIALS SCIENCE AND ENGINEERING B-SOLID STATE MATERIALS FOR ADVANCED TECHNOLOGY Volume: **131** Issue: **1-3** Pages: **27-31 2006**

Erbium-implanted silica microsphere laser

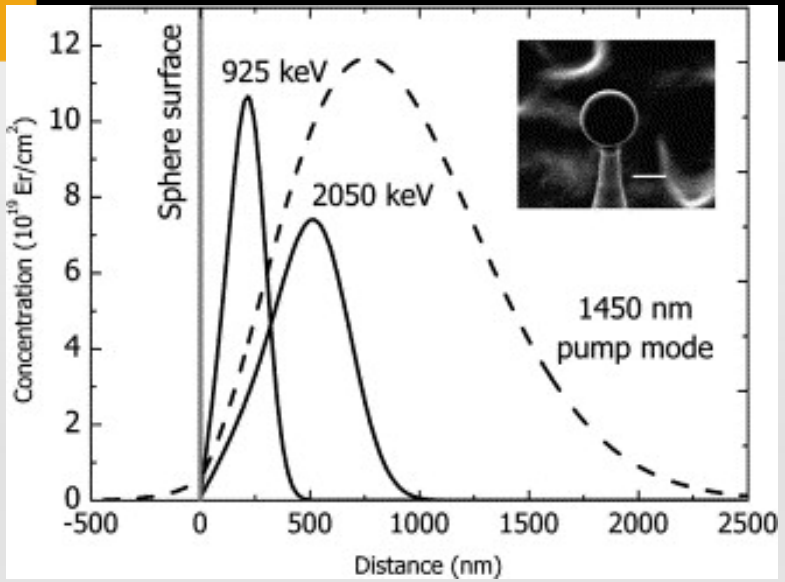

Calculated Er implantation profiles for 22 μm-diameter silica microspheres implanted with 925 keV Er+ (7.2 × 1015 cm−2) and 2.05 MeV Er2+ (1.1 × 1016 cm−2) using a rotating geometry. Measured ion ranges and straggles for planar samples were used as input. Also indicated is the 1450 nm pump mode profile (dashed line) for a 22 μm radius sphere. The inset shows an optical micrograph of a microsphere on the fiber stem (scale bar 50 μm).

Optical transmission spectrum around λ = 1450 nm measured in the under-coupled regime. Solid line shows a fit from which the quality factor (Q = 1.9 × 107) was derived. The inset shows a top view of the fiber-microresonator coupling geometry.

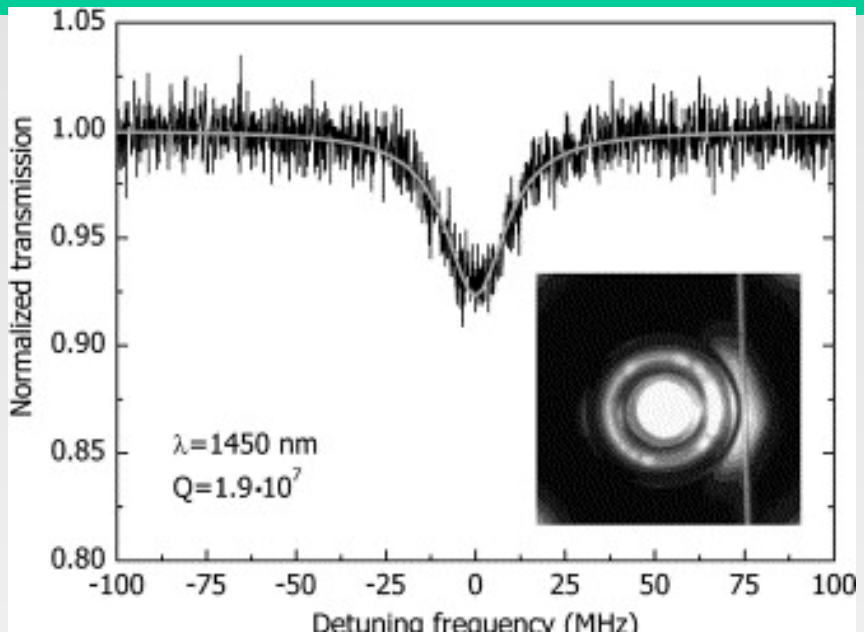

Nuclear Instruments and Methods in Physics Research Section B: Beam Interactions with Materials and Atoms
Volume 242, Issues 1-2, January 2006, Pages 182-185

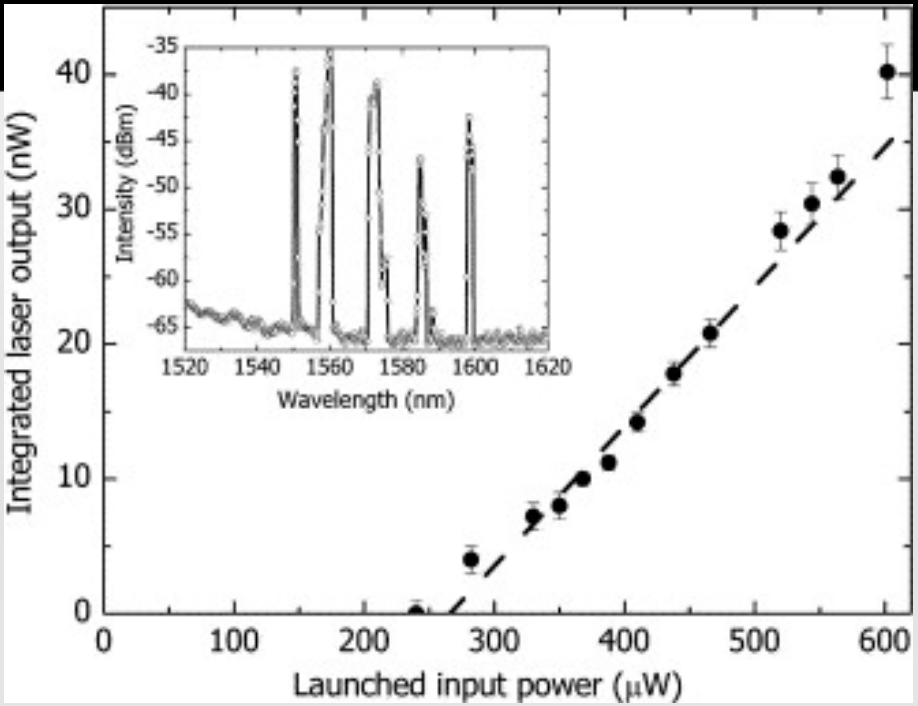

Lasing output power integrated over all lasing lines plotted as a function of pump power at 1450 nm for a microcavity doped with 925 keV Er. A lasing threshold of 250 μ W is observed. The inset shows a typical lasing spectrum

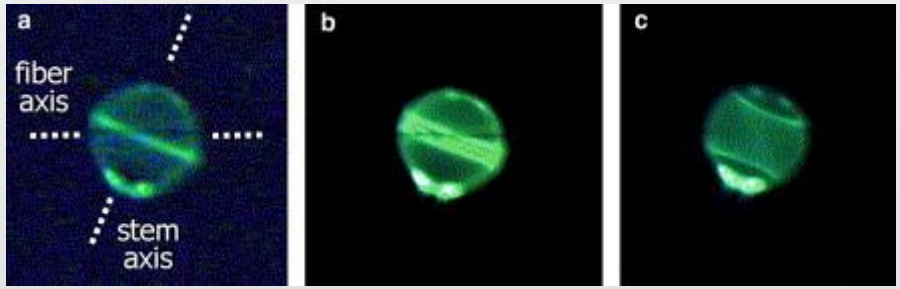

Optical micrographs of an Er-implanted microsphere (2.05 MeV) under lasing conditions. Green upconversion emission is imaged (printed in black and white).

L-band Er3+-telluite glass microlaser

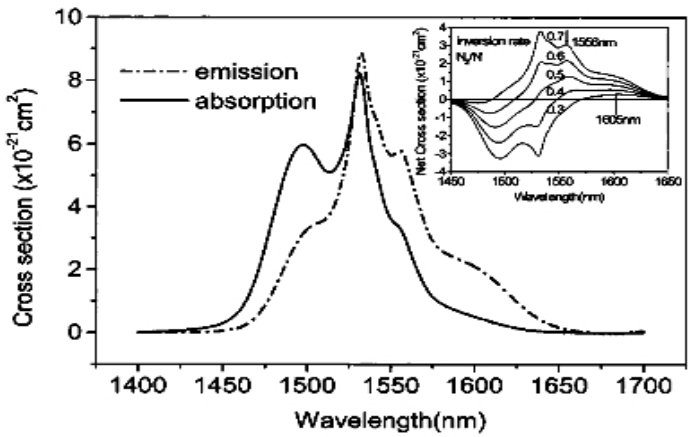

FIG. 1. Absorption cross section and emission cross section of the Er^{3+}-doped tellurite glass. The inset shows the net cross section $[\sigma_e(N_2/N)-\sigma_a(N_1/N)]$ of Er^{3+} in tellurite glass near communication window, for different values of the fractional upper-state population (N_2/N) (indicated adjoining each curve).

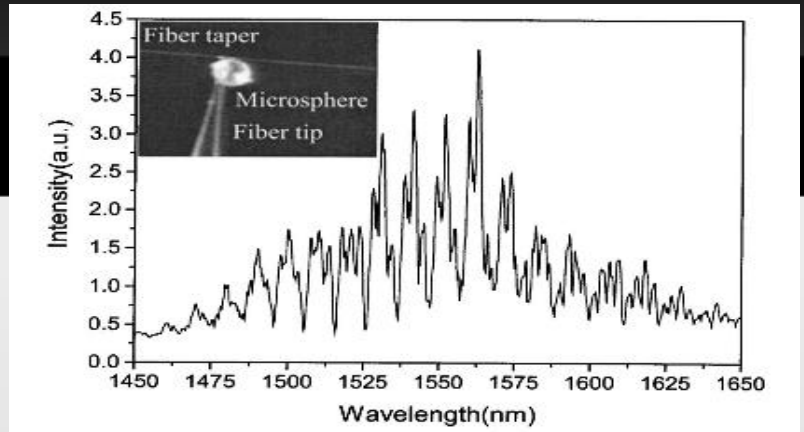

FIG. 2. Whispering-gallery modes measured by the fiber taper coupling configuration. The pump power is below the threshold. The inset shows the experimental fiber taper coupling setup.

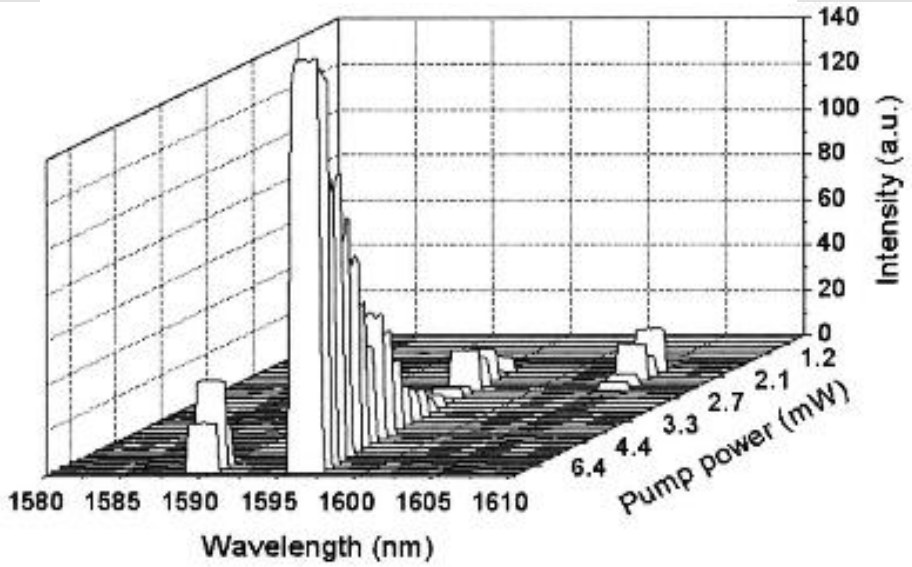

FIG. 4. Wavelength shift of the microsphere lasing mode as the pump power increased.

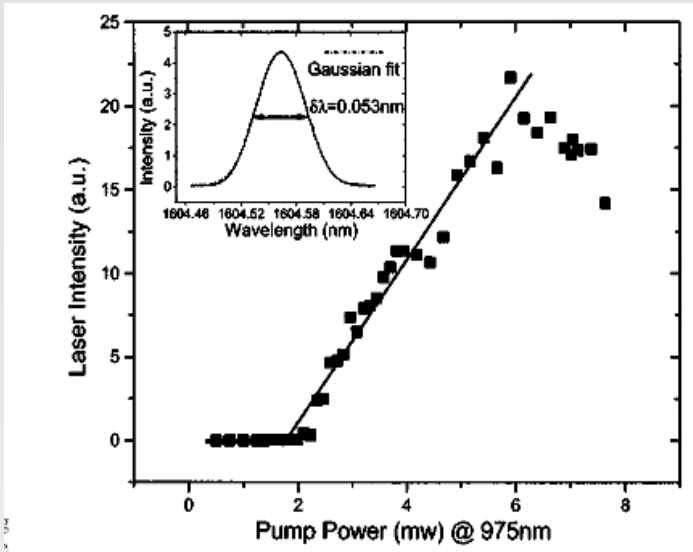

FIG. 3. Microsphere laser output power vs pump power at 975 nm. The inset shows the Gaussian fit of the laser mode profile.

APL Vol. 82, no. 10, 2003

S-band Tm3+-tellurite microlaser

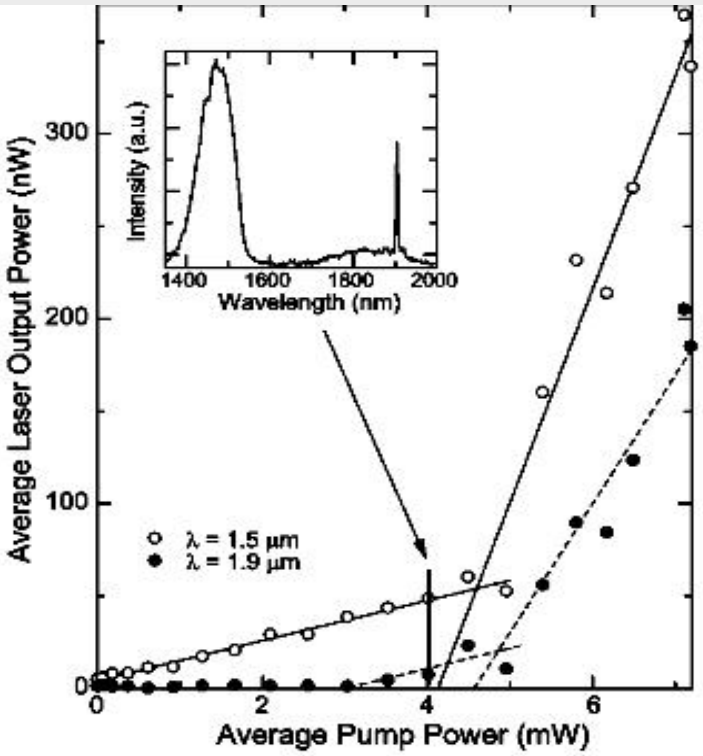

FIG. 3. Average laser output power against average pump power for a Tm^{3+}-doped tellurite microsphere laser. (Inset) Laser emission spectrum at average pump power of 4.0 mW.

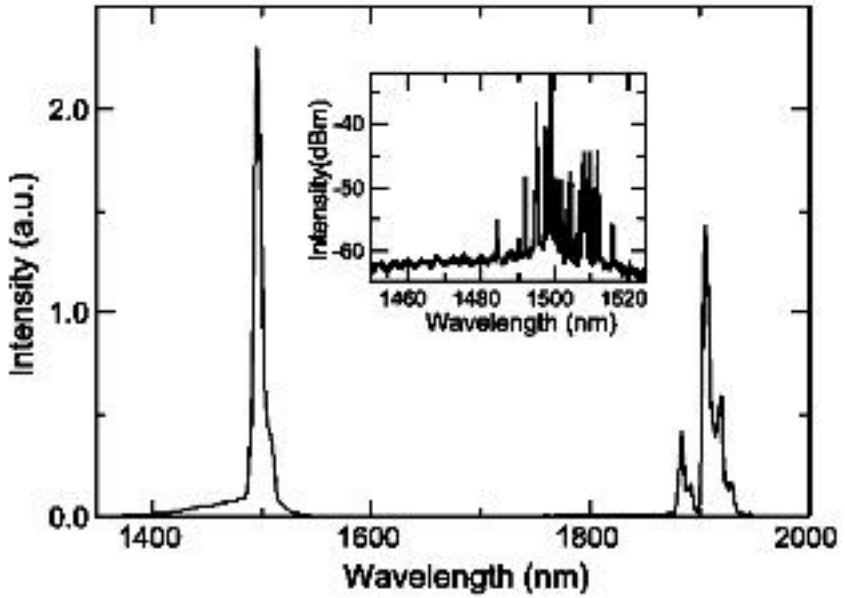

FIG. 2. Emission spectrum of a Tm^{3+}-doped tellurite microsphere laser with diameter of 104 μm. (Inset) OSA emission spectrum.

APL Vol. 85, no. 19, 2004

APL Vol. 87, no. 21, 2005

Yb3+-doped microlaser@1040nm

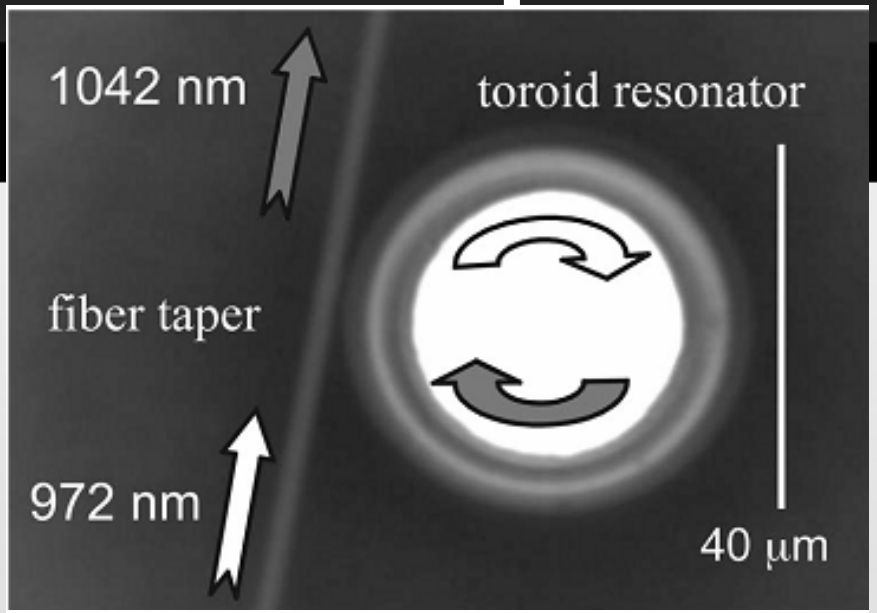

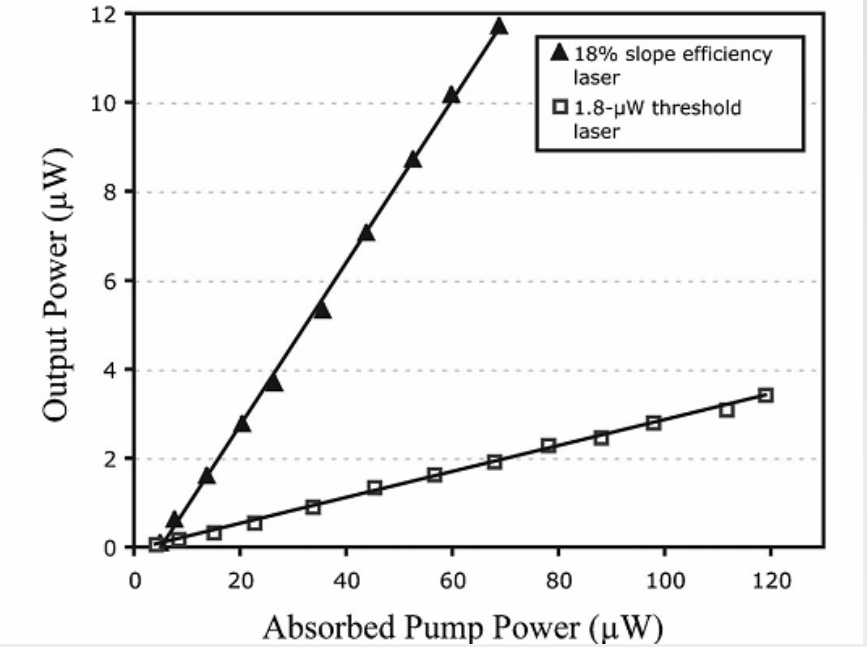

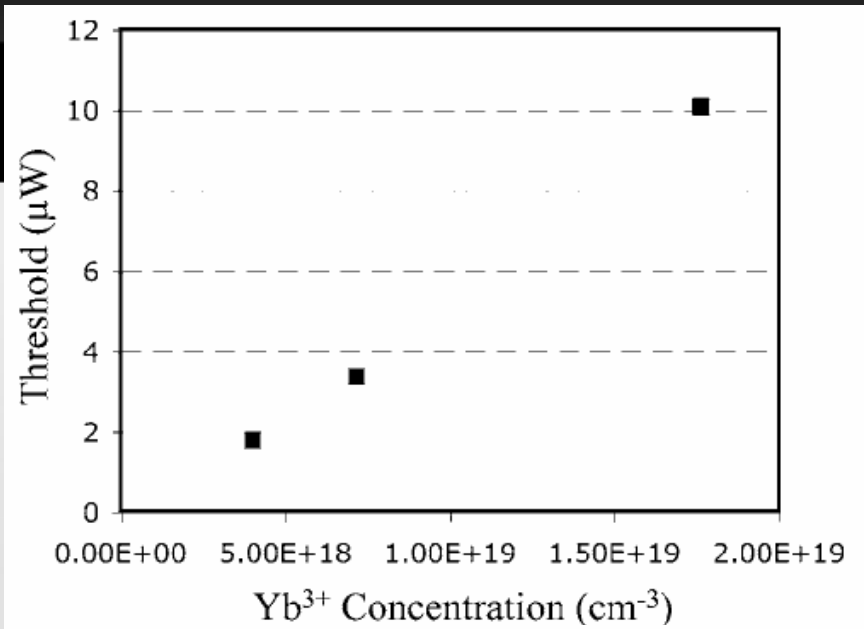

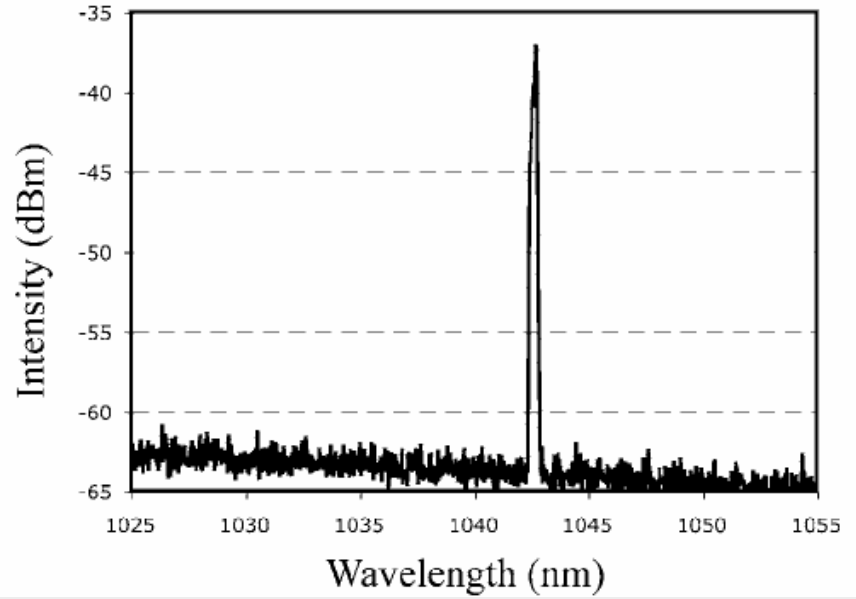

OPTICS LETTERS / Vol. 32, No. 18 2007

Lasing in WGR with Semiconductor Gain Material

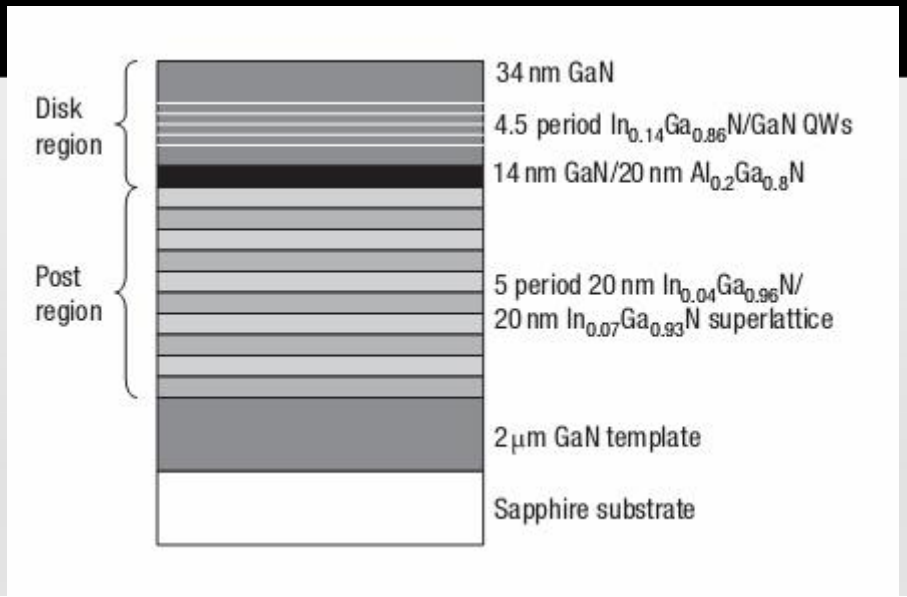

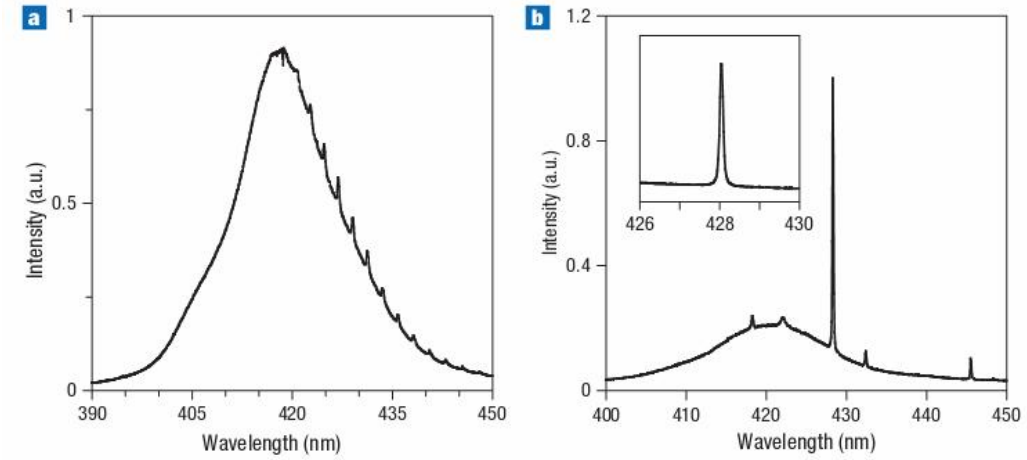

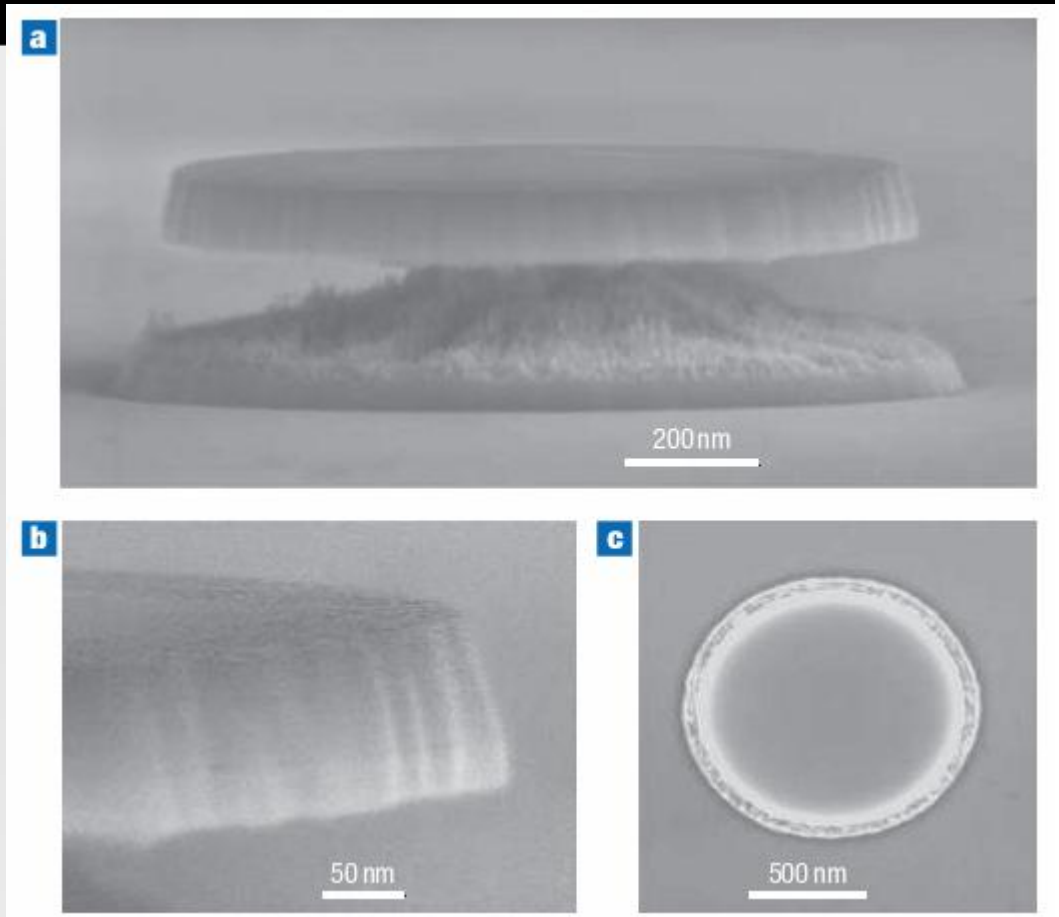

Nature Photonics Vol. 1 Jan, 2007

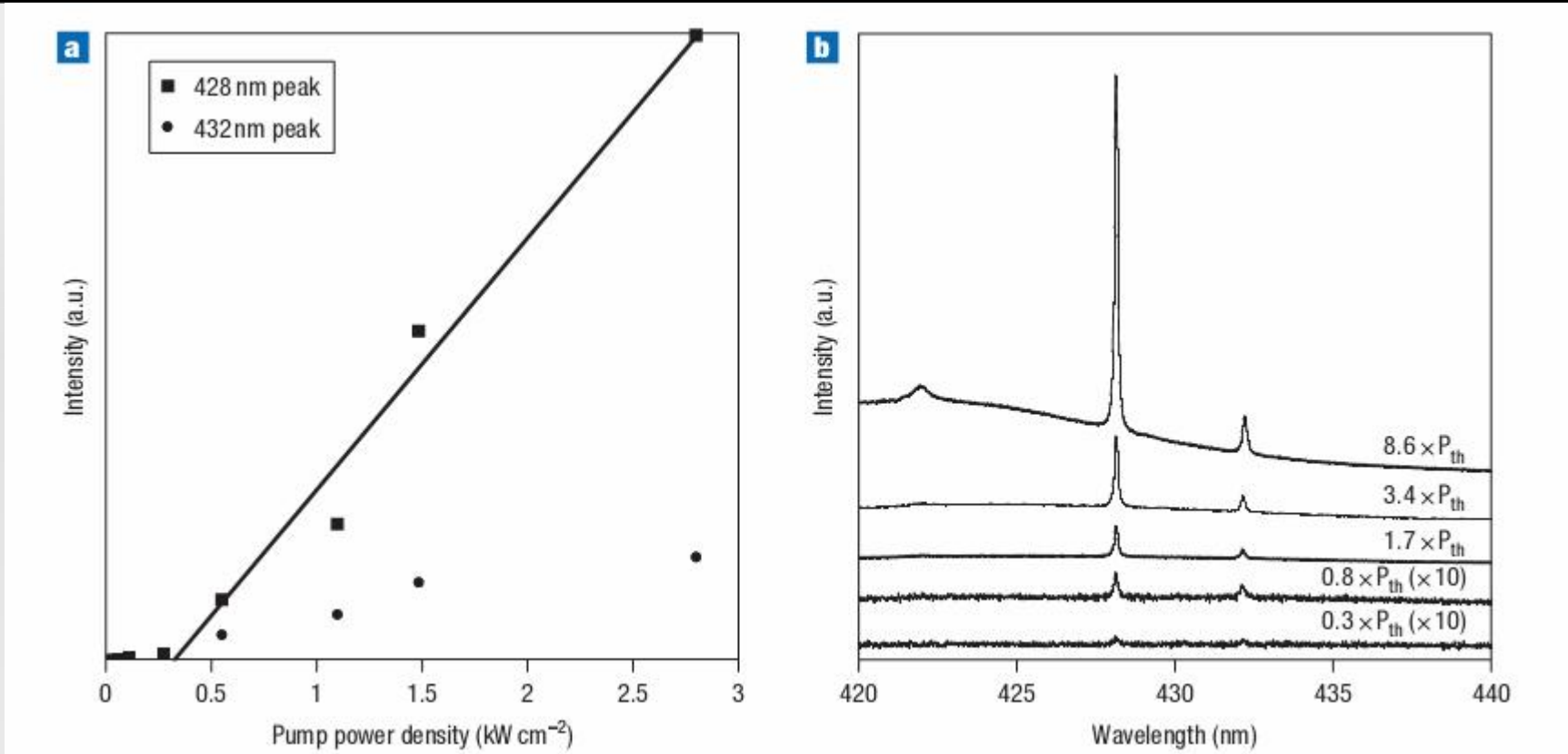

Power-dependent data for 1.2-mmdisk.a, Peak intensity versus pump power for two modes: the lasing mode at 428 nm, which exhibits a clear threshold at about 300 W cm , and another mode at 432 nm. b, PL spectra taken at different pump powers.

Submicro scale microdisk laser

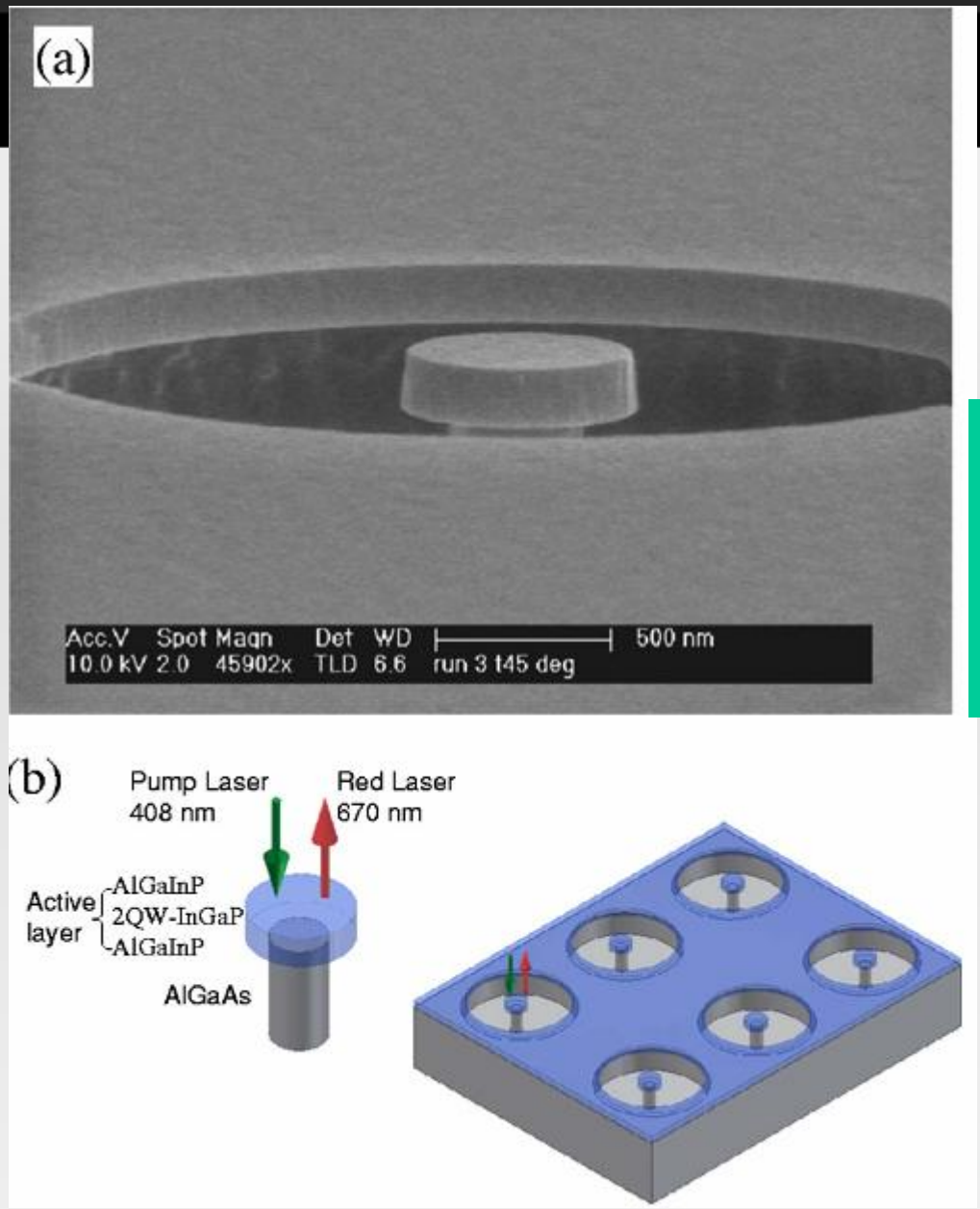

a) Scanning electron microscope image of one of the 645 nm diameter submicron microdisk laser structures.b) Illustration of mushroom shape structure and pumping scheme not to scale.

APL Vol. 90 111119, 2007

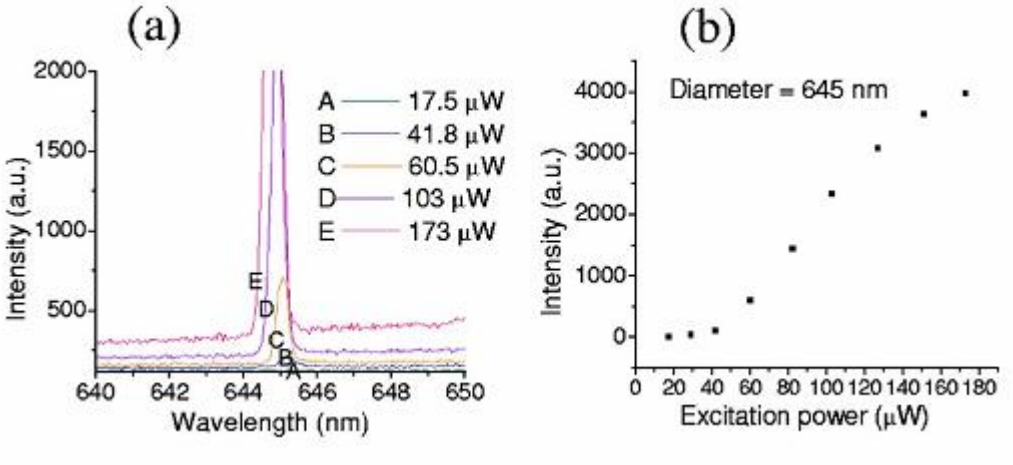

a) Typical spectrum of different excitation powerand b)L-Lcurve of one of the 645 nm diameter microdisk.

a) Typical spectrum and b) semilogarithmic L-Lcurve of one of the 650 nm diameter microdisks.

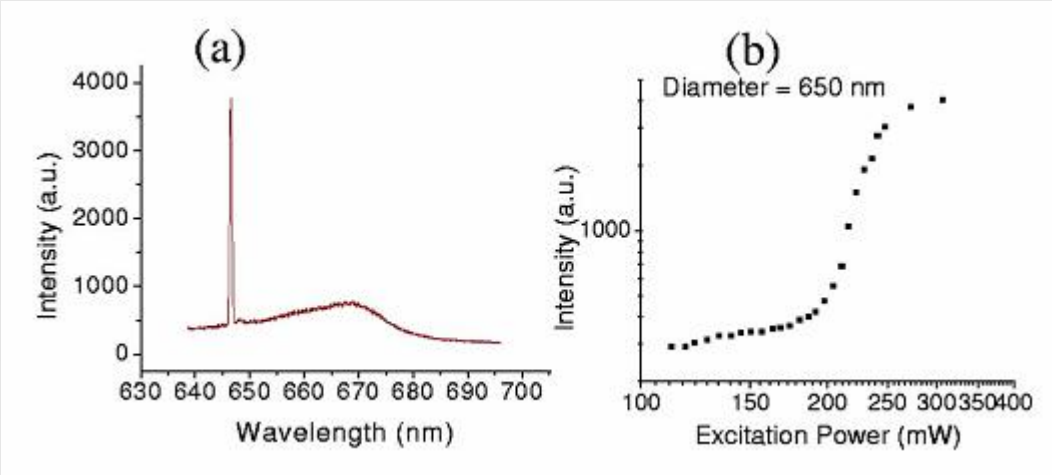

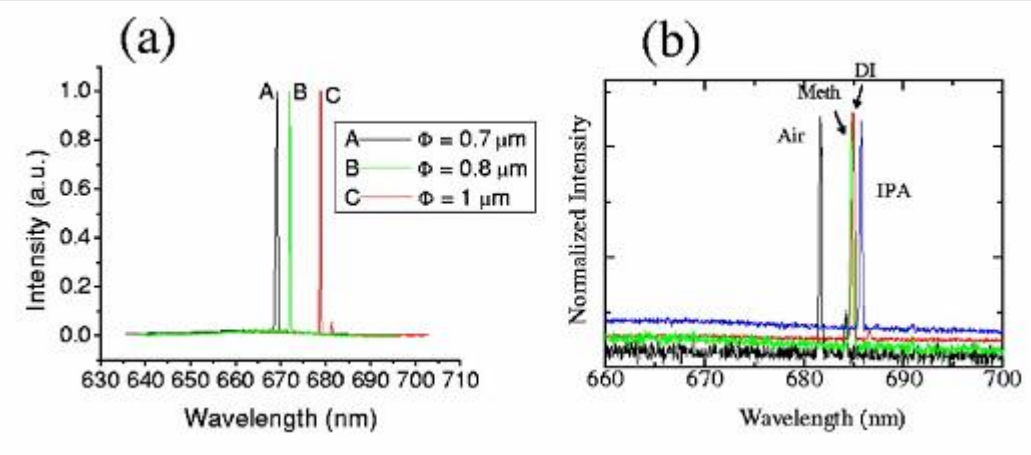

a) Laser spectra with different diameter microdisks and b) lasing peak wavelength shift obtained with different chemical environments.

Quantum dot Microlaser

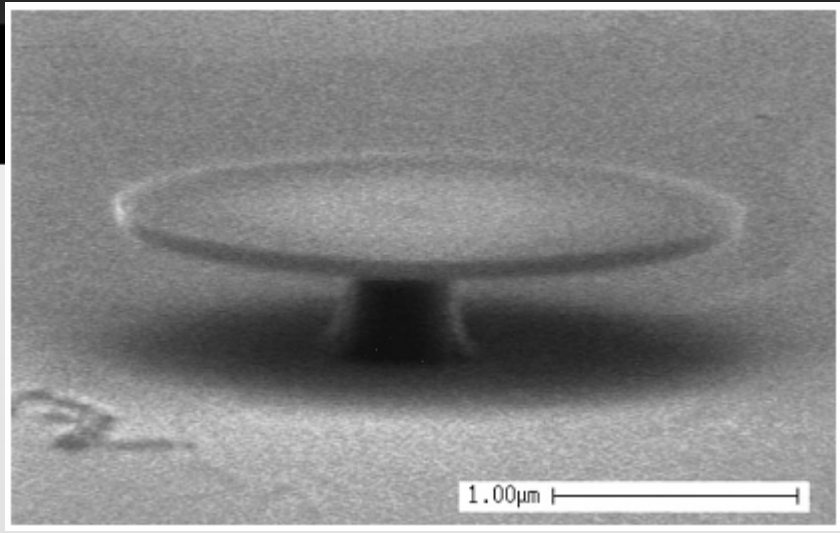

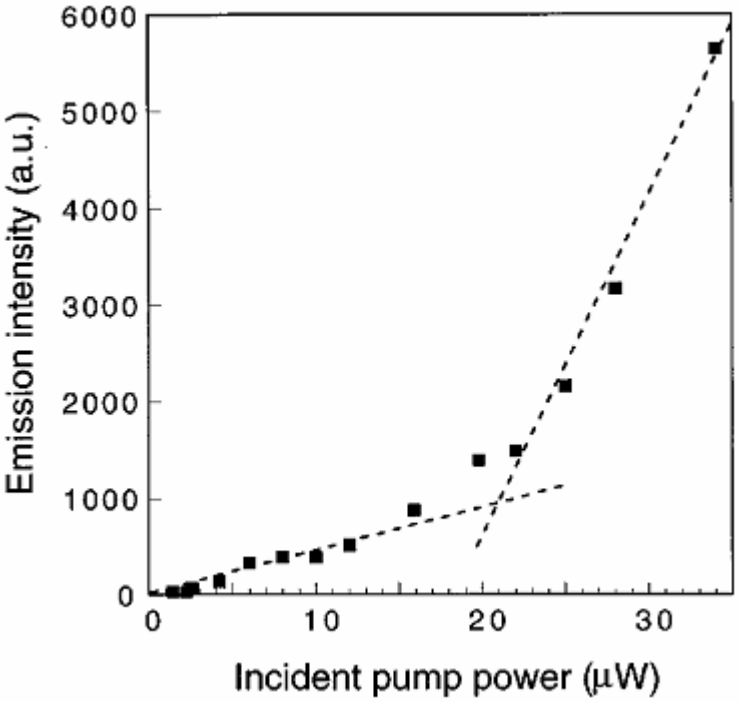

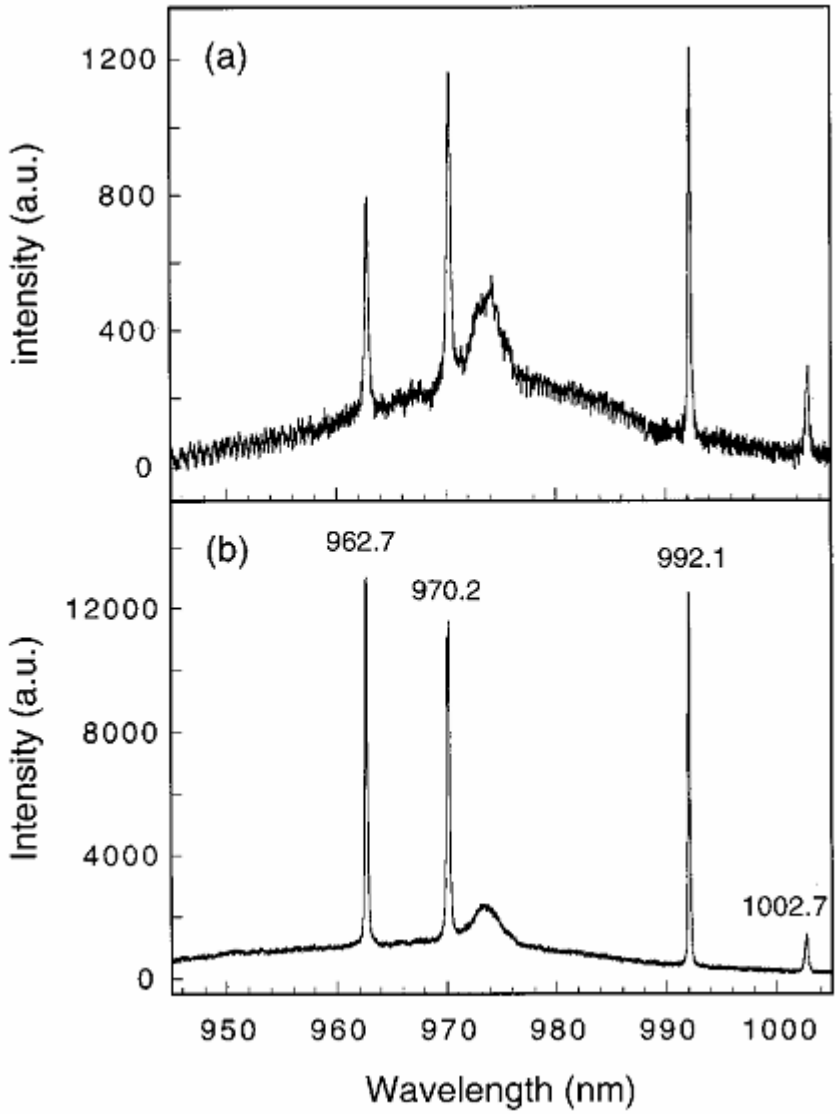

Optically pumped InAs quantum dot microdisk lasers

APL Vol. 76, 24, 2000

Other QDs in Microcavity

- CdTe nanocrystal attached to organic microsphere.
- Room temperature HgTe QDs on fused silica microsphere:Ultralow-threshold (about 2uW) near communication wave band.
- Zinc Oxide film based microdisks:UV laser for chemical detection.

Highlights in research of microlaser

- Toward integration ,to nanoscale
- Lower threshold, even higher Q-factor
- All kinds of wavelength
- Improving coupling methods

Integration

Eight-Channel Microdisk CW Laser Arrays Vertically Coupled to Common Output Bus Waveguides

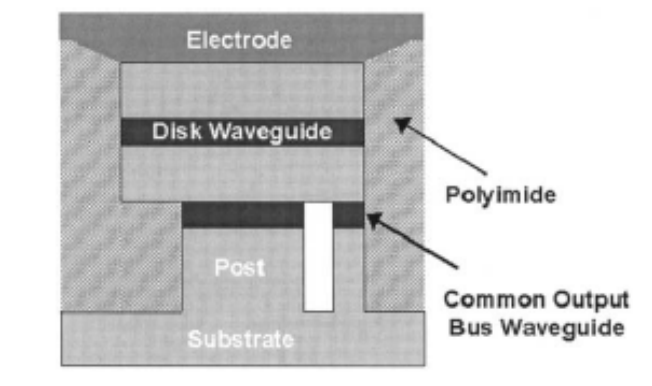

Schematic cross-sectional view of a bus-coupled microdisk laser

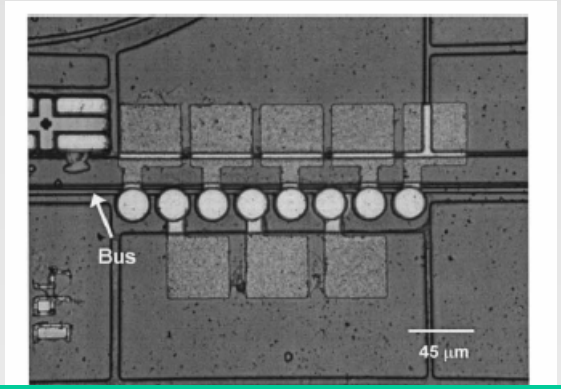

Micrograph showing the top view of the fabricated eight-channel microdisk array vertically coupled to a single bus waveguide.

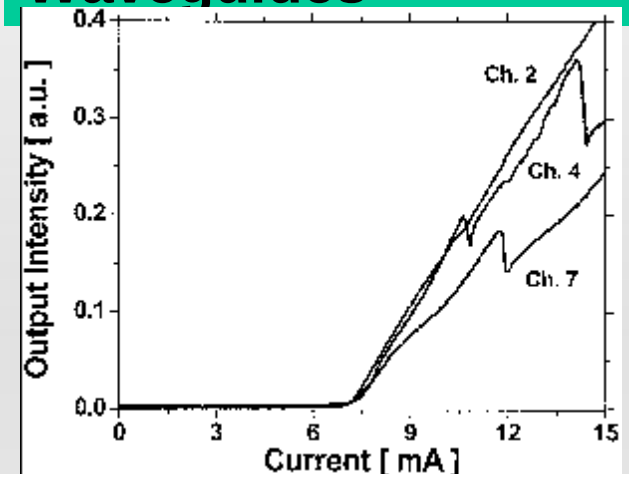

L–I curves measured from different microdisks corresponding to channels 2, 4, and 7, respectively.

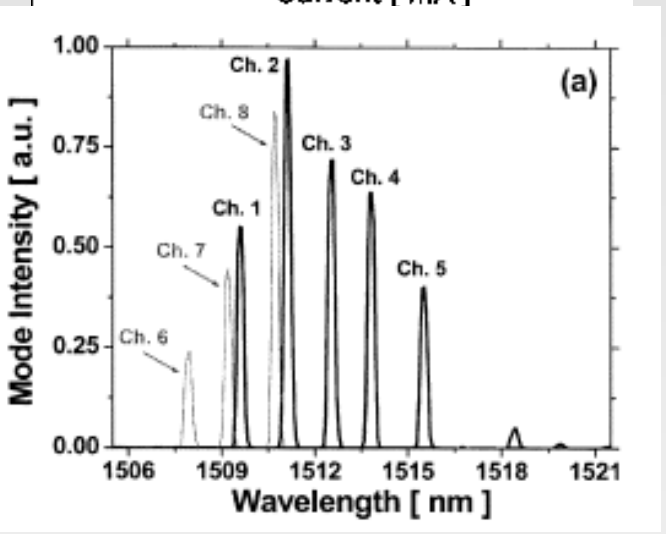

Superimposed lasing spectra measured from an eight-channel microdisk laser array.

IEEE PHOTONICS TECHNOLOGY LETTERS, VOL. 16, NO. 2, FEBRUARY 2004

To Improve Q factor

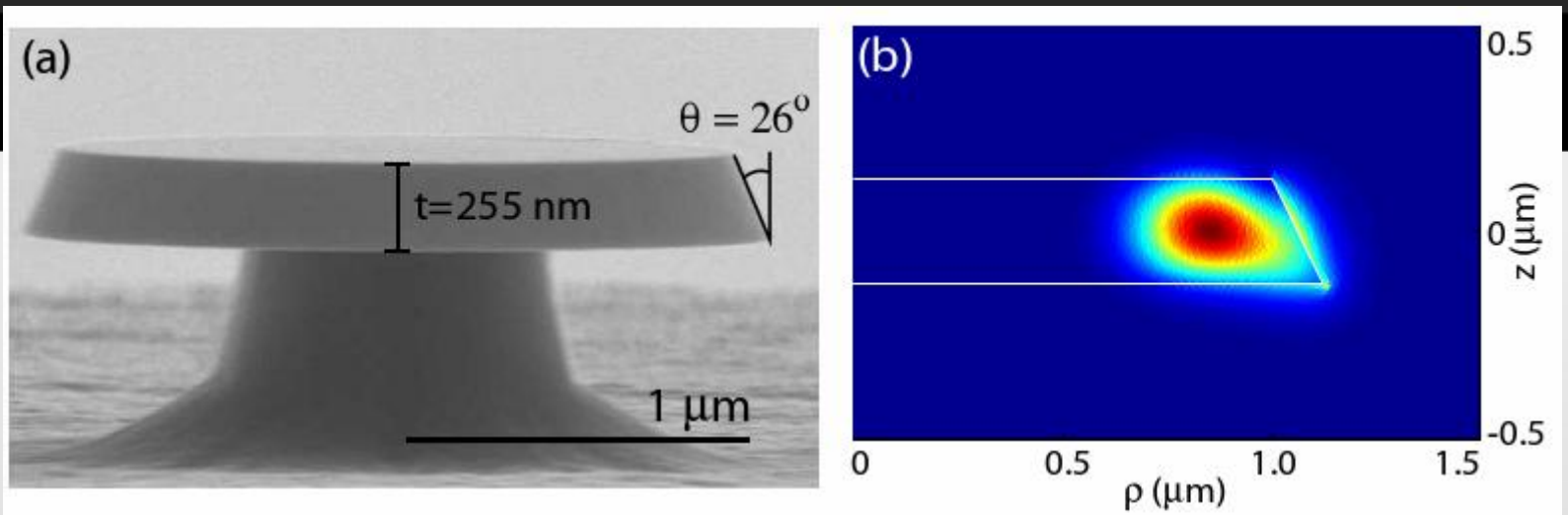

Fig. 1. (a) Scanning electron microscope (SEM) image of a fabricated microdisk device. The disk thickness t=255 nm and sidewall angle $\theta = 26°$ from vertical are taken as fixed in the finite-element simulations presented in the work. The measured average diameter for this device (i.e., the diameter at the center of the slab) is ~ 2.12 μm. (b) Finite-element-calculated $|\mathbf{E}|^2$ distribution for the $TE_{p=1,m=11}$ WGM of a microdisk with a diameter of ~ 2.12 μm at the center of the slab. For this mode, $\lambda \sim 1265.41$ nm, $Q_{rad} \sim 10^7$, and $V_{eff} \sim 2.8(\lambda/n)^3$.

Opt. Expr. Vol. 14, no. 3, 2006

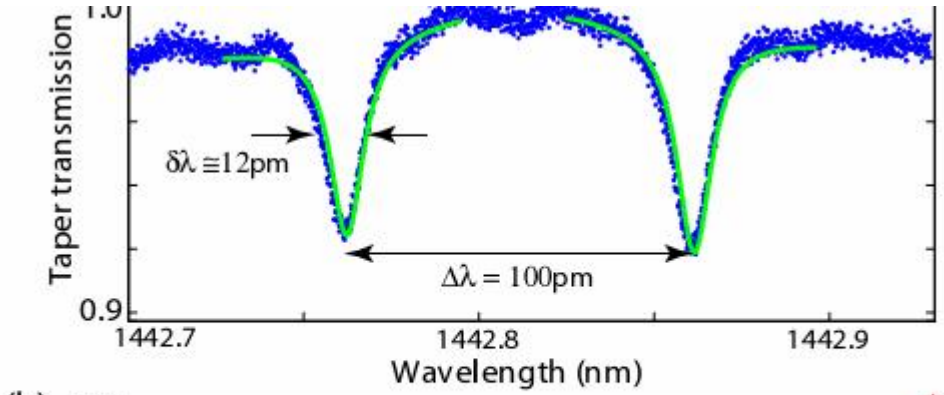

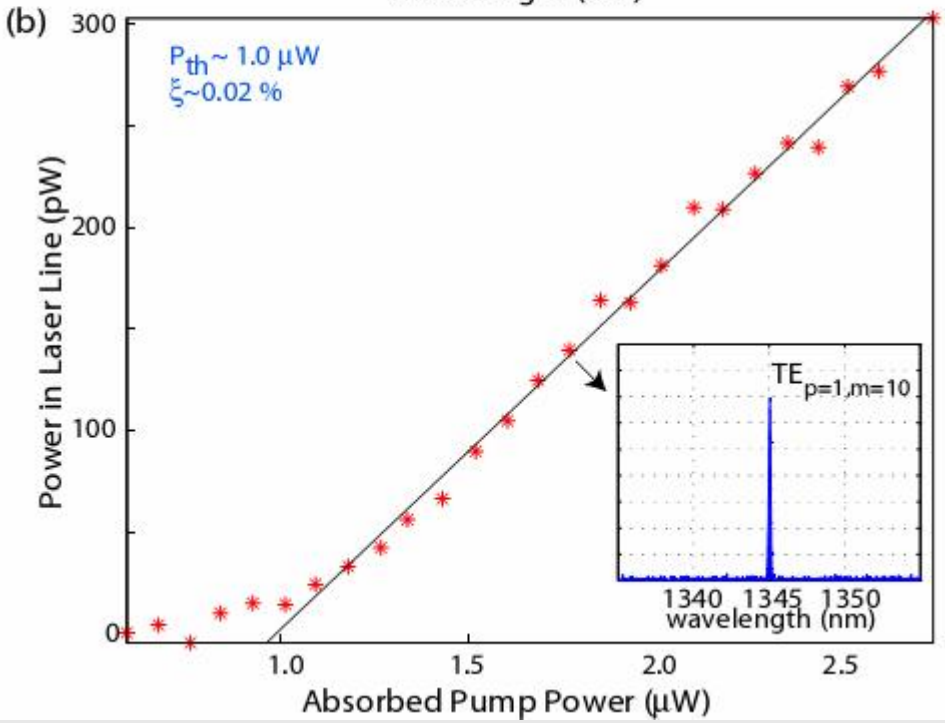

a)Normalized transmission spectrum when a fiber taper is positioned a few for hundred nm away from the microdisk edge.(b)L-L)curve a device operated with free-space collection. The laser threshold absorbed pump power Pth is $\sim$1.0 μ W

Directional Laser in Deformed Cavity

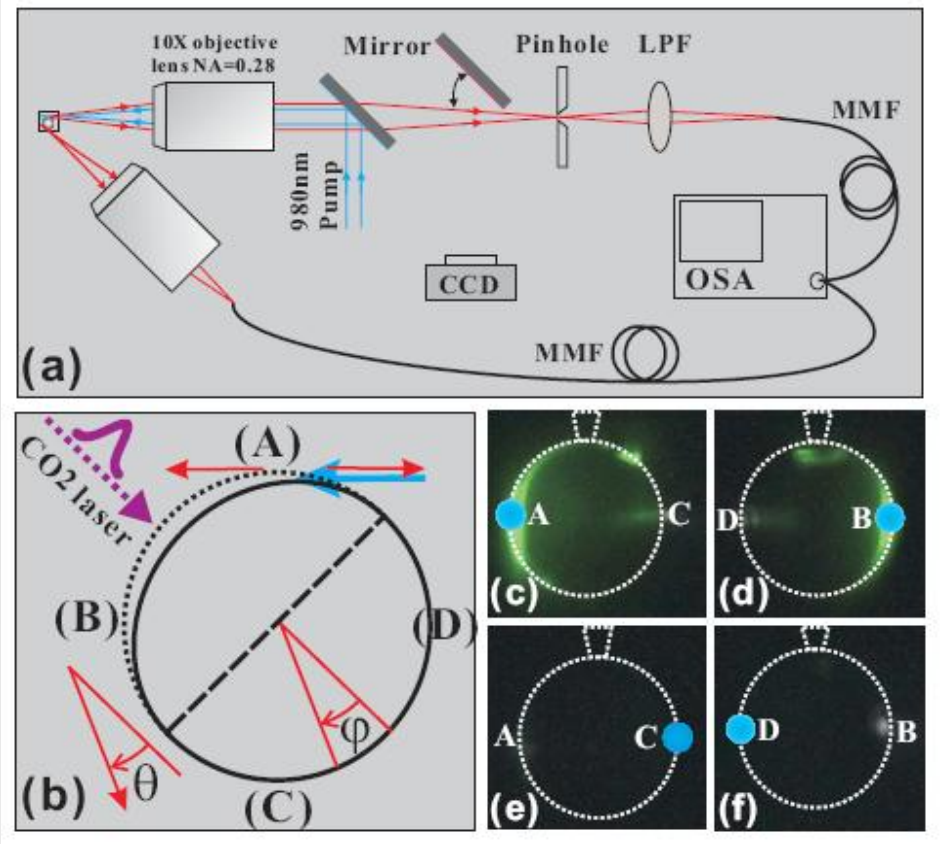

Fig. (a) Sketched experimental setup.
Pump laser(977nm) is coupled in deformation microsphere in free space.

Fig. (b) Sketched the deformation microsphere.

Fig. (c)- (f) Optical images when the coupling different points.
In (c) and (d), we can see obvious green light near points *A* and *B*. This indicates that our deformed-cavity support two emission directions.

Submitted

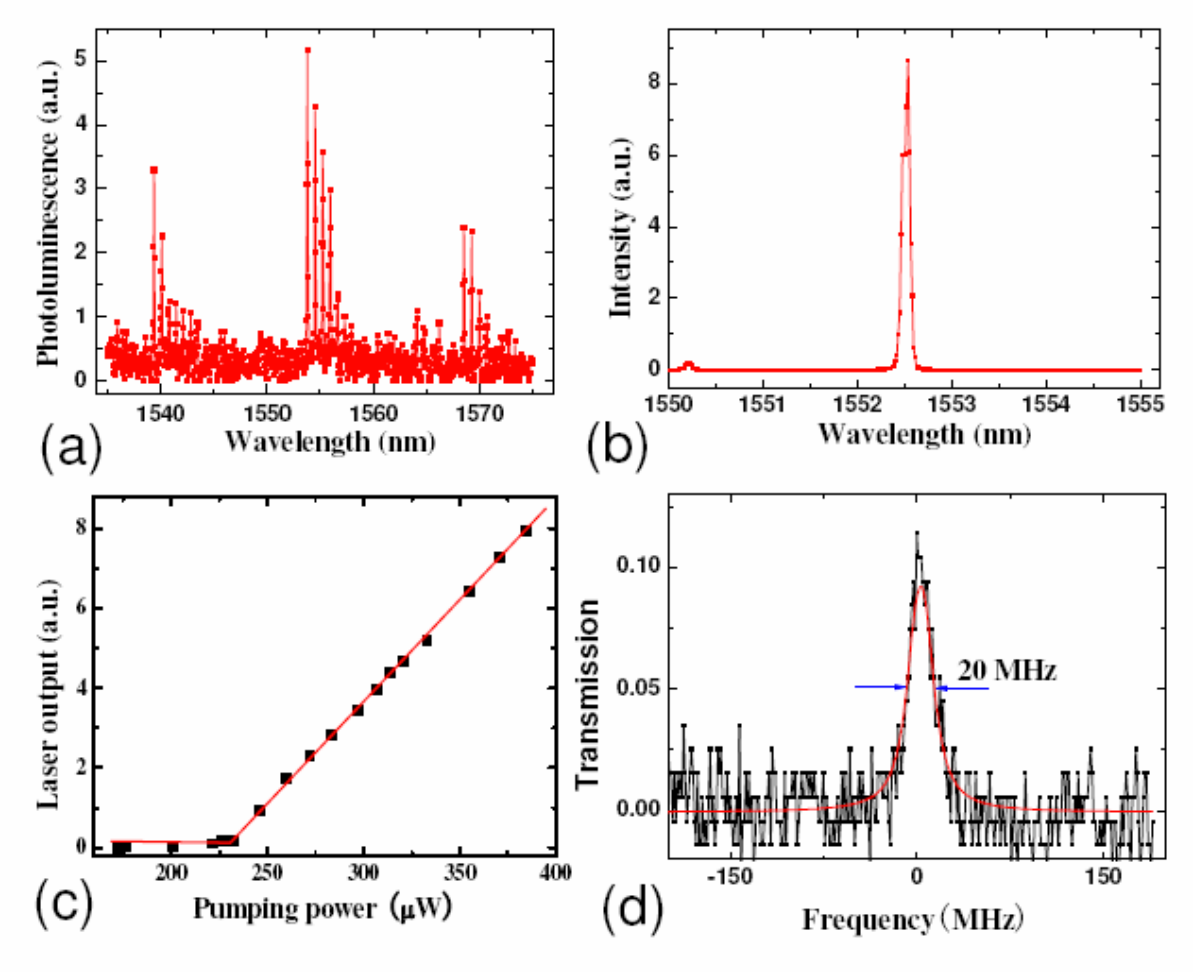

Fig. (a) PL spectrum in 1550nm band when absorbed power below threshold.
Fig. (b) Lasing emission with the pump power above the threshold.
Fig. (c) Threshold behavior of lasing emission.
Fig. (d) A typical transmission peak of the deformed microsphere in 780 nm band, correspond to Q~2*10^7.

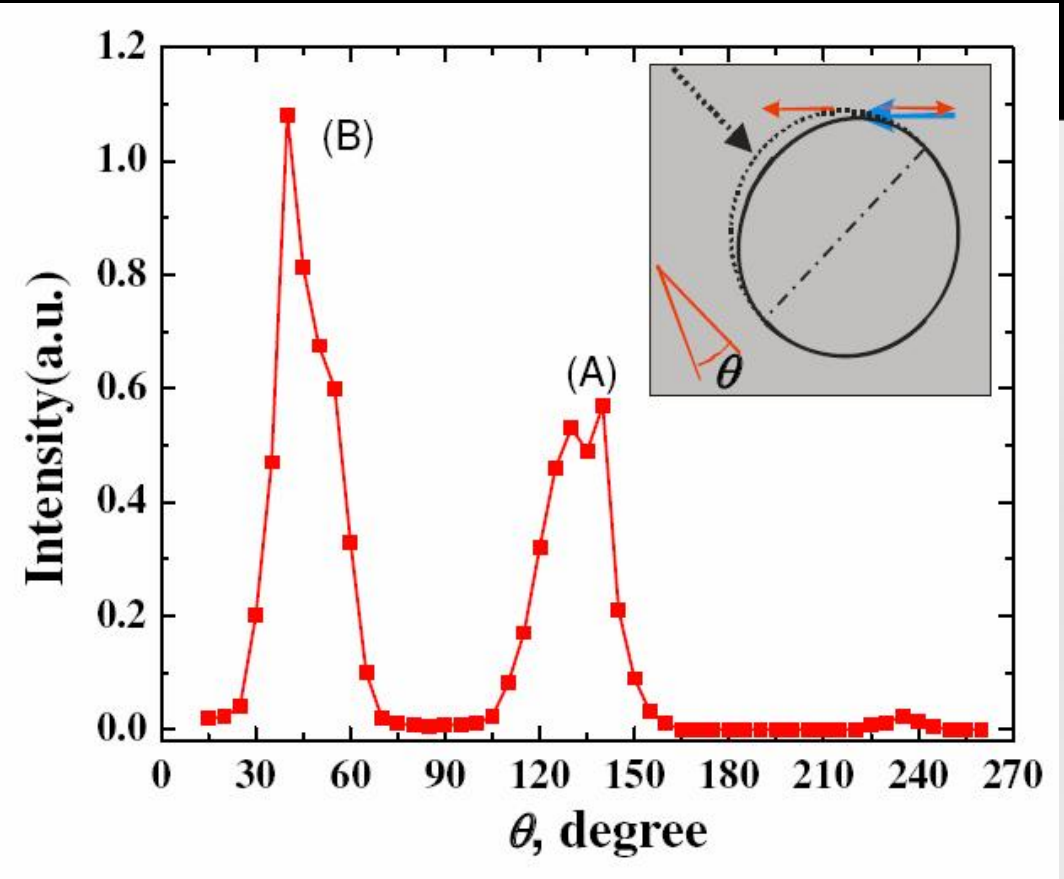

Far-field emission distribution of the lasing in the deformed microsphere. Here we excite the WGMs in free space close to the point *A*. Inset: the description of the deformed microsphere.

Other type of microlaser: microgears

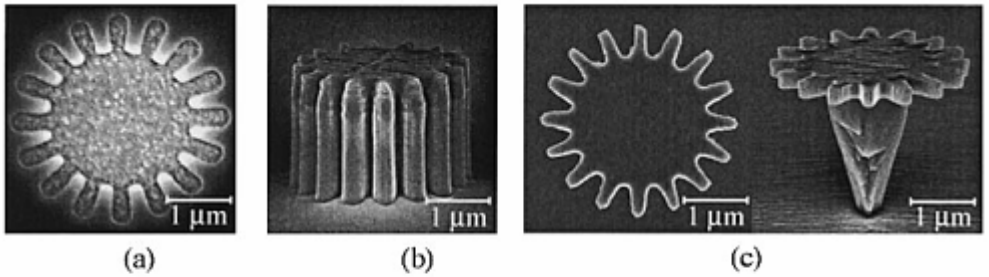

Fig. 3. Scanning electron micrographs of devices after each fabrication process. (a) Resist pattern by EB lithography. (b) Microgear mesa formed by Cl_2/Xe ICP etching. (c) Microgear disk formed by HCl wet etching.

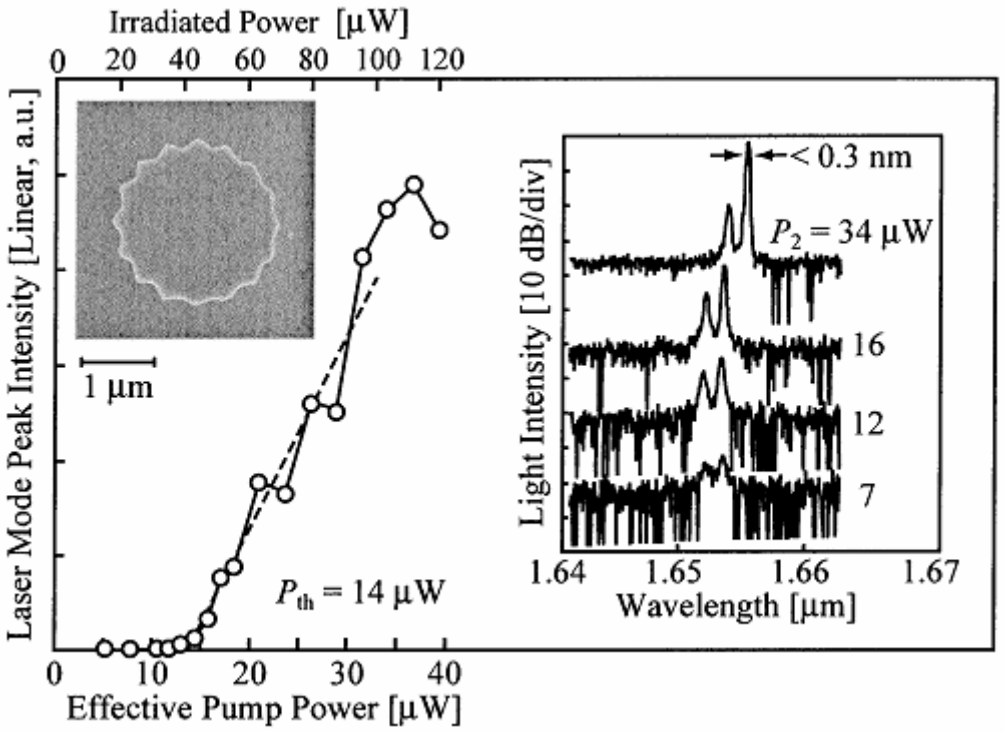

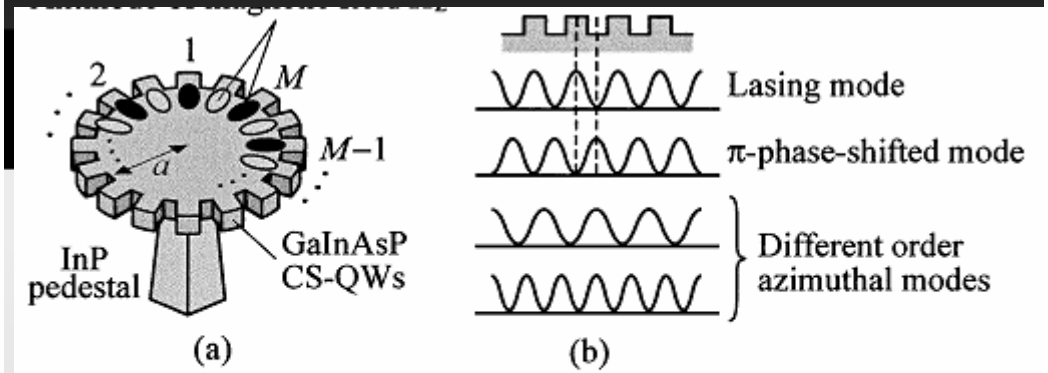

Fig. 1. Schematics of microgear laser and resonant modes. (a) Microgear laser with H_z standing wave of WG mode matched with the grating. M is the azimuthal mode order. (b) $|H_z|^2$ of resonant modes.

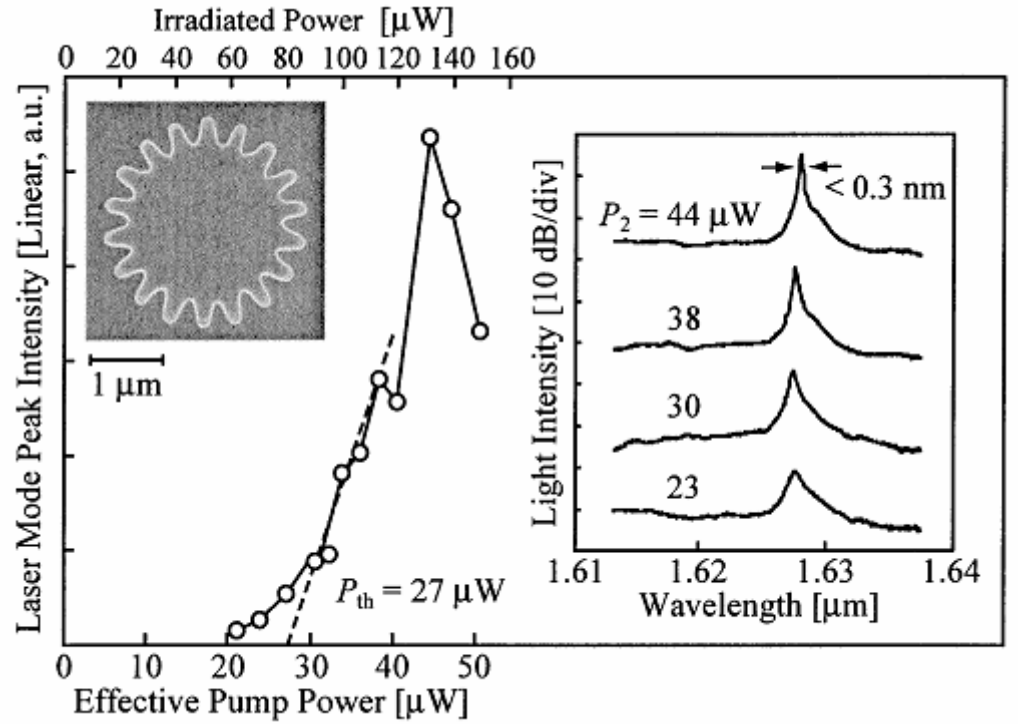

IEEE quant electro Vol. 9 ,5 , 2003

Microring Microdisk THz Laser Source

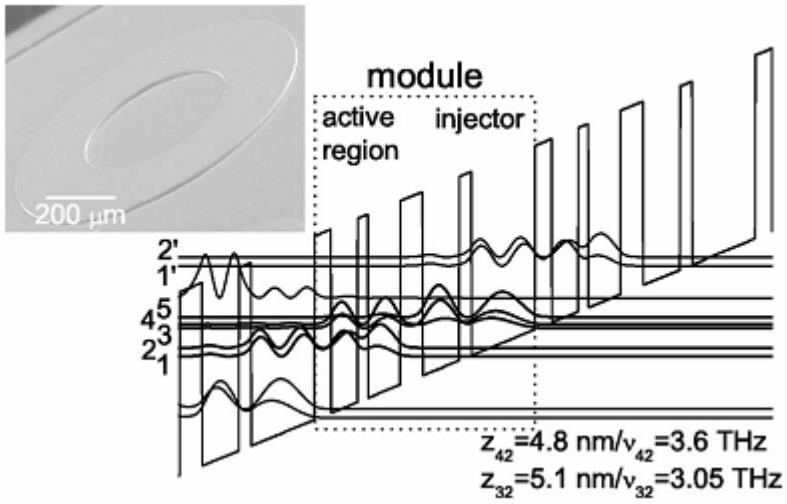

APL 87, 211112, 2005

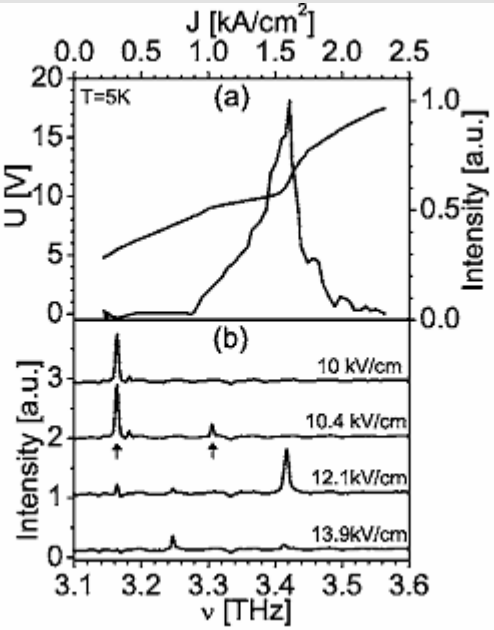

circular-shaped microcavity quantum-cascade lasers emitting in the THz region between 3.0 and 3.8 THz. The band structure design of the GaAs/Al0.15Ga0.85As heterostructure is based on longitudinal-optical phonon scattering for depopulation of the lower radiative state. A double metal waveguide is used to confine the whispering gallery modes in the gain medium. The threshold current density is 900 A/cm at 5 K. Lasing takes place in pulsed-mode operation up to aheat-sink temperature of 140K.

Microring Laser as Optical Memory

Nature 432, 11, 2004

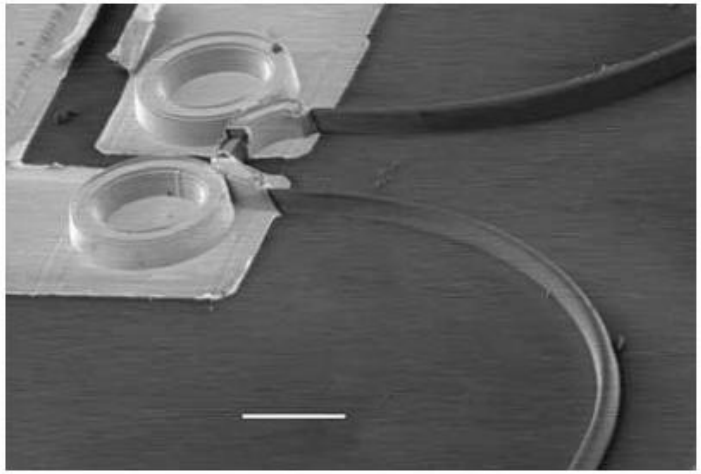

Figure 2 A memory element formed by two 16 μm diameter micro-ring lasers coupled via a waveguide on a InP/InGaAsP photonic integrated circuit. Scale bar, 10 μm. The micro-ring lasers were fabricated in active areas of the integrated circuit containing bulk 1.55 μm bandgap InGaAsP in the light guiding layer. Separate electrical contacts allowed each laser's wavelength to be individually tuned by adjusting the laser current. Passive waveguides connected the micro-ring lasers to the integrated circuit edges.

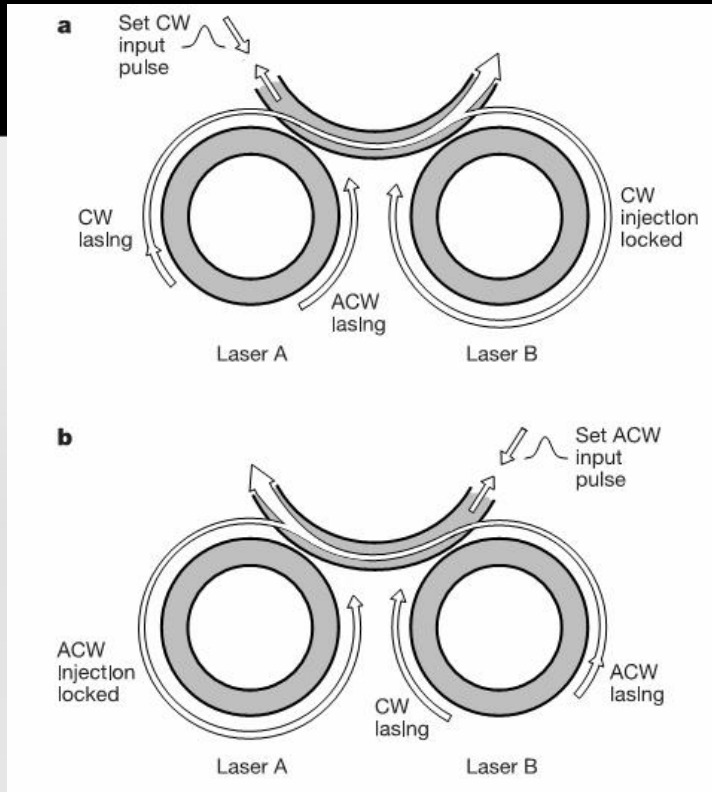

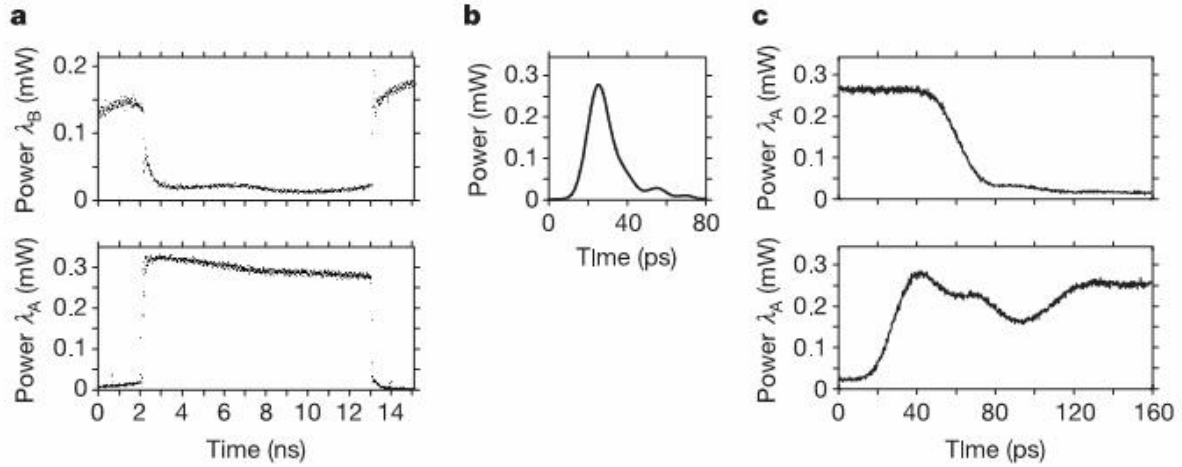

Other Applications

- Fundamental research on chaos
- Opto-electro oscillation
- Modulator and switcher
- Opto-Mechanics based on light pressure
- Surface Plasma
- Cavity QED and Quantum Information

Strong Coupling

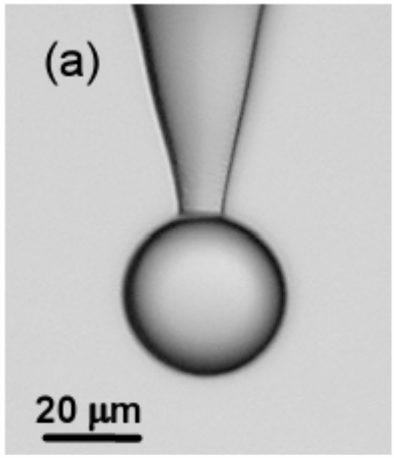

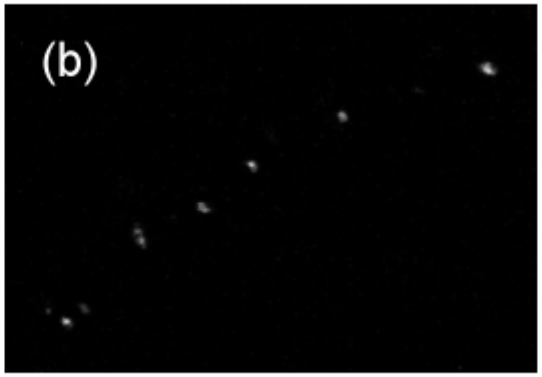

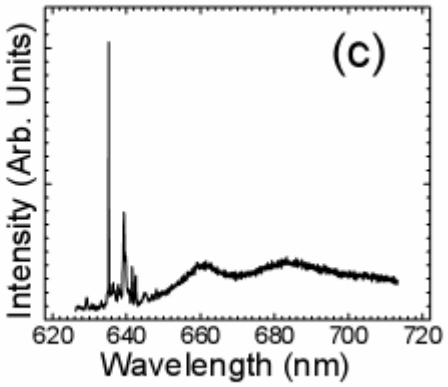

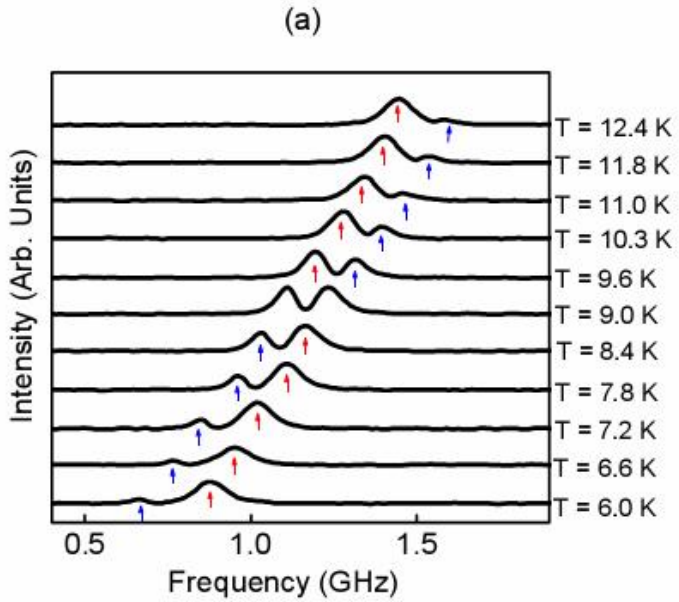

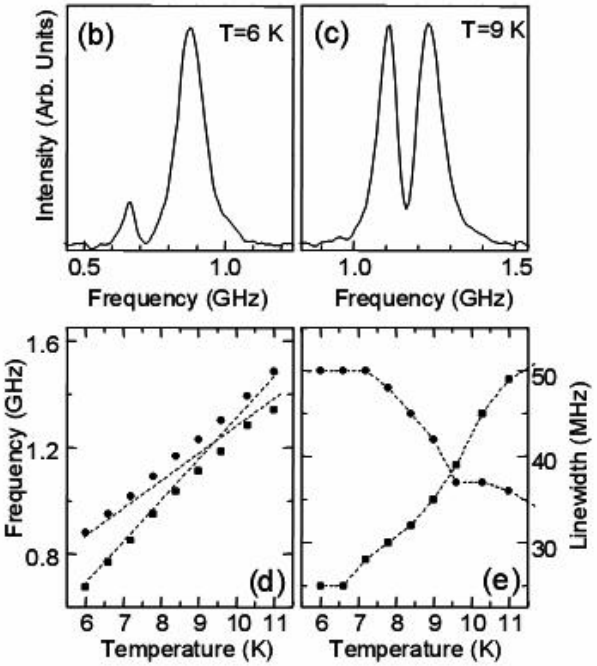

Strong coupling between NV center and microsphere

Strong coupling with CdSe nano crystal and polymer microsphere

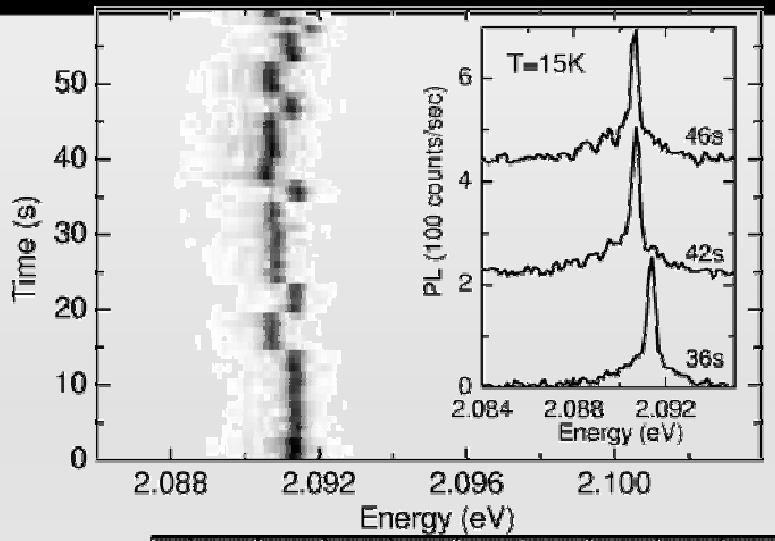

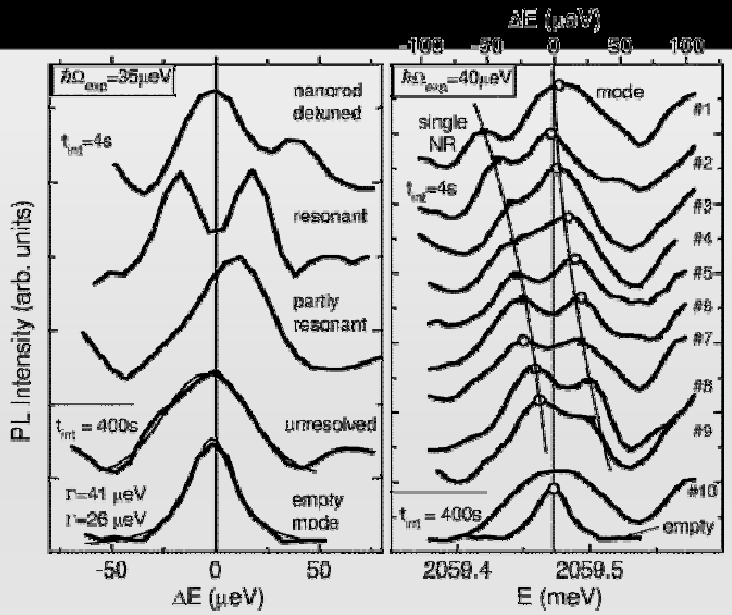

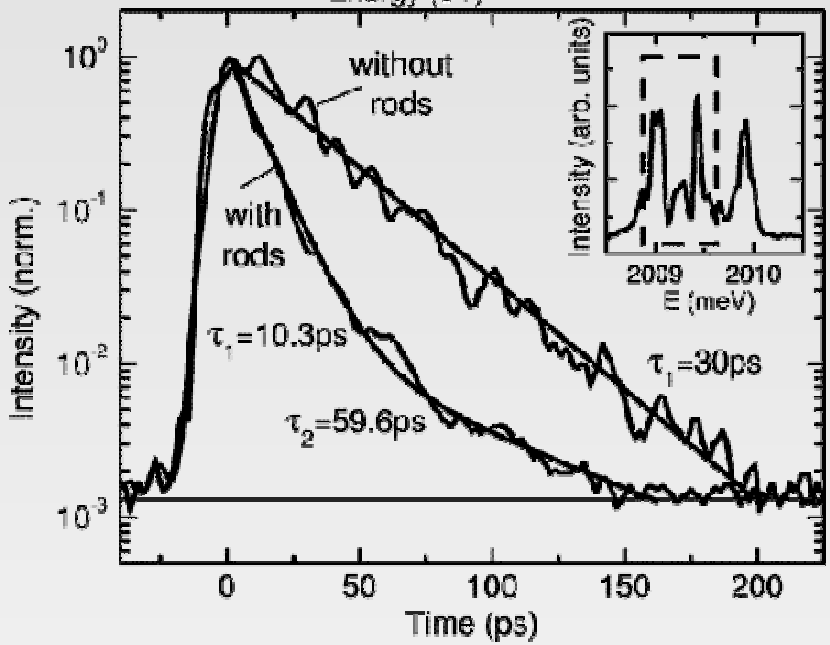

Nano Lett., **6** (3), 557 -561, 2006.

In GaAs QDs

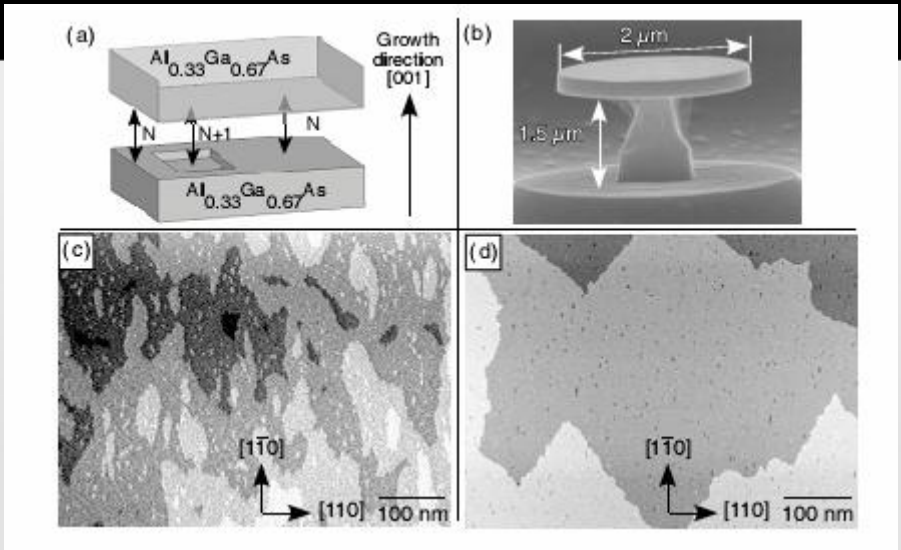

PRL 95, 067401 (2005)

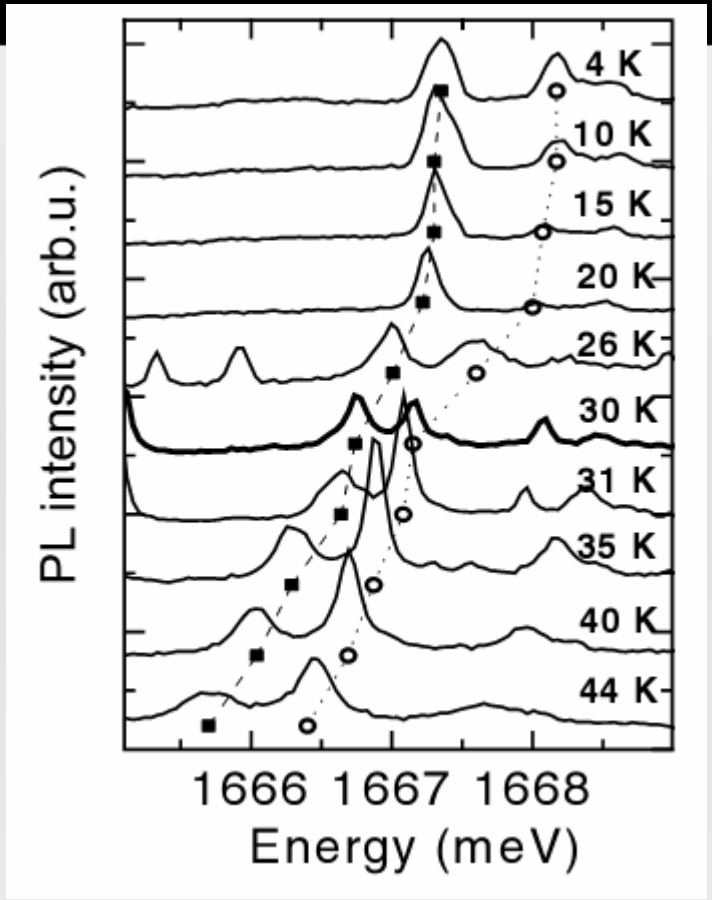

Modal Coupling together with Strong coupling

Considering Modal Coupling in real microcavity ,by defining normal mode of forward (CW) a and backward (CCW) b, the Hamiltonian can be written:

$$
\begin{aligned}
H \;=\; & \Delta_{\mathrm{A}}\sigma^{+}\sigma^{-} + (\Delta + h)A^{\dagger}A + (\Delta - h)B^{\dagger}B \\
& + \frac{1}{\sqrt{2}}\left[\mathcal{E}_{\mathrm{p}}^{*}\left(A + B\right) + \mathcal{E}_{\mathrm{p}}\left(A^{\dagger} + B^{\dagger}\right)\right] \\
& + g_A\left(A^{\dagger}\sigma^{-} + \sigma^{+}A\right) \\
& - ig_B\left(B^{\dagger}\sigma^{-} - \sigma^{+}B\right).
\end{aligned}
$$

Numerical simulation gives a spectra property of transmission Tf:

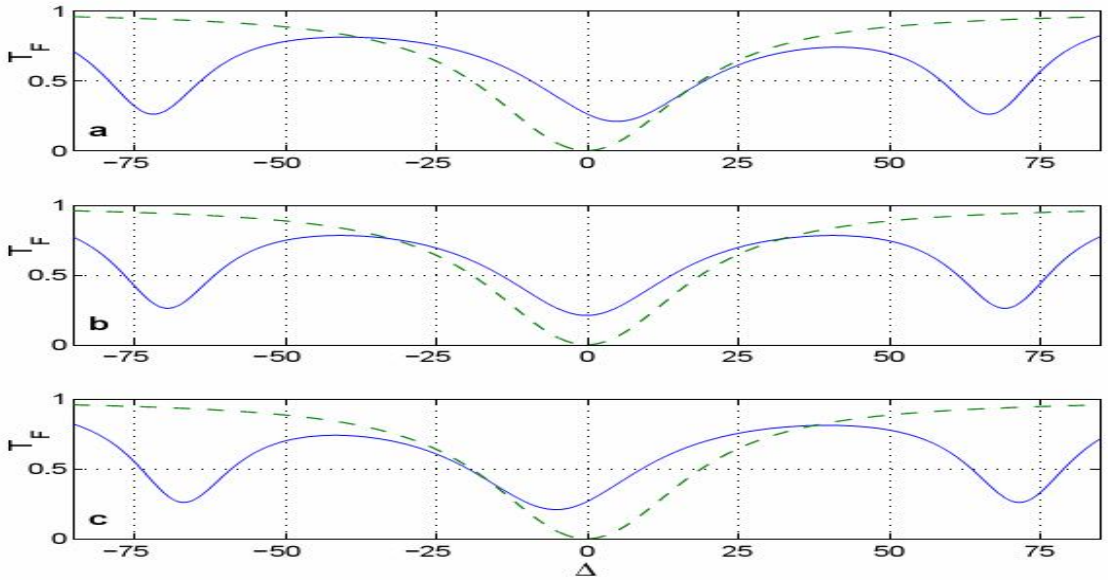

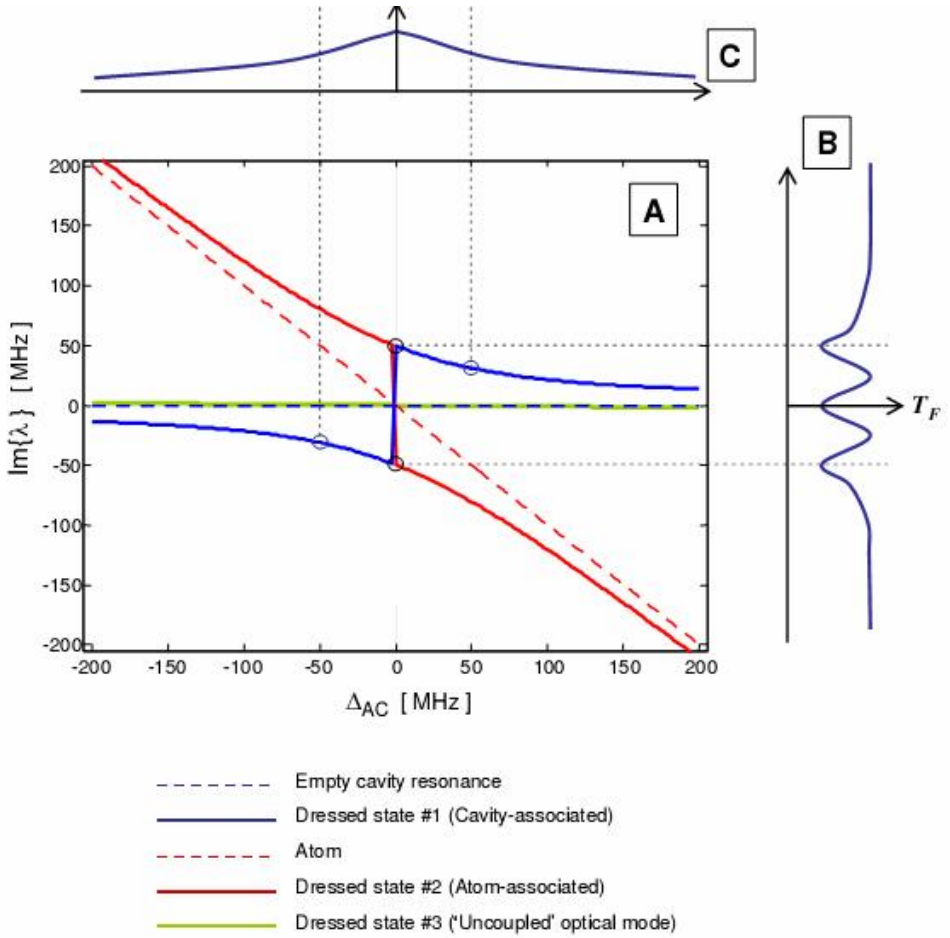

$$T_{\mathrm{F}}\big|_{\omega_{\mathrm{p}}=\omega_{\mathrm{C}}} = \frac{4\kappa_{\mathrm{i}}^2\left|g_{\mathrm{tw}}\right|^4 + h^2\left(g_{\mathrm{tw}}^2 + (g_{\mathrm{tw}}^*)^2\right)^2}{\left[(\gamma/2)\left(h^2+\kappa^2\right) + 2\kappa\left|g_{\mathrm{tw}}\right|^2\right]^2 + \left[\Delta_{\mathrm{AC}}\left(h^2+\kappa^2\right) - h\left(g_{\mathrm{tw}}^2 + (g_{\mathrm{tw}}^*)^2\right)\right]^2} .$$

$$\beta = \frac{\gamma}{2} + \frac{2\kappa\left|g_{\mathrm{tw}}\right|^2 + h\left(g_{\mathrm{tw}}^2 + (g_{\mathrm{tw}}^*)^2\right)}{h^2+\kappa^2} \simeq \frac{2\left|g_{\mathrm{tw}}\right|^2}{\kappa} = \frac{|g_0|^2}{\kappa} ,$$

A more precise theory must include different case ,which is discussed :PRA 75, 023814, 2007

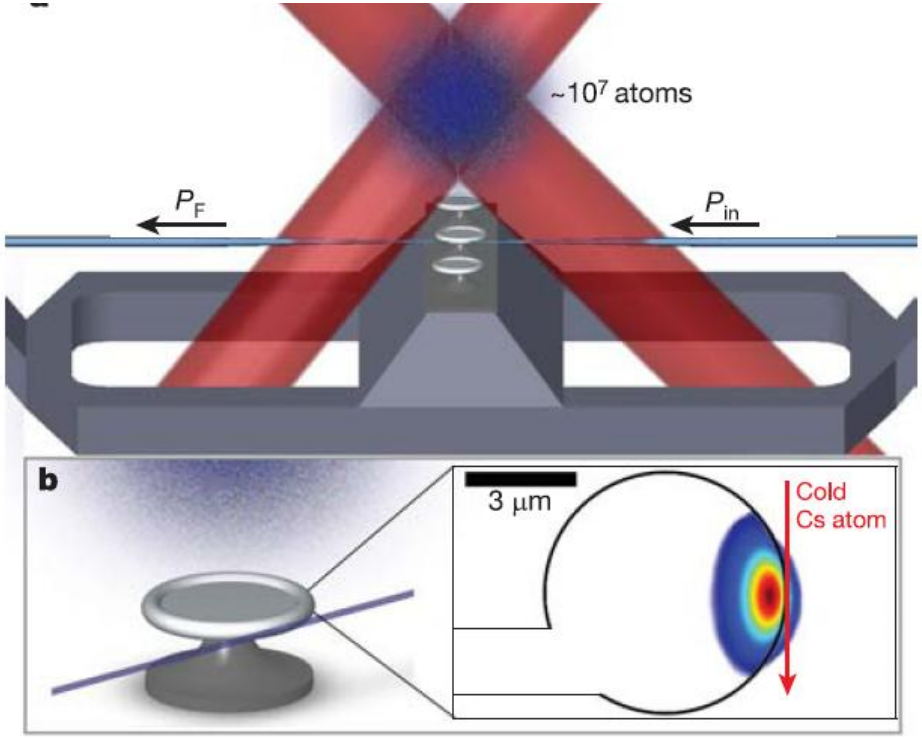

strong coupling between one atom
and a monolithic microresonator

Nature05147 Vol 443 2006

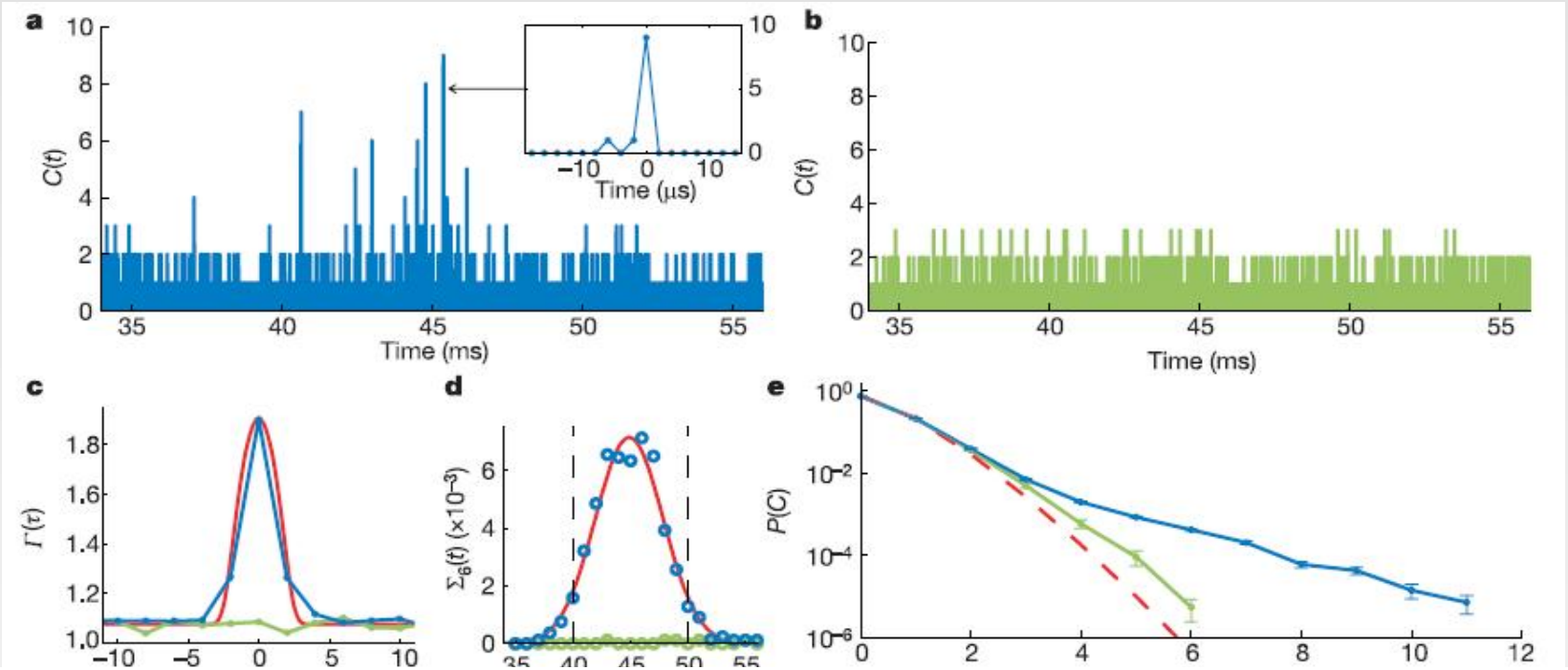

Turnstile Device with Microtoroid

Science 319, 1062, 2008

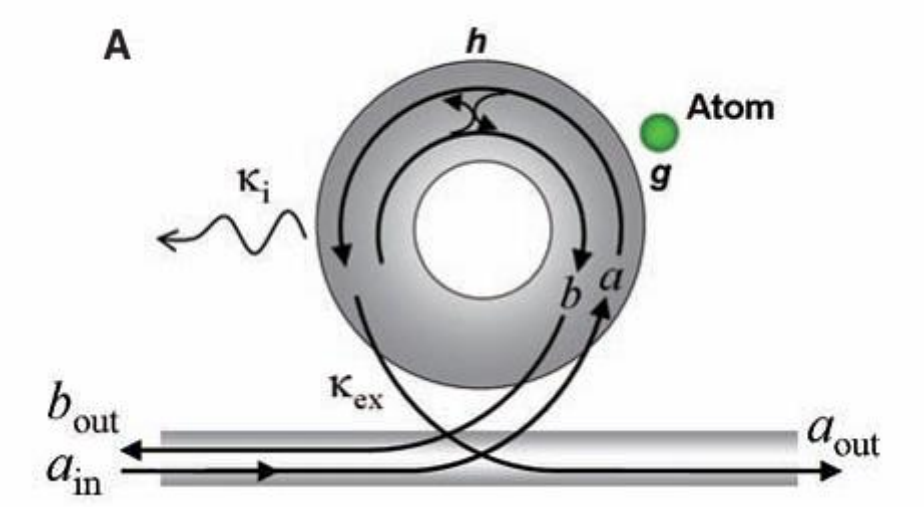

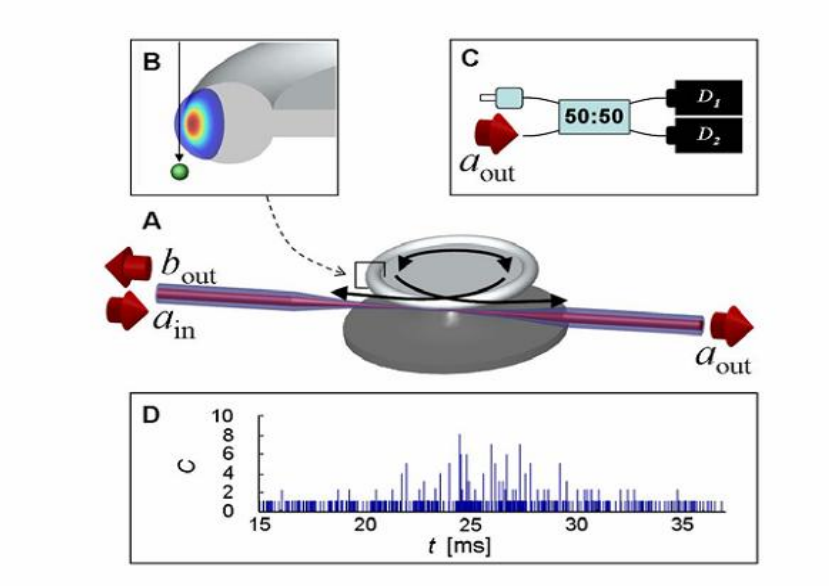

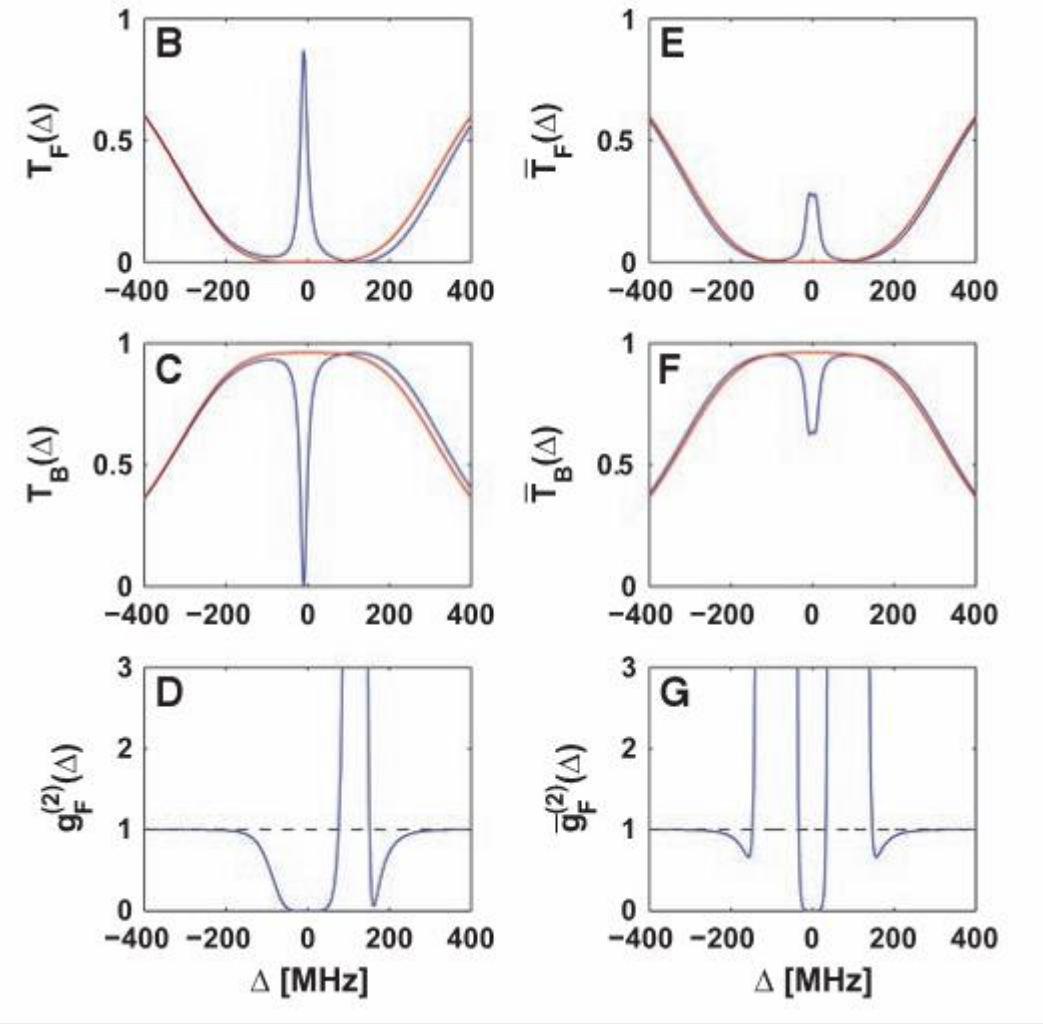

Fig. 4. Intensity correlation function $g^{(2)}(\tau)$ versus time delay τ for individual atomic transit events. $g^{(2)}(\tau)$ exhibits photon antibunching $g^{(2)}(0) < g^{(2)}(\tau)$, and sub-Poissonian photon statistics $g^{(2)}(0) = (0.14 \pm 0.04) < 1$, over an interval $\Delta\tau \approx 6$ ns (half width at half maximum) due to the operation of the atom-cavity system as a photon turnstile. The red trace is from our theoretical model.

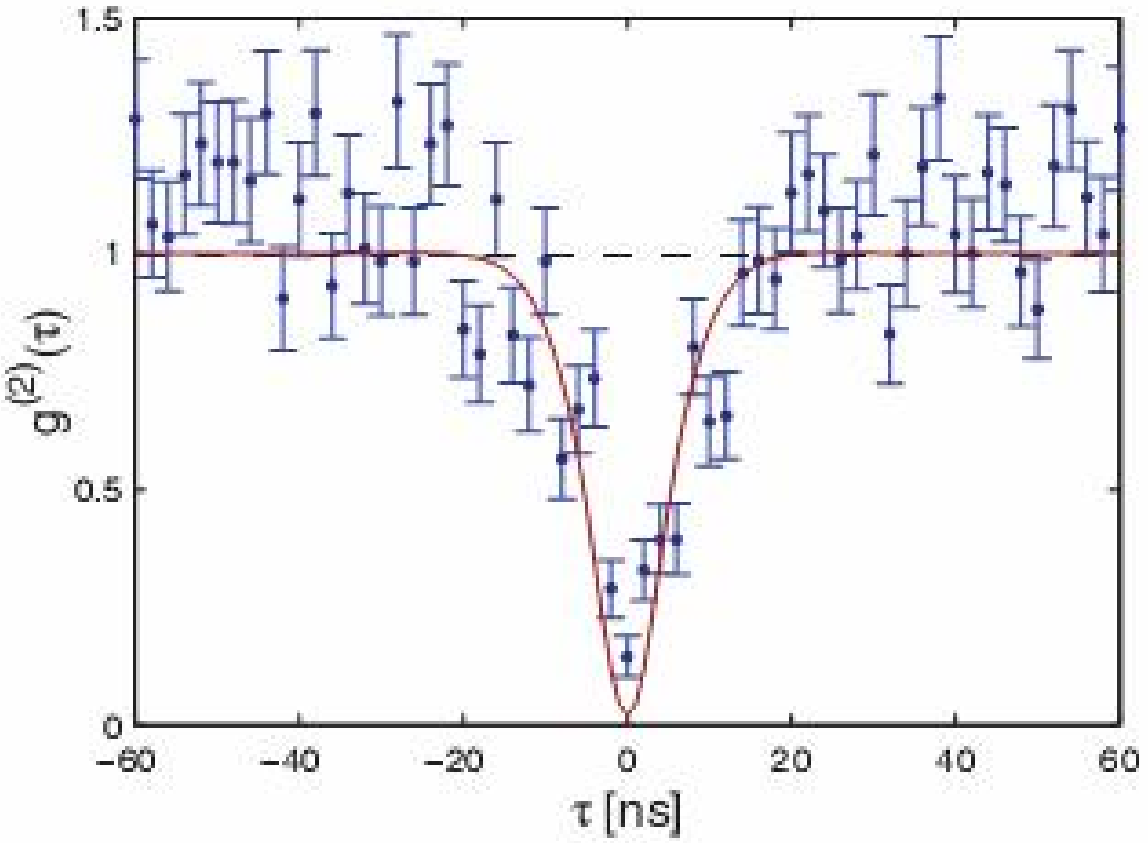

Nonlinear optical spectroscopy of a strongly coupled microdisk–quantum dot system

Nature06274 Vol 450 2007

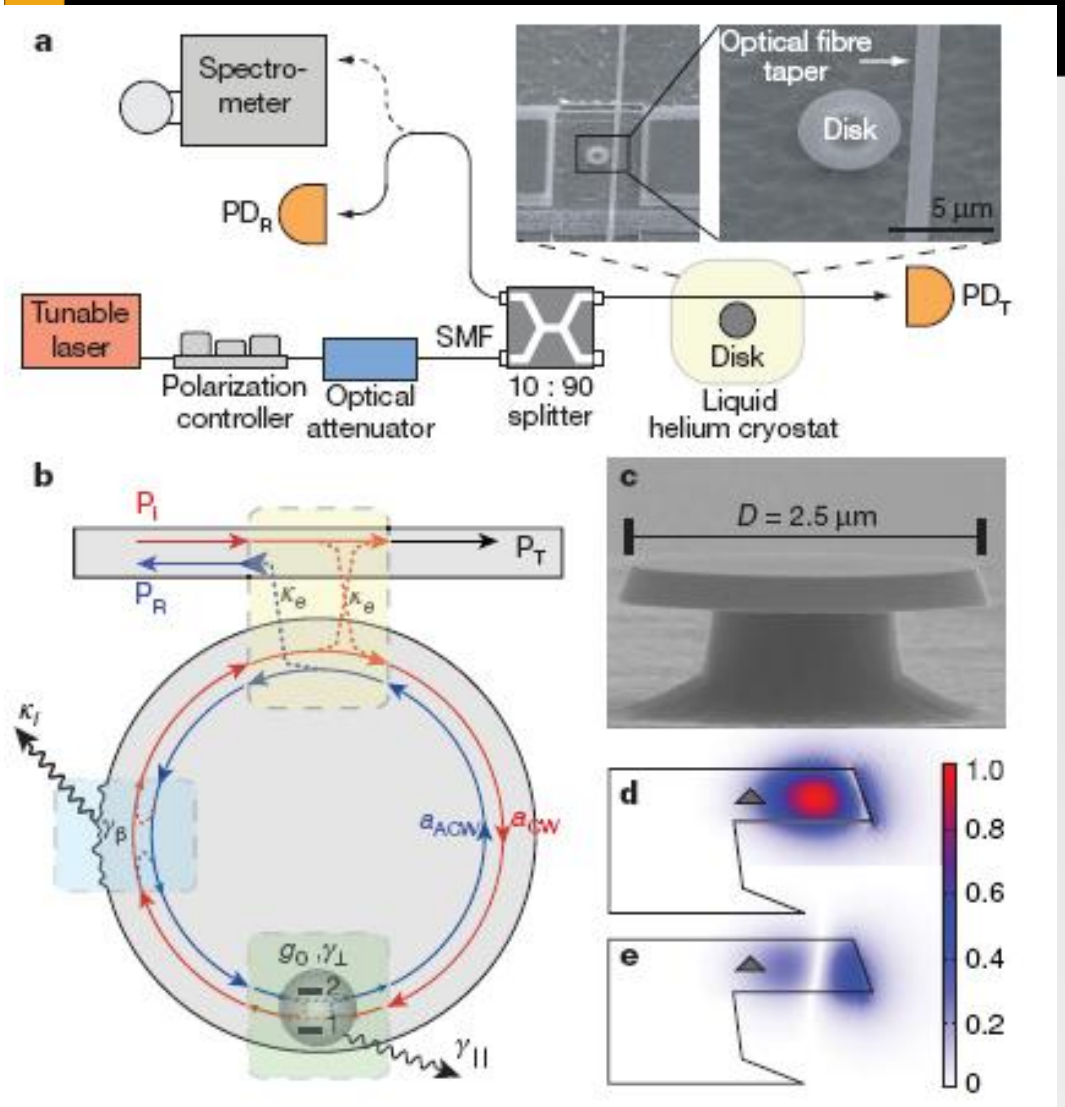

Experiment scheme

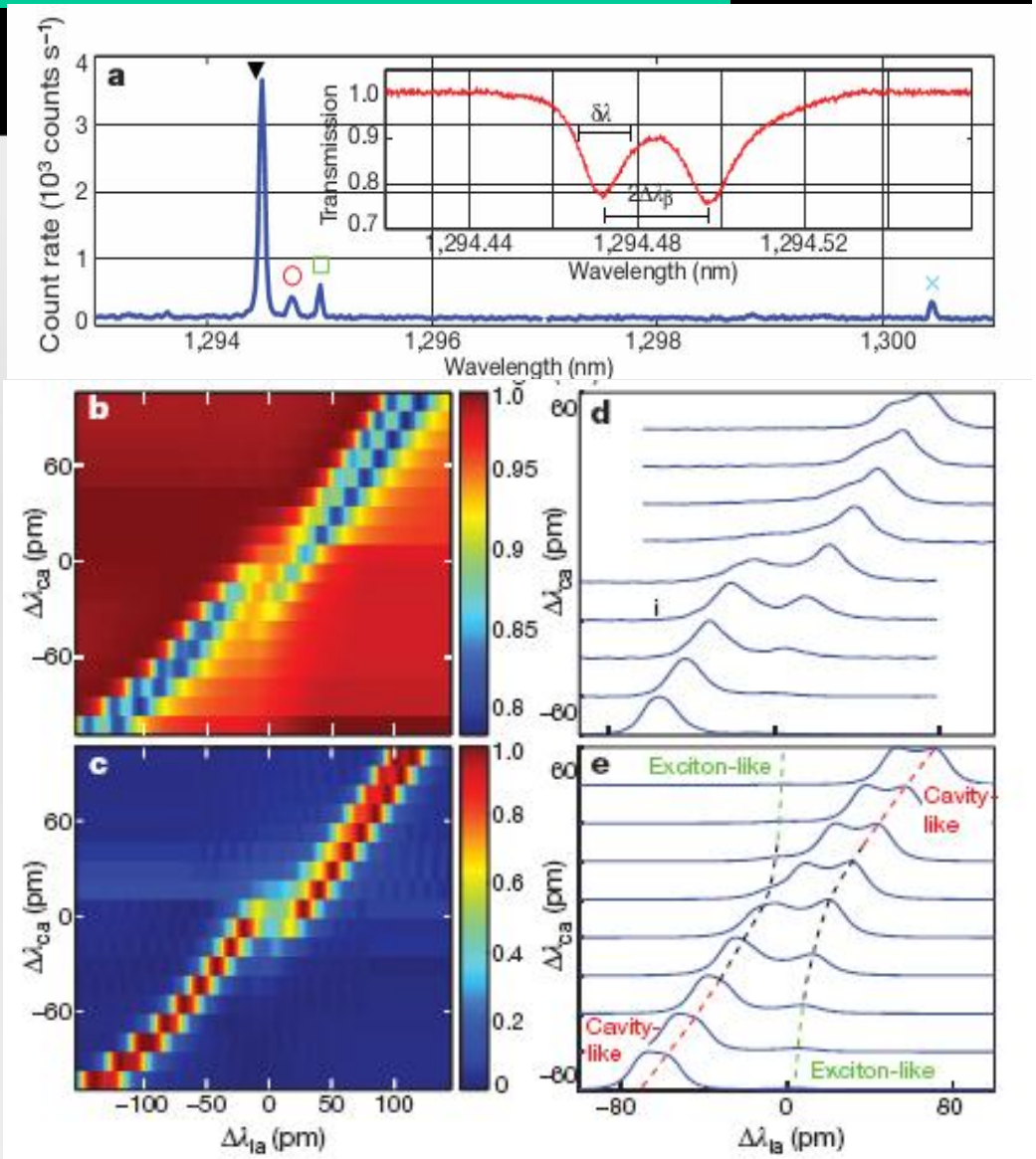

Anti crossing image

Table 1 | Parameters of quantum master equation model

Parameter	V_{tw}	η	$\kappa_e/2\pi$	$\kappa_i/2\pi$	$\gamma_\beta/2\pi$	ξ	τ_{rad}	$g_{sw1}/2\pi$	$g_{sw2}/2\pi$	$\gamma_\perp/2\pi$	$\gamma_\parallel/2\pi$
	$((\lambda_0/n)^3)$		(GHz)	(GHz)	(GHz)	(rad)	(ns)	(GHz)	(GHz)	(GHz)	(GHz)
Value	6.4	0.21	0.171	0.91	1.99	0.25π	1	2.93	1.21	1.17	0.55

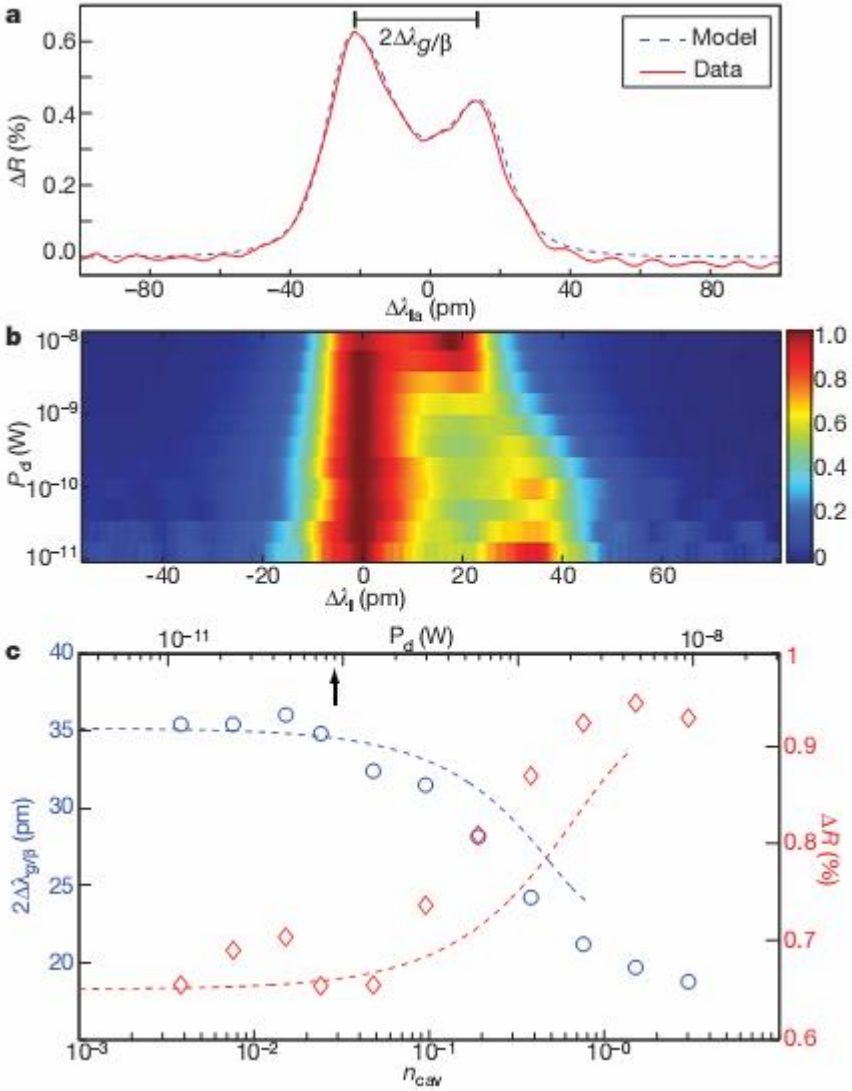

Calculated result see Fig 2 e, which shows it is strong coupling

Tuning of WGMs

Appl. Phys. Lett. 90, 0311142007

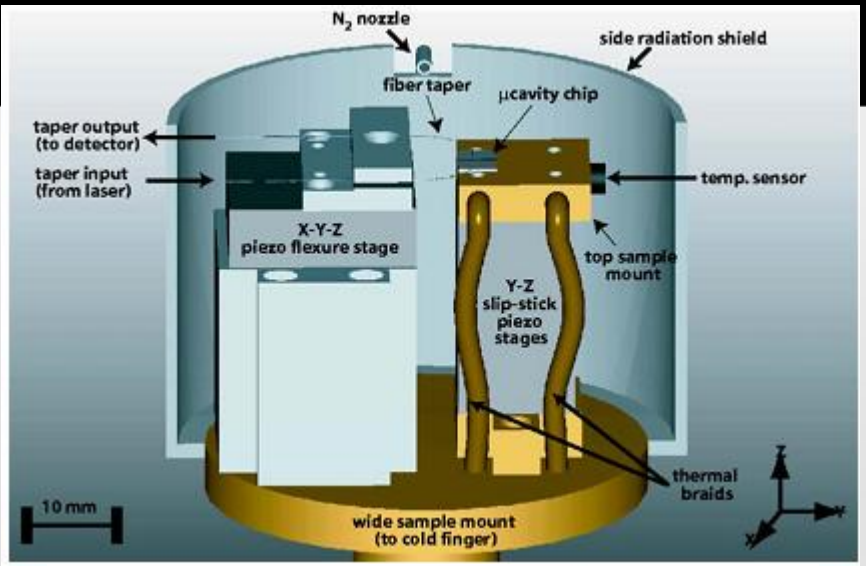

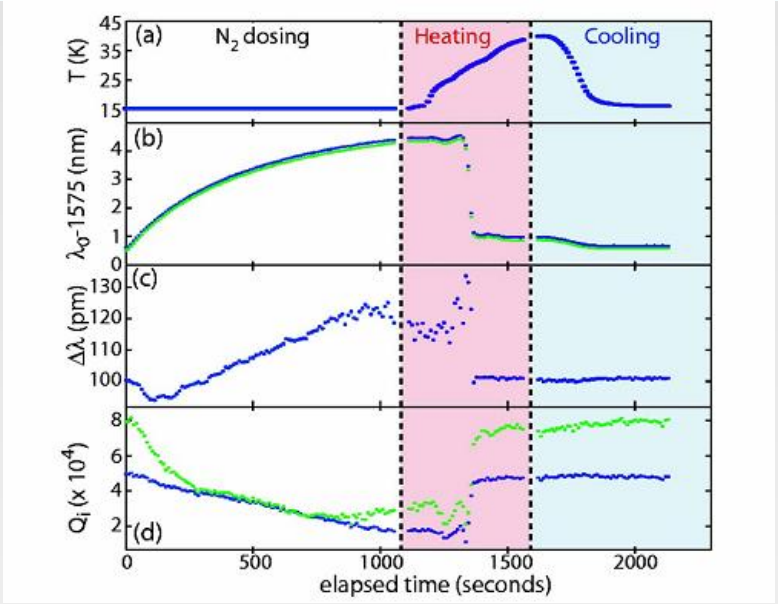

N2 gas pressure tuning

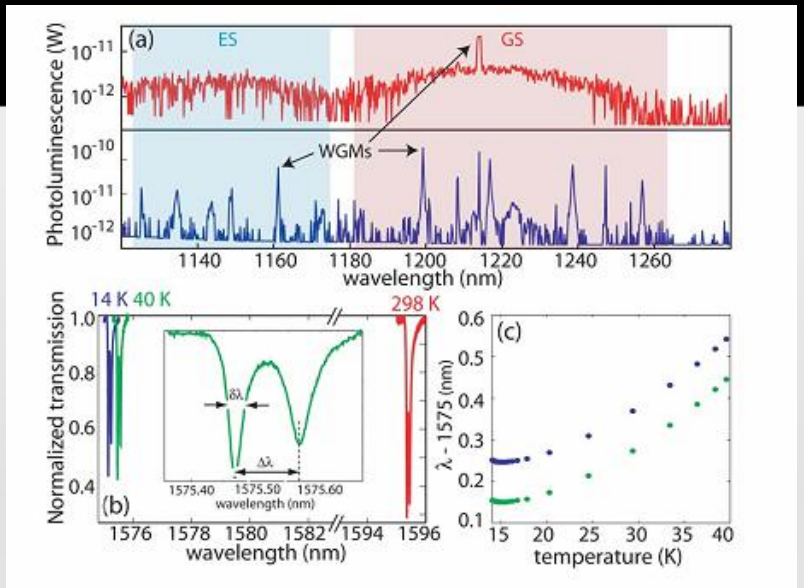

Temperature tuning

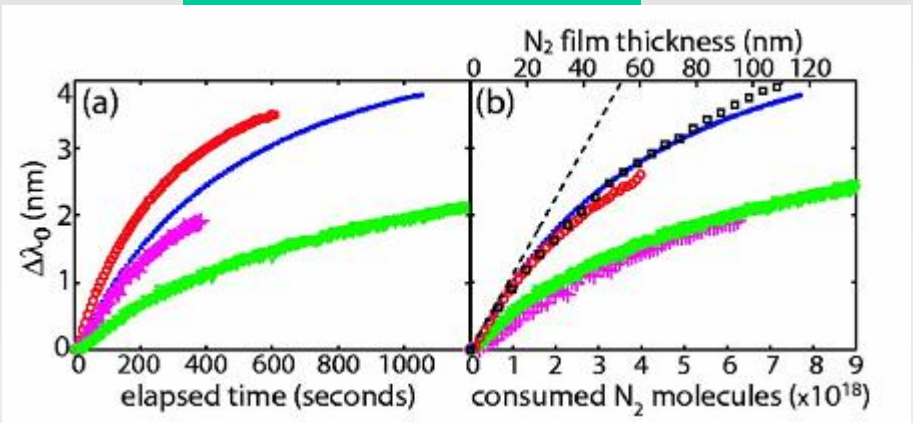

(a)Wavelength shift vs time and (b) N2 consumption

Aim of our Group

"Single-photon source"
"单光子源", "Photon gun"

✓量子密码
✓线性量子计算

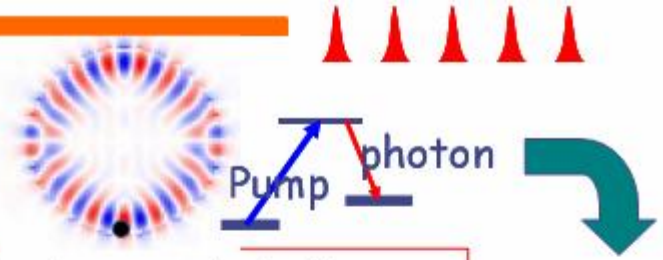

1. 极好的方向性
2. 完全固体化
3. 发射速率完全可控

可控单光子源

"Quantum Computaion" "量子计算"

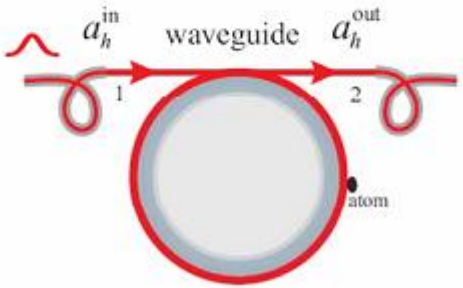

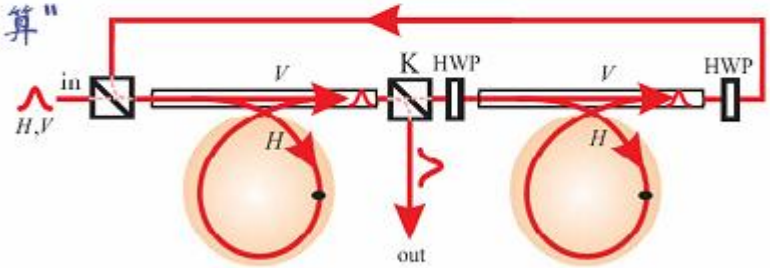

Y.-F. Xiao et al., Phys. Rev. A 70, 042314 (2004)
Y.-F. Xiao, Z.-F. Han, G.-C. Guo PRA (2006)

High gate fidelity
Low error rate
No strict strong coupling

First Step is Strong Coupling

Possible Candidate for CQED

特性 材料	单原子	单分子	胶质量子点	自组织量子点	金刚石NV中心	金刚石NE8中心	稀土离子
工作波长	可见光近红外	可见光近红外	~ 550 nm	wide	~ 637 nm	782, 793, 797, 802.	500~550
上能级寿命	~10 ns	~ 10 ns	1 ns 10 ns	< ns	~ 12 ns	2 ns	> 50 ns
非均匀加宽	Small	Large	~ nm	~ nm	~ 100 nm	~ 1.5 nm	~ nm
均匀加宽	Small	?	< 5 GHz	< 5 GHz	~ 100 nm	?	< 1 GHz
相干性	Good	Bad	Medium	Medium	Good	?	Good
样品是否方便制备	Medium	Medium	Easy	Difficult	Easy	?	in Silica?
工作时间(是否稳定)	Second	Bleaching Minute	Blinking	Long, Year	Long, Day	Long, Day	Yes
已实现否	YES	NO	YES	YES	YES	NO	NO

工作平台：微芯圆环，低温

Thank You!

Any comments are welcome